Novel Autocatalytic Mechanism and a Variety of Electrochemical Oscillations, Strongly Depending on the Atomic-Level Structure of the Electrode Surface

Shuji Nakanishi

Division of Chemistry

Graduate School of Engineering Science

Osaka University

2002

Novel Autocatalytic Mechanism and a Variety of Electrochemical Oscillations, Strongly Depending on the Atomic-Level Structure of the Electrode Surface

Shuji Nakanishi

Division of Chemistry

Graduate School of Engineering Science

Osaka University

2002

Contents

General Introduction

1. *Chemical oscillations*

The coupling of nonlinear chemical reactions and diffusion in non-equilibrium chemical systems in general or often leads to spontaneous formation of dynamic spatiotemporal patterns. Highly organized structures and functions of living bodies are known to appear on the basis of this principle. The dynamic self-organized patterns in non-equilibrium systems in general show the following unique characteristics, which are never seen in equilibrium systems.

1. The multiplicity of the state appears.
2. Rhythms and patterns with the self-restoration ability appear spontaneously.
3. The present state of the system depends on the previous history.
4. Chaotic oscillations often appear.
5. Coupling phenomena are observed.

Chemical oscillations are typical examples of the dynamic spatiotemporal patterns, and very interesting from the view-point of dynamic self-organization of molecular systems. The elucidation of the mechanisms will give new and important insights into understanding of the principles of highly organized molecular systems such as living bodies.

Chemical oscillations have been reported in various systems, such as reactions in homogeneous solutions[1-3], those in biological/organic membranes[4], electrochemical reactions[5-8], and heterogeneous surface-catalyzed reactions[9]. Of these, the Belousov-Zhabotinsky (BZ) reaction[1-3] in homogeneous solutions has been studied most extensively. This reaction was first found by Belousov in 1950's, and later progressed largely by Zhabotinsky in 1960's. In addition, a few mathematical models, such as a Brusselator and an Oregonator, have been proposed. The BZ reaction now becomes to play a central role in the study of dynamic spatiotemporal patterns.

2. *Oscillatory phenomena in electrochemical systems*

Electrochemical systems have a number of advantages for mechanistic studies of oscillations over other chemical systems, as listed below.

1. The Gibbs energies of reactions, which play a crucial role in the appearance of oscillations, can be controlled continuously.
2. Oscillatory reactions can be easily and directly observed as current or

potential oscillations.

3. The coupling of two or more oscillations can be easily detected. It can also be easily controlled by regulating the size, shape, number, of the working electrode(s), together with relative arrangements of the working electrodes, and the counter electrodes.

Thus, electrochemistry has been a powerful area for understanding the essentials of chemical oscillations.

The first oscillatory phenomenon in electrochemical systems was reported as early as the beginning of the 19th century[10]. However, modern scientific active researches have been made only since 1950's. in various reactions including anodic metal dissolution[11,12], cathodic metal deposition[13], oxidation of hydrogen[14,15] and small organic compounds[16,17], and electrocatalytic reactions[18-25], as summarized in recent reviews[5-8]. Mechanistic studies have also made rapid progress recently[8,26,27], especially since the work by Koper and Sluyters[28,29]. Growing attention has also been paid to observation and mechanistic studies of spatiotemporal patterns[30-35].

3. *Previous studies on oscillations in the laboratory to which the author has belonged*

The studies on electrochemical oscillations in the laboratory to which the author has belonged started at around 1994. The author entered the laboratory in the early stage of the studies in 1996 as a senior student. The studies had been focused on exploration of new oscillations and classification of the mechanisms in a system of electrochemical H_2O_2 reduction on Pt electrodes in acidic solutions. Fortunately the author and collaborators could later discover seven oscillations of different types (named oscillation A, B, C, D, E, F, and G).

At the beginning of our study, only one oscillation (oscillation A) was known in the system. Thus, we investigated the mechanism of oscillation A,[36,37] and in the course of the studies, we found that a new oscillation (oscillation B) was observed when the H_2O_2 concentration was made higher[38-40]. We further found that other new oscillations (oscillations C and D) were observed when small amounts of halide ions were added to the solution[41,42].

In addition to the above work, we also studied the mechanism of oscillatory coupling[43,44], the effect of deposition of foreign metal atoms such as Cu, Ag and Au on Pt electrodes[45,46], the influence of external potential pulses[47],

the effect of light illumination[40], and the mechanism of transitions from stationary-current states to oscillatory-current states[48].

In the course of the author's study, rapid progress has been made on the oscillation mechanisms and the classification by effort of Koper[7], Krischer[8], Strasser[27], et al. We found new mechanisms in the H_2O_2 reduction system[42] and developed a more refined classification on the basis of the results.

4. The outline of the present thesis

This thesis collects the work of the author concerning the effect of the atomic-level structure of the electrode surfaces on electrochemical oscillations. The main aim of the work is to clarify the detailed mechanisms of the oscillations on a molecular level as well as to investigate the interrelation between the oscillation behavior and the structure of the electrode surface.

In chapter 1, the author applied for the first time the atomically flat single crystal Pt electrodes to the oscillations in the H_2O_2-reduction system, and found a new oscillation (called oscillation E) as characteristic of atomically flat Pt(111) electrodes. The appearance of oscillation E strongly depends on the atomic-level structure of electrode surfaces, i.e., the oscillation never appears on Pt(100), Pt(110), Pt(poly), and even on Pt(111) electrodes with atomically non-flat surfaces. Mechanistic studies have revealed that adsorbed OH has an autocatalytic effect on the dissociative adsorption of H_2O_2 (the first step of the H_2O_2 reduction), and the effects strongly depend on the crystallographic structure of electrode surfaces[49,50].

In Chapter 2, the author has found that there are two stationary states of low and high H_2O_2-redcution currents, called LC- and HC-mechanism states, respectively. It is concluded that the HC-mechanism state results from double positive feedback mechanisms, i.e., the increase in adsorbed OH due to the increase in the surface H_2O_2 concentration by effective solution stirring through catalytic oxygen-gas evolution arising from the increased adsorbed OH, and the increase of adsorbed OH due to the increased dissociative adsorption of H_2O_2 as an autocatalytic effect of the increased adsorbed OH[51].

In Chapter 3, the effect of adsorbed iodine on enhancement of oscillation E is discovered and investigated. For Pt(111) electrodes, oscillation E is enhanced by iodine adsorption i.e., the potential region of oscillation E spreads toward the positive. For Pt(100), on which oscillation E does not appear, oscillation E

becomes to appear by iodine adsorption, though oscillation E never appears for Pt(110) even by the iodine adsorption. Experiments and mathematical simulation have shown that the enhancement effect is caused by the catalytic effect of adsorbed iodine on the dissociative adsorption of H_2O_2[52].

In Chapter 4, another system, i.e., the "$S_2O_8^{2-}$ reduction on Pt and Au electrodes" is investigated for generalizing the new concept found in the H_2O_2-reduction system. In the new system, the author found five oscillations of different kinds (oscillation α, β, γ, δ, and ζ) not reported before. The detailed studies have been made on oscillation γ, which appears in the most positive potentials. Experiments by use of single crystal Au(111), (100), and (110) electrodes revealed that adsorbed OH have also a catalytic effect on the $S_2O_8^{2-}$ reduction[50].

In Chapter 5, it is revealed that adsorbed bromide has a catalytic effect on the dissociative adsorption of H_2O_2 and $S_2O_8^{2-}$, causing new oscillations, named oscillations F and ζ, respectively[53]. The results further show the generality of the new concept of the (auto)catalytic effect of adsorbed anions such as OH, I, and Br, on the dissociative adsorption of peroxides (H_2O_2 and $S_2O_8^{2-}$).

In Chapter 6, a new aspect, i.e., the influence of the surface structures of electrodes on electrochemical oscillations is investigated. The control of the oscillation period by the atomic-level or nanometer-scale modulation of electrode surfaces with metal (Au, Ru, Ag, or Cu) atoms is achieved. Experiments and mathematical simulation revealed that the oscillation period is determined by the term of the low current state.

References

1. I. Shreiber, Y. Hung, J. Ross, *J. Phys. Chem.*, **100**, 8556 (1996).
2. I. R. Epstein, K. Showalter, *J. Phys. Chem.*, **100**, 13132 (1996).
3. M. Eiswirth, A. Freund, J. Ross, *Advances in Chemical Physics, Vol. 80*; I. Prigogine, S. A. Rice, Eds.; John Wiley & Sons: New York (1991), p.127.
4. R. Larter, *Chem. Rev.*, **90**, 355 (1990).
5. J. L. Hudson and T. T. Tsotsis, *Chem. Eng. Sci.*, **49**, 1493 (1994).
6. T. Z. Fahiday and Z. H. Gu, "Modern Aspects of Electrochemistry Vol. 27", ed by R. E. White, J. O'M. Bockris, and R. E. Conway, Plenum, New York (1995), p.383.
7. M. T. M. Koper, "Advances in Chemical Physics Vol. 92", ed by I. Prigogine and S. A. Rice, John Willey & Sons, New York (1996), p.161.
8. K. Krischer, "Modern Aspects of Electrochemistry Vol. 32", ed by R. E. White, J. O'M. Bockris, and R. E. Conway, Plenum, New York (1995), p.1.
9. A. V. Oertzen, H. H. Rotermund, A. S. Mikhailov, G. Ertl, *J. Phys. Chem. B*, **104**, 3155 (2000).
10. G. T. Fechner, Schweigg. *J. Chemie Physik*, **53**, 129 (1828).
11. U. F. Franck, R. FitzHugh, *Z. Elektrochem.*, **65**, 156 (1961).
12. S. Nakabayashi, K. Zama, K. Uosaki, *J. Electrochem. Soc.*, **143**, 2258 (1996).
13. J. St-Pierre, D. L. Piron, *J. Electrochem. Soc.*, **137**, 2491 (1990).
14. T. Yamazaki, T. Kodera, *Electrochim. Acta*, **34**, 969 (1989).
15. K. Krischer, M. Luebke, W. Wolf, M. Eiswirth, G. Ertl, *Electrochim. Acta*, **40**, 69 (1995).
16. S. Nakabayashi, A. Kita, *J. Phys. Chem.*, **96**, 1021 (1992).
17. H. Okamoto, N. Tanaka, M. Naito, *Electrochim. Acta*, **39**, 2471 (1994).
18. H. Tributsch, *Ber. Bunsenges. Phys. Chem.*, **79**, 570 (1975).
19. H. Tributsch, J. C. Bennett, *Ber. Bunsenges. Phys. Chem.*, **80**, 321 (1976).
20. S. Catterin, H. Tributsch, *J. Electrochem. Soc.*, **137**, 3475 (1990).
21. S. Catterin, H. Tributsch, U. Stimming, *J. Electrochem. Soc.*, **139**, 1320 (1992).
22. N. Fetner, J. L. Hudson, *J. Phys. Chem.*, **94**, 6506 (1990).
23. M. T. M. Koper, E. A. Meulenkemp, D. Vanmaekelbergh, *J. Phys. Chem.*, **97**, 7337 (1993).
24. T. G. J. Verooij, M. T. M. Koper, *Electrochim. Acta*, **40**, 1689 (1995).
25. G. Flätgen, K. Krischer, G. Ertl, *J. Electroanal. Chem.*, **409**, 183 (1996).
26. M. T. M. Koper, J. H. Sluyters, *J. Electroanal. Chem.*, **371**, 149 (1994).
27. P. Strasser, M. Eiswirth, M. T. M. Koper,*J. Electroanal. Chem.*, **478**, 50 (1999).

28. M. T. M. Koper, J. H. Sluyters, *J. Electroanal. Chem.*, **303**, 73 (1991).
29. M. T. M. Koper, J. H. Sluyters, *J. Electroanal. Chem.*, **347**, 31 (1993).
30. G. Flätgen, K. Krischer, B. Pettinger, K. Doblhofer, H. Junkes, G. Ertl, *Science*, **269**, 668 (1995).
31. I. Z. Kiss, V. Gaspar, J. L. Hudson, *J. Phys. Chem. B*, **104**, 7554 (2000).
32. J. Christoph, R. D. Otterstedt, M. Eiswirth, N. I. Jaeger, J. L. Hudson, *J. Chem. Phys.* **110**, 8614 (1999).
33. P. Strasser, J. Christoph, W. F. Lin, M. Eiswirth, J. L. Hudson, *J. Phys. Chem. A*, **104**, 1854 (2000).
34. N. Mazouz, K. Krischer, G. Flätgen, G. Ertl, *J. Phys. Chem. B*, **101**, 2403 (1997).
35. T. Matsuda, H. Hommura, Y. Mukouyama, S. Yae, Y. Nakato, *J. Electrochem. Soc.*, **144**, 1988 (1997).
36. Y. J. Li, J. Oslonovitch, N. Mazouz, F. Plenge, K. Krischer, G. Ertl, *Science*, **291**, 2395 (2001).
37. Y. Mukouyama, H. Hommura, S. Nakanishi, T. Nishimura, H. Konishi, Y. Nakato, *Bull. Chem. Soc. Jpn.*, **72**, 1247 (1999).
38. H. Hommura, Y. Mukouyama, T. Matsuda, S. Yae, Y. Nakato, *Chem. Lett*, 391 (1996).
39. Y. Mukouyama, S. Nakanishi, Y. Nakato, *Bull. Chem. Soc. Jpn.*, **72**, 2573 (1999).
40. Y. Mukouyama, S. Nakanishi, H. Konishi, Y. Ikeshima, Y. Nakato, *J. Phys. Chem. B*, **105**, 10905 (2001).
41. Y. Mukouyama, S. Nakanishi, H. Konishi, and Y. Nakato, *J. Electroanal. Chem.*, **473**, 156 (1999).
42. Y. Mukouyama, S. Nakanishi, T. Chiba, K. Murakoshi, Y. Nakato, *J. Phys. Chem. B*, **105**, 7246 (2001).
43. Y. Mukouyama, H. Hommura, T. Matsuda, S. Yae, Y. Nakato, *Chem. Lett.*, 463 (1996).
44. T. Matsuda, Y. Mukouyama, H. Hommura, S. Yae, Y. Nakato, *J. Electrochem. Soc.*, 144, 2296 (1997).
45. S. Nakanishi, Y. Mukouyama, Y. Nakato, *J. Electrochem. Soc.*, **148**, E405 (2001).
46. S. Nakanishi, H. Hommura, Y. Mukouyama, T. Matsuda, S. Yae, Y. Nakato, *Chem. Lett.*, 977 (1998).
47. T. Nishimura, Y. Mukouyama, S. Nakanishi, H. Konishi, Y. Nakato, *Kagaku Kogaku Ronbunshu*, 25, 510 (1999).
48. Y. Mukouyama, T. Nishimura, S. Nakanishi, Y. Nakato, *J. Phys. Chem. B*, **104**, 11186 (2000).

49. S. Nakanishi, Y. Mukouayma, K. Karasumi, A. Imanishi, N. Furuya, Y. Nakato, *J. Phys. Chem. B*, **104**, 4181 (2000).
50. S. Nakanishi, S. –I. Sakai, M. Hatou, K. Fukami, Y. Nakato, *J. Electrochem. Soc.*, submitted for publication.
51. Y. Mukouyama, S. Nakanishi, H. Konishi, K. Karasumi, Y. Nakato, *Phys. Chem. Chem. Phys.*, 3, 3284 (2001).
52. S. Nakanishi, Y. Mukouyama, Y. Nakato, *J. Phys. Chem. B*, **105**, 5751 (2001).
53. S. Nakanishi, S. –I. Sakai, M. Hatou, Y. Mukouyama, Y. Nakato, *J. Phys. Chem. B*, **106**, 2287 (2002).

Chapter 1

Appearance of an Oscillation through Autocatalytic Mechanism by Control of the Atomic-Level Structure of Electrode Surfaces in Electrochemical H_2O_2 Reduction at Pt Electrodes

Introduction

Chemical and electrochemical oscillations are attractive phenomena from a view-point of dynamic self-organization of molecular systems. Electrochemical oscillations have been reported for a variety of systems as summarized in recent reviews.[1-3] Recently low-index single-crystal metal electrodes with well-defined surface structures have been used for mechanistic studies of oscillations.[4-10] Ertl et. al.[4] reported that the oscillatory patterns for H_2 oxidation on Pt in the presence of Cu^{2+} and halide ions depended on the crystallographic surface structures of Pt electrodes, and explained it to be due to a difference in the binding strength of halogen atoms on different single-crystal surfaces.

The author has been studying electrochemical oscillations for H_2O_2 reduction on Pt electrodes in acidic solutions.[11-16] Interestingly, various oscillations of different types, named oscillation A, B, C, and D, have been found to appear. Oscillation A is observed in a potential region just before hydrogen evolution,[11,12] whereas oscillation B is observed in a potential region of hydrogen evolution.[11,12] Oscillations C and D are observed in the presence of a small amount of halide ions such as Cl^-, Br^-, and I^- in the electrolyte.[13-15] Moreover, the oscillation period for oscillation A is modulated by adsorption of inert metal atoms, such as Cu, Au, Ag, and Ru, to sub-monolayer amounts.[16] These results indicate that the oscillations in the "H_2O_2-acid-Pt electrode" system are sensitive to the atomic-level structures of electrode surfaces.

In the present paper, the author reports that the atomic-level structures of the electrode surfaces affect not only the adsorption behavior but also the reaction mechanism, resulting in an appearance of another-type oscillation, named oscillation E, at the crystallographically most-flat Pt(111) surface. The result is important for deeper understanding of the mechanisms of electrochemical reactions themselves as well as the oscillation mechanisms.

Experimental

The electrochemical cell used is schematically illustrated in Fig. 1. A half-spherical single-crystal or polycrystalline Pt disc electrode (about 1 to 2 mm in diameter), used as the working electrode (WE), was held such that only the flat surface was in contact with the electrolyte by use of its meniscus. The electrolyte was 0.3 M H_2SO_4 or $HClO_4$ (pH 0.55) with or without H_2O_2 (M = mol/dm^3). A gold plate was used as the counter electrode (CE). A hydrogen electrode, composed of a platinized platinum electrode, 1.0 M H_2SO_4 or $HClO_4$, and highly pure hydrogen gas, was used as the reference electrode (RE). Either 1.0 M H_2SO_4 or $HClO_4$ in the hydrogen electrode was chosen so that the common acid was used in the WE and RE compartments. The WE and RE compartments were separated with a cation exchange membrane (Nafion 117).

Single-crystal Pt(111), (100), and (110) electrodes with atomically *flat* surfaces were prepared by the method of Clavilier et al.[17] Single-crystal Pt spheres were prepared by heating Pt wires (99.97% in purity) in a hydrogen flame. They were cut in parallel to the Pt(111), (100), and (110) faces, and polished with diamond slurry. They were then annealed in a hydrogen flame for 30 min for Pt(111), and 180 min for Pt(100) and (110). Just before measurements, all the electrodes were annealed again in a hydrogen flame for 60 s and immediately quenched in Ar-bubbled pure water. Single-crystal Pt(111) electrodes with atomically *non-flat* surfaces were also used for reference. The details of their preparation will be described later. Polycrystalline Pt electrodes, having nearly the same shape as the single-crystal Pt electrodes, were also used. They were prepared by cutting and polishing of polycrystalline spheres, which were obtained by heating Pt wires in a hydrogen flame.

Aqueous electrolytes were prepared using special grade chemicals and pure water, the latter of which was obtained by purification of de-ionized water with a Milli-Q water purification system. Current density (j) vs. potential (U), and j vs. time (t) were measured with a potentio-galvanostat (Nikko-Keisoku NPGS-301) and a potential programmer (Nikko-Keisoku NPS-2). They were either recorded with an X-Y recorder (Riken-Denshi F-35C) or stored digitally at 1 kHz with a Mac ADIOS II/16 (GW Instruments). Ohmic drops in the solution are not corrected in the present work. Argon gas was bubbled through the electrolyte in the working-electrode compartment for 30 min to remove dissolved oxygen when j-U curves for adsorption and desorption of hydrogen atoms (upd-H) were measured in 0.3 M H_2SO_4 or $HClO_4$. No bubbling of argon gas was carried out in solutions containing H_2O_2, because oxygen is more or less evolved by decomposition of H_2O_2 on Pt. The structure of electrode surfaces was

inspected with a scanning tunneling microscope (STM) (Nanoscope IIIa, Digital Instruments), using a Pt-Ir wire as a tip. The tunnel current was held at 1 nA, and the scan rate was 5.086 Hz.

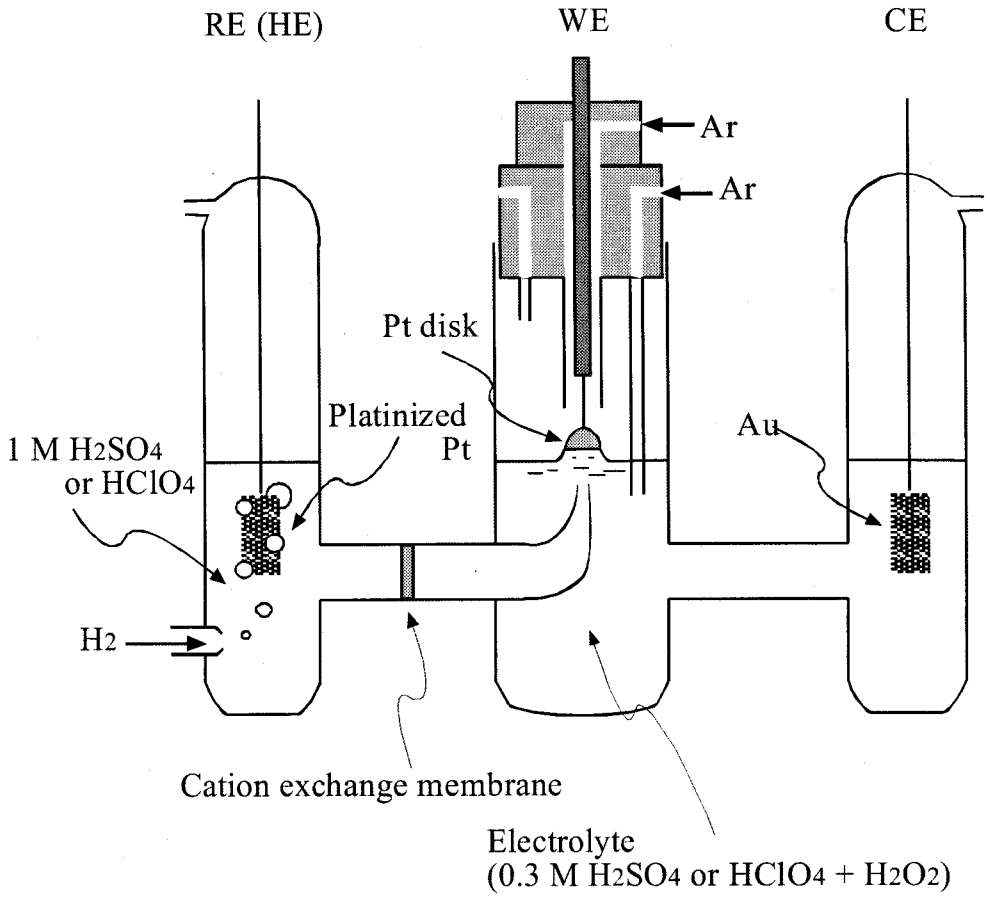

Fig. 1 An electrochemical cell used for measurements of current oscillations. WE: working electrode (single-crystal or polycrystalline Pt disc), CE: counter electrode (Au plate), RE: reference electrode (a hydrogen electrode, composed of platinized Pt, 1.0 M H_2SO_4 or $HClO_4$, and 1 atm hydrogen gas).

Results

Figure 2 shows current density (j) vs. potential (U) curves for a polycrystalline Pt electrode (hereafter abbreviated as a poly-Pt electrode), observed under potential-controlled conditions. Figure 2a is a curve in 0.3 M H_2SO_4 not containing H_2O_2 (pH 0.55). Two current peaks on both cathodic and anodic sides are attributed to formation and disappearance of electrochemically adsorbed hydrogen atoms, called upd-H (under-potential deposited hydrogen).[11,18,19] The appearance of such two peaks on both sides are characteristic of poly-Pt electrodes. Figure 2b is a curve in 0.3 M H_2SO_4 containing low-concentration (0.2 M) H_2O_2. A current in a potential region from about 0.65 to 0.00 V vs. NHE is attributed to H_2O_2 reduction, which starts at about 0.80 V. A hydrogen evolution current appears in potentials more negative than ca. –0.02 V. The current peaks for upd-H are missing in Fig. 2b because the j-scale in Fig. 2b is much larger than that in Fig. 2a. It is to be noted that the H_2O_2-reduction current is independent of the electrode potential in a region above 0.07 V, whereas it shows the "negative slope" in a region from +0.07 V to –0.02 V. The potential-independent H_2O_2-reduction current is explained by assuming that the H_2O_2 reduction is initiated by dissociative adsorption of H_2O_2

$$2Pt + H_2O_2 \xrightarrow{k_1} 2Pt\text{-}OH \qquad (1)$$

followed by electrochemical reduction of the resultant Pt-OH

$$Pt\text{-}OH + H^+ + e^- \xrightarrow{k_2} Pt + H_2O \qquad (2)$$

and that the former (reaction (1)) is a rate-determining step.[15]

The "negative" slope (or "negative" resistance) is caused by the suppression of the dissociative adsorption of H_2O_2 on Pt by formation of upd-H of a nearly full coverage.[11-13] This explanation is in harmony with the fact that the "negative" slope starts at a potential of the most negative end of the current peaks for upd-H. Figure 2c shows a j-U curve in 0.3 M H_2SO_4 containing high-concentration (0.7 M) H_2O_2. Current oscillations, called oscillation A and B,[11] are both observed. Oscillation B is less pronounced in Fig. 2c than in our previous work[11] probably because a *meniscus* electrode (see Fig. 1) is used in the present work instead of a wholly immersed electrode in the previous work.

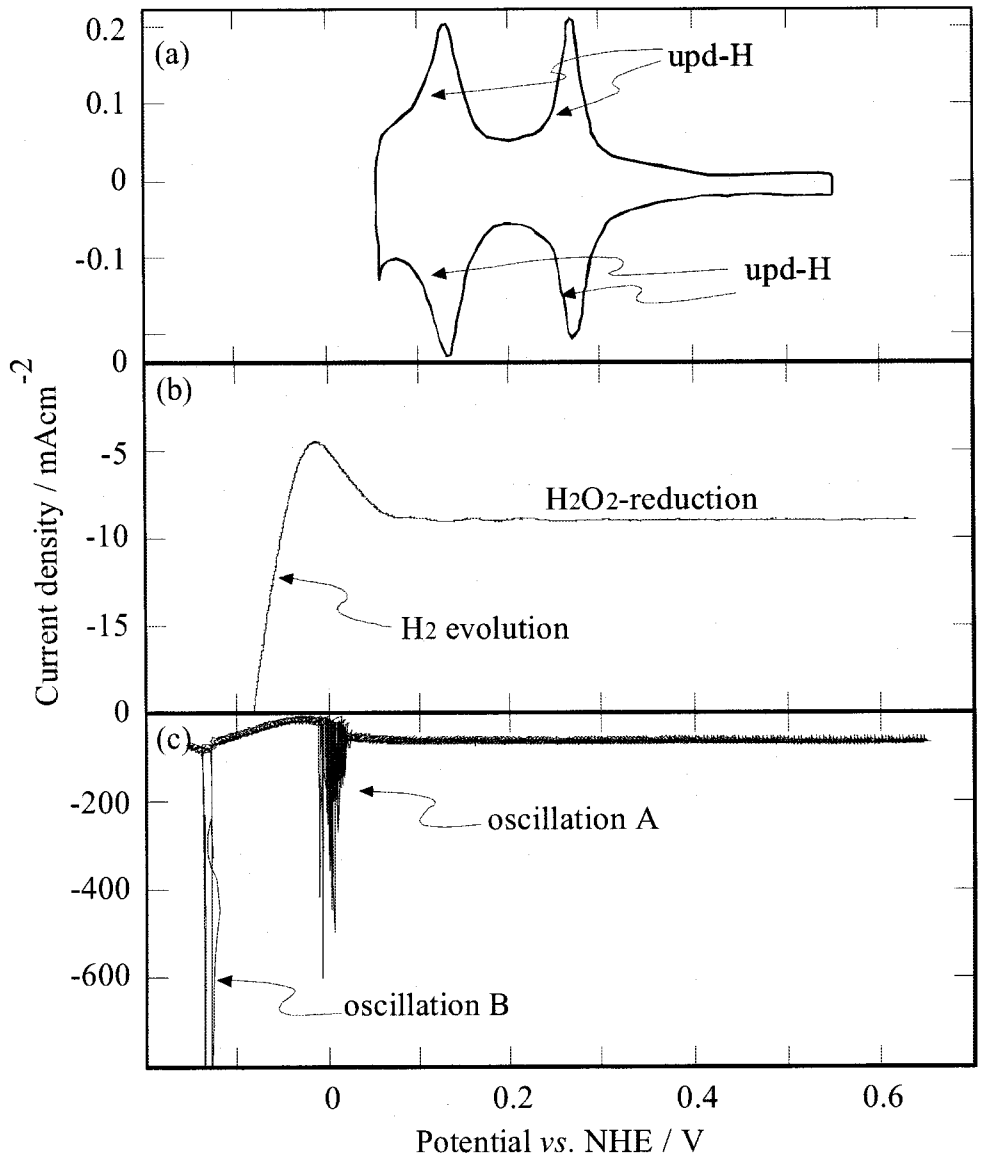

Fig. 2 Current density (j) vs. potential (U) curves for a polycrystalline Pt (poly-Pt) electrode, obtained under potential-controlled conditions. Electrolyte: (a) 0.3 M H_2SO_4 (pH 0.55), (b) 0.2 M H_2O_2 + 0.3 M H_2SO_4, and (c) 0.7 M H_2O_2 + 0.3 M H_2SO_4. Scan rate: (a) 100 mV/s, and (b) and (c) 10 mV/s.

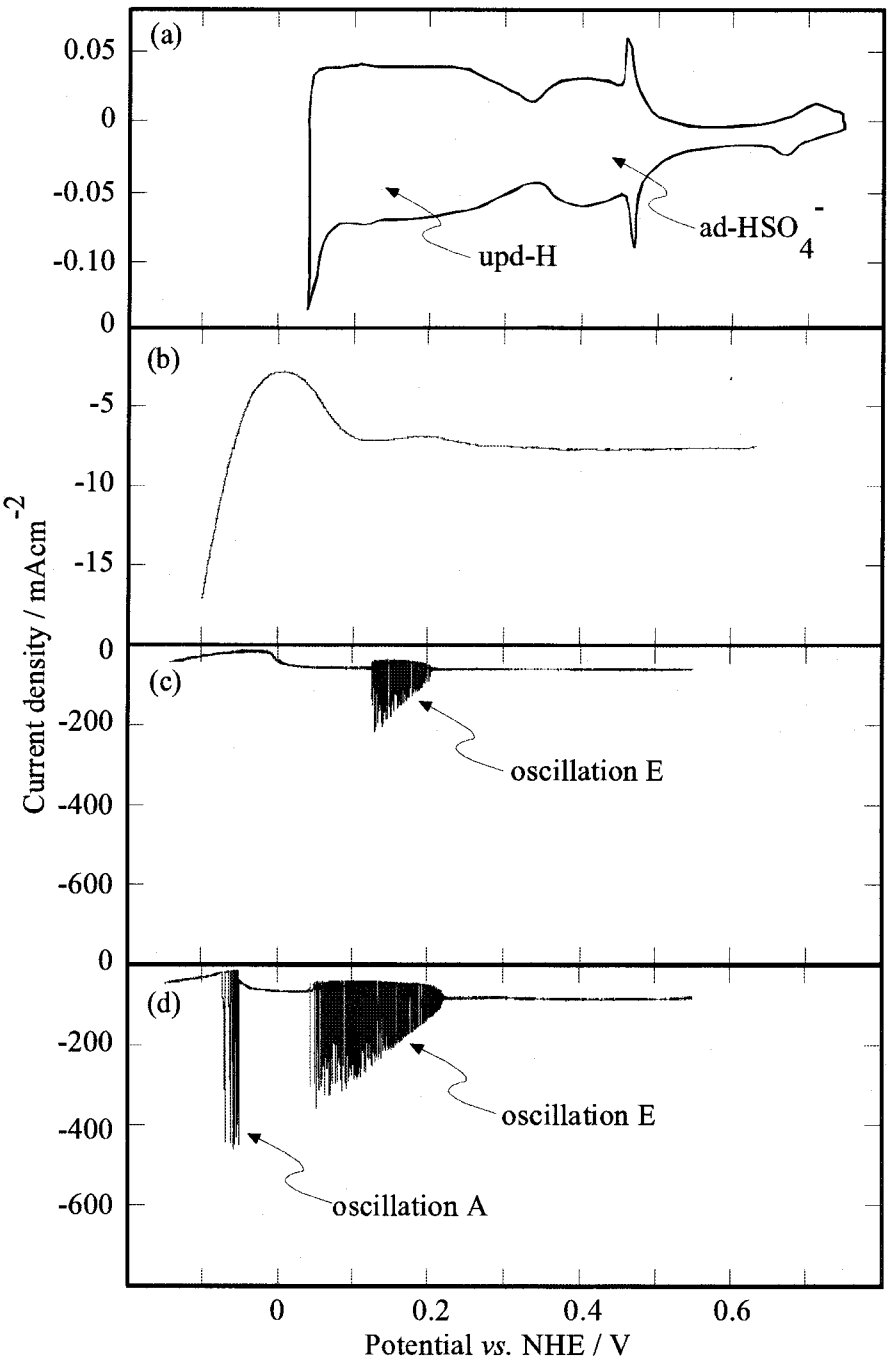

Fig. 3 *j-U* curves for an atomically *flat* Pt(111) electrode, drawn in the same way as Fig. 2. Electrolyte: (a) 0.3 M H_2SO_4, (b) 0.2 M H_2O_2 + 0.3 M H_2SO_4, (c) 0.7 M H_2O_2 + 0.3 M H_2SO_4, and (d) 1.0 M H_2O_2 + 0.3 M H_2SO_4. Scan rate: (a) 100 mV/s, (b) and (c) 10 mV/s, and (d) 5 mV/s.

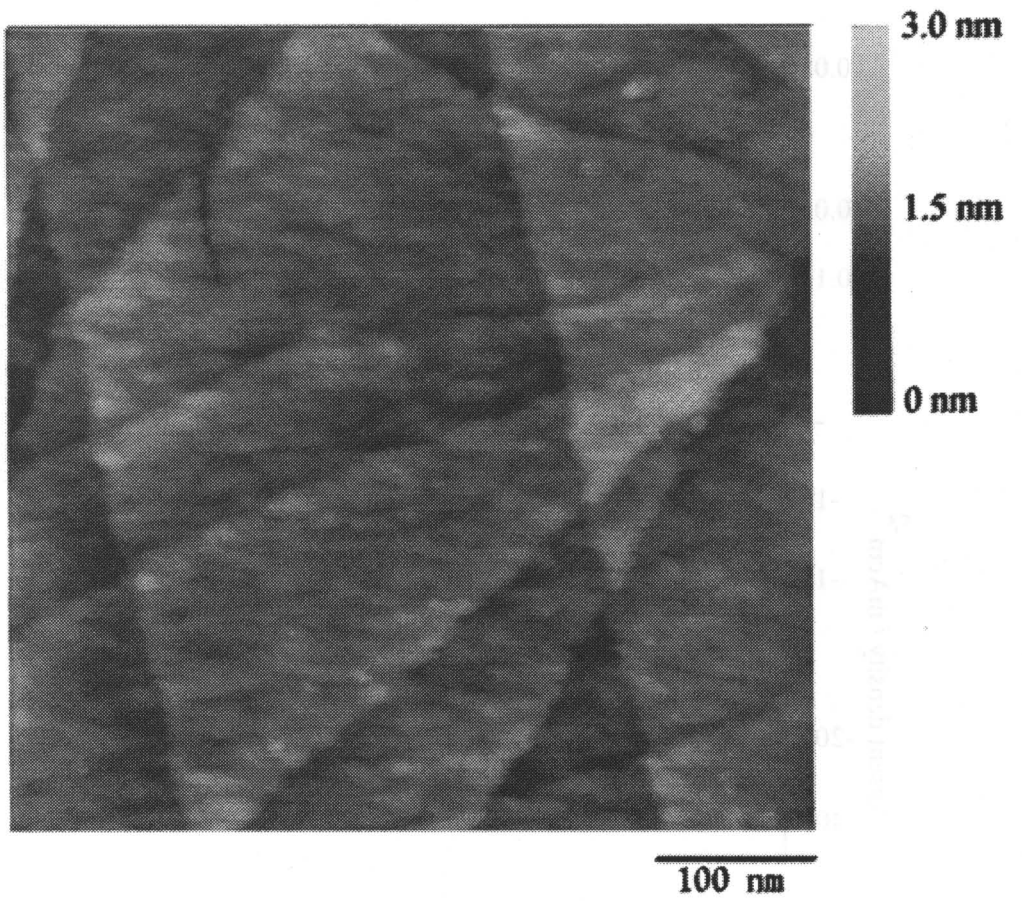

Fig. 4 An STM image of the surface of an atomically *flat* Pt(111) electrode used in the present work.

Figure 3 shows *j-U* curves for an atomically *flat* Pt(111) electrode, drawn in the same way as Fig. 2. It is well known[17] that the Pt(111) electrode shows broad current peaks in a potential region from ca. 0.35 to 0.05 V vs. NHE due to the formation and disappearance of upd-H, as shown in Fig. 3a. Anodic and cathodic current peaks in a potential region from ca. 0.55 to 0.35 V with sharp spikes at about 0.47 V in Fig. 3a are attributed to adsorption and desorption of HSO_4^-.[20,21] The observation of the upd-H and adsorbed-HSO_4^- peaks characteristic of the Pt(111) electrode, in agreement with the literature,[17] clearly shows that a well-defined atomically *flat* Pt(111) surface is obtained in the present work. This conclusion was also confirmed by STM inspection, which gave an image with a clear "step and terrace" structure, as displayed in Fig. 4, similar

STM images are reported in the literature.[22]

Figure 3b shows that a "negative" resistance is observed for the atomically *flat* Pt(111) electrode in 0.3 M H_2SO_4 containing low-concentration (0.2 M) H_2O_2, similarly to the case of Fig. 2b. However, the negative resistance in Fig. 3b shows a two-step structure and its potential range extends to a more positive potential of around 0.35 V. As explained later, the negative resistance in a region from 0.10 to 0 V is attributed to the formation of upd-H, similarly to the case of Fig. 2b, whereas that in a region from 0.35 to 0.10 V is attributed to another reason. In harmony with the appearance of the new negative resistance in 0.35 to 0.10 V, a new current oscillation, named oscillation E, appears in potentials of about 0.22 to 0.13 V in case where the H_2O_2 concentration is made high, 0.7 M (Fig. 3c). The conclusion that oscillation E is distinguished from oscillation A and truly a new oscillation is clearly shown by the fact that oscillation A itself appears in a region of reasonable potentials (-0.05 to –0.07 V) in addition to oscillation E when the H_2O_2 concentration is made much higher (Fig. 3d).

In order to investigate whether the appearance of oscillation E is due to an effect of the atomic-level flatness of the electrode surface, atomically *non-flat* Pt(111) electrodes were prepared and examined. Itaya et al.[22] reported, by in-situ STM experiments, that surface roughening, such as schematically shown in Fig. 5d, is caused by a procedure of oxidation and re-reduction of an atomically *flat* Pt(111) surface. In the present work, the surface roughening was carried out by shifting the electrode potential stepwise to 1.75 V where Pt-oxide was formed and oxygen evolution occurred. The electrode potential was kept at 1.75 V for 3 min, and then shifted back to 0.65 V where the surface Pt-oxide was reduced and removed. This procedure was repeated 3 times. Figures 5a ~ 5c show *j-U* curves for an atomically *non-flat* Pt(111) electrode thus prepared, drawn in the same way as Figs. 2 and 3. It is seen that the curves in Fig. 5 are rather similar to those for poly-Pt (Fig. 2) than those for atomically *flat* Pt(111) (Fig. 3). The negative resistance in Fig. 5b appears only in a narrow potential region (0.10 to 0.00 V) and no oscillation E appears as seen in Fig. 5c, similar to the cases of Figs. 2b and 2c. The *j-U* curves for the atomically *flat* Pt(111) such as shown in Fig. 3 were restored when the atomically *non-flat* Pt(111) electrodes giving the curves of Fig. 5 were annealed in a hydrogen flame, suggesting that the atomic non-flatness of the atomically *non-flat* Pt(111) was restricted only to a narrow surface region (see Fig. 5d).

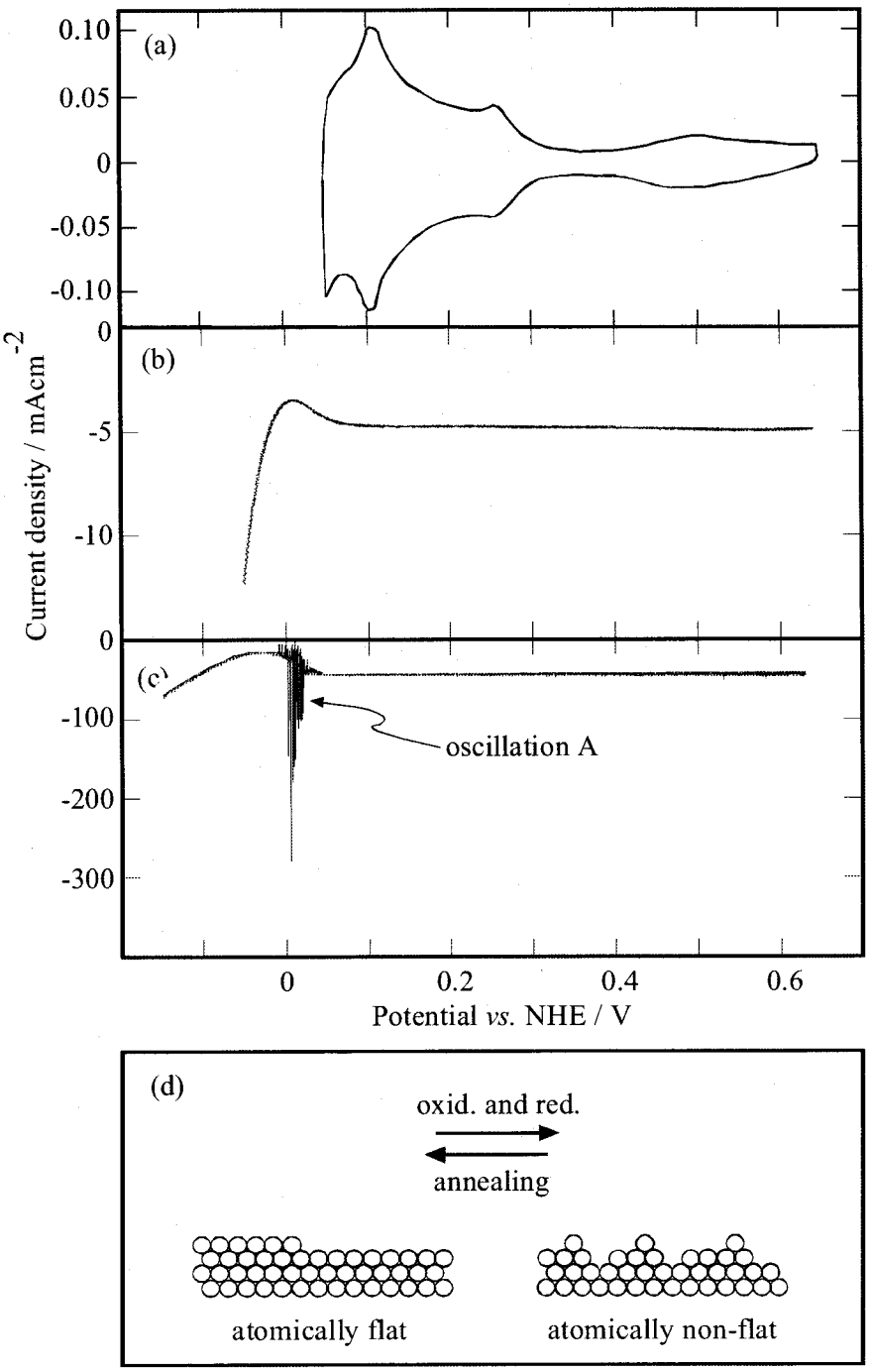

Fig. 5 (a) ~ (c) *j-U* curves for an atomically *non-flat* Pt(111) electrode prepared by a procedure of repeated electrochemical oxidation and re-reduction, drawn in the same way as Figs. 2 and 3. Electrolyte: (a) 0.3 M H_2SO_4, (b) 0.2 M H_2O_2 + 0.3 M H_2SO_4, and (c) 0.7 M H_2O_2 + 0.3 M H_2SO_4. Scan rate: (a) 100 mV/s, and (b) and (c)

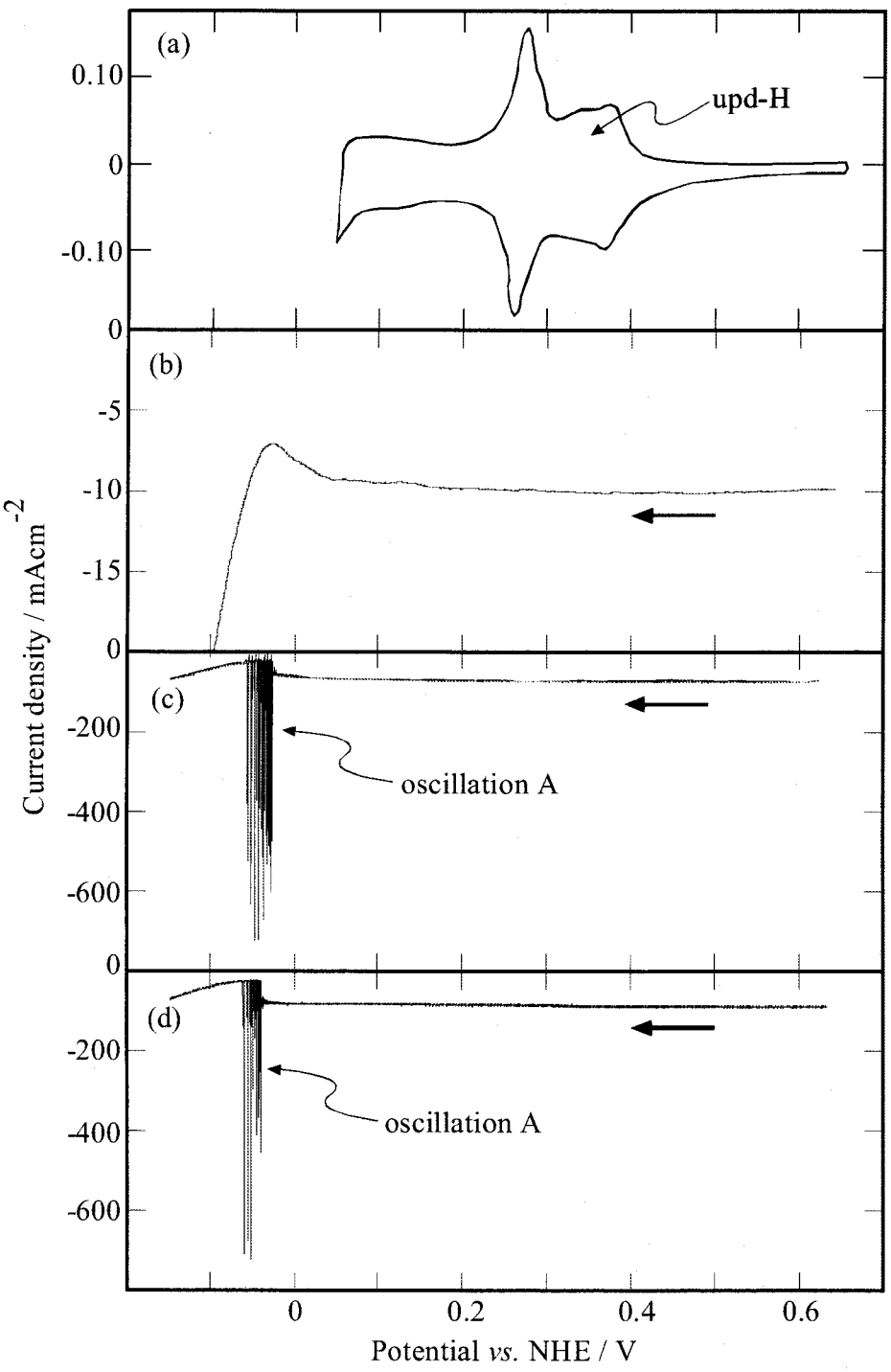

Fig. 6 *j-U* curves for an atomically *flat* Pt(100) electrode, drawn in the same way as Fig. 2. Electrolyte: (a) 0.3 M H_2SO_4, (b) 0.2 M H_2O_2 + 0.3 M H_2SO_4, (c) 0.7 M H_2O_2 + 0.3 M H_2SO_4, and (d) 1.0 M H_2O_2 + 0.3 M H_2SO_4. Scan rate: (a) 100 mV/s, (b) and (c) 10 mV/s, (d) 5 mV/s.

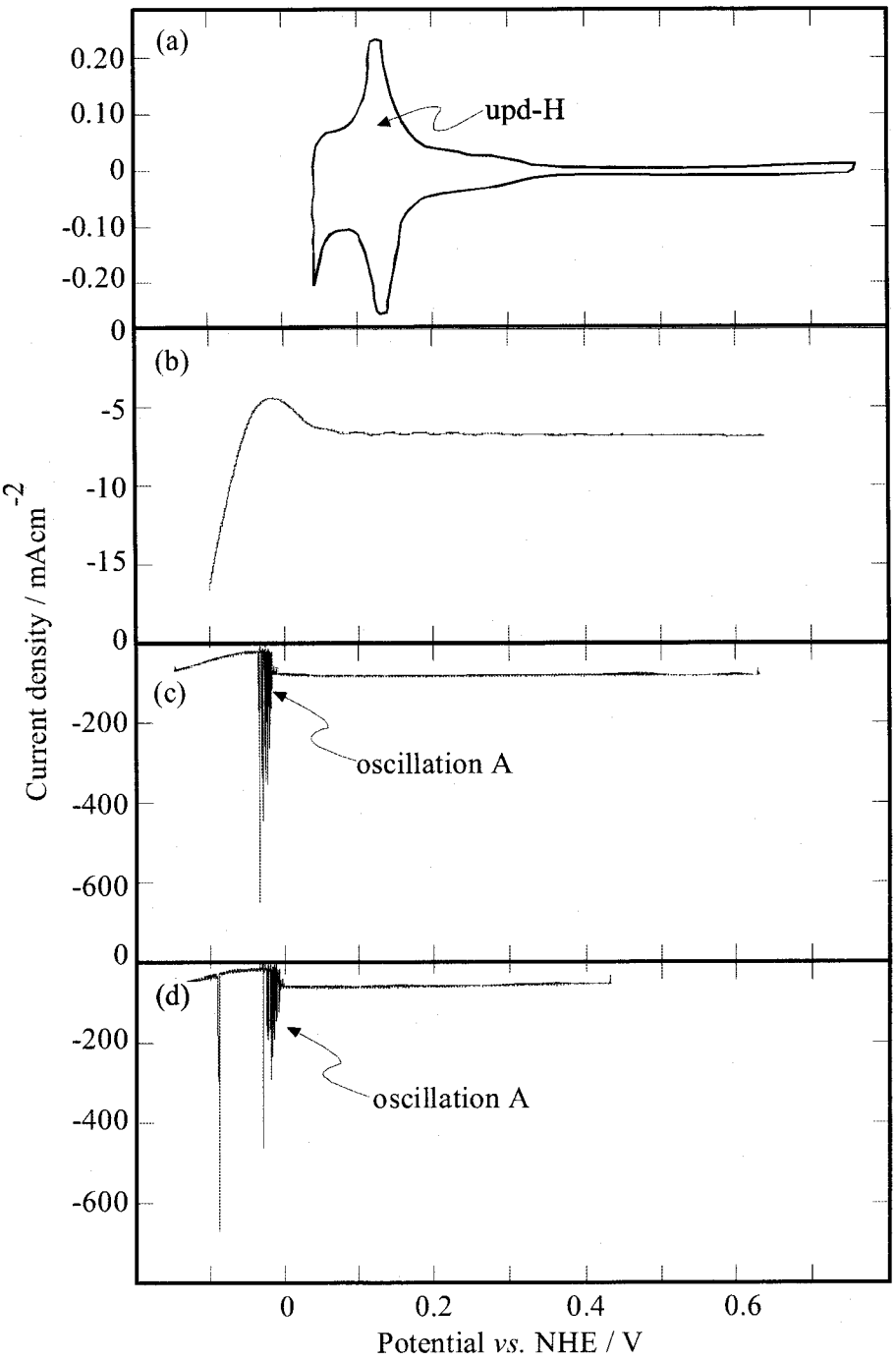

Fig. 7 *j-U* curves for an atomically *flat* Pt(110) electrode, drawn in the same way as Fig. 2. Electrolyte: (a) 0.3 M H_2SO_4, (b) 0.2 M H_2O_2 + 0.3 M H_2SO_4, (c) 0.7 M H_2O_2 + 0.3 M H_2SO_4, and (d) 1.0 M H_2O_2 + 0.3 M H_2SO_4. Scan rate: (a) 100 mV/s, (b) and (c) 10 mV/s, (d) 5 mV/s.

Figures 6 and 7 show *j-U* curves for atomically *flat* Pt(100) and (110) electrodes, respectively, drawn in the same way as Figs. 2 and 3. The observed cathodic and anodic current peaks attributed to upd-H (Figs. 6a and 7a) agreed with those reported for well-defined atomically *flat* Pt(100) and (110),[23] indicating that the electrodes in the present work had well-defined atomic structures. The *j-U* curves for both the Pt(100) and (110) are rather similar to those for poly-Pt (Fig. 2) than those for atomically *flat* Pt(111) (Fig. 3). However, Pt(100) electrodes showed the negative resistance of a two-step structure (Fig. 6b) though much less prominent than for Pt(111) (Fig. 3b). In harmony with this result, some of the Pt(100) electrodes showed oscillation E in addition to oscillation A when the potential sweep was in the *positive* direction.

Figure 8 shows current (*j*) vs. time (*t*) curves for atomically *flat* Pt(111) and poly-Pt electrodes. Figure 8a shows the waveshape of oscillation E at 0.13 V vs. NHE. Figures 8b and 8c are the waveshapes of oscillation A for atomically *flat* Pt(111) and poly-Pt, respectively. It is clear that the wave shapes for oscillations E and A are quite different from each other. In addition, the oscillation period for oscillation E (2 ~ 10 ms) is much shorter than that for oscillation A (0.2 ~ 1 s).

Figure 9 shows *j-U* curves in 0.3 M $HClO_4$-based solutions (instead of the 0.3 M H_2SO_4-based ones thus-far described) for atomically *flat* Pt(111) to see an effect of the kind of anions in the electrolyte. The cathodic and anodic current peaks for upd-H in 0.3 M $HClO_4$ (Fig. 9a) are located in nearly the same potentials as in 0.3 M H_2SO_4 (Fig. 3a), in agreement with the literature.[20,21] A current peak attributed to the adsorption of ClO_4^- is not observed[20,21], contrary to the case of HSO_4^-. Cathodic and anodic current peaks in 0.60 to 0.85 V (Fig. 9a) are attributed to the adsorption and desorption of OH^-.[21] Though the adsorption and desorption behavior of HSO_4^- and ClO_4^- is quite different from each other, as mentioned above, the observed negative slope and oscillation E is nearly the same between the HSO_4^-- and ClO_4^--based solutions (Figs. 3 and 9). This indicates that the appearance of oscillation E is not due to the effect of anion adsorption.

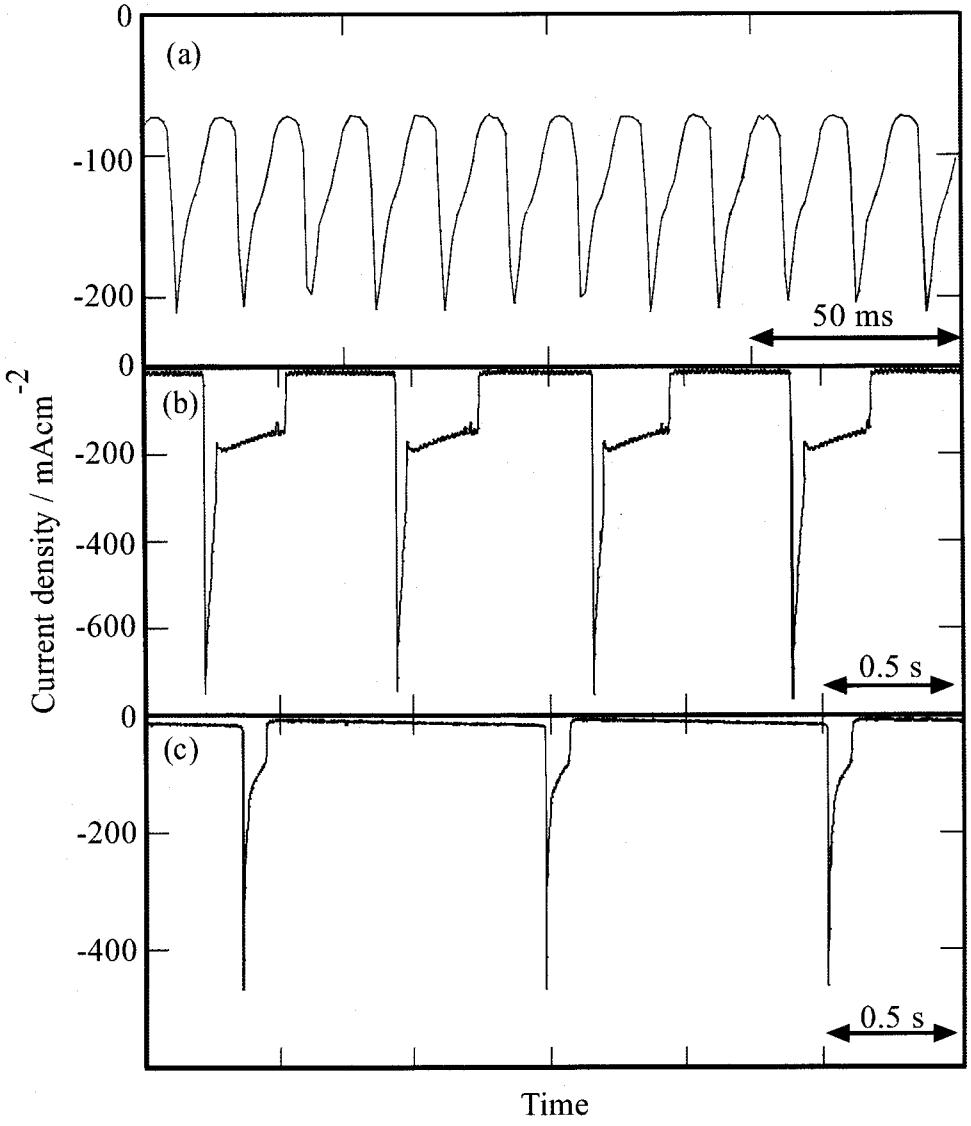

Fig. 8 Current density (j) vs. time (t) curves, (a) and (b) for atomically *flat* Pt(111), and (c) for poly-Pt. Electrolyte: (a) and (b) 1.0 M H_2O_2 + 0.3 M H_2SO_4, and (c) 0.7 M H_2O_2 + 0.3 M H_2SO_4. Electrode potential: (a) 130 mV (oscillation E), (b) –30 mV (oscillation A), and (c) –20 mV (oscillation A).

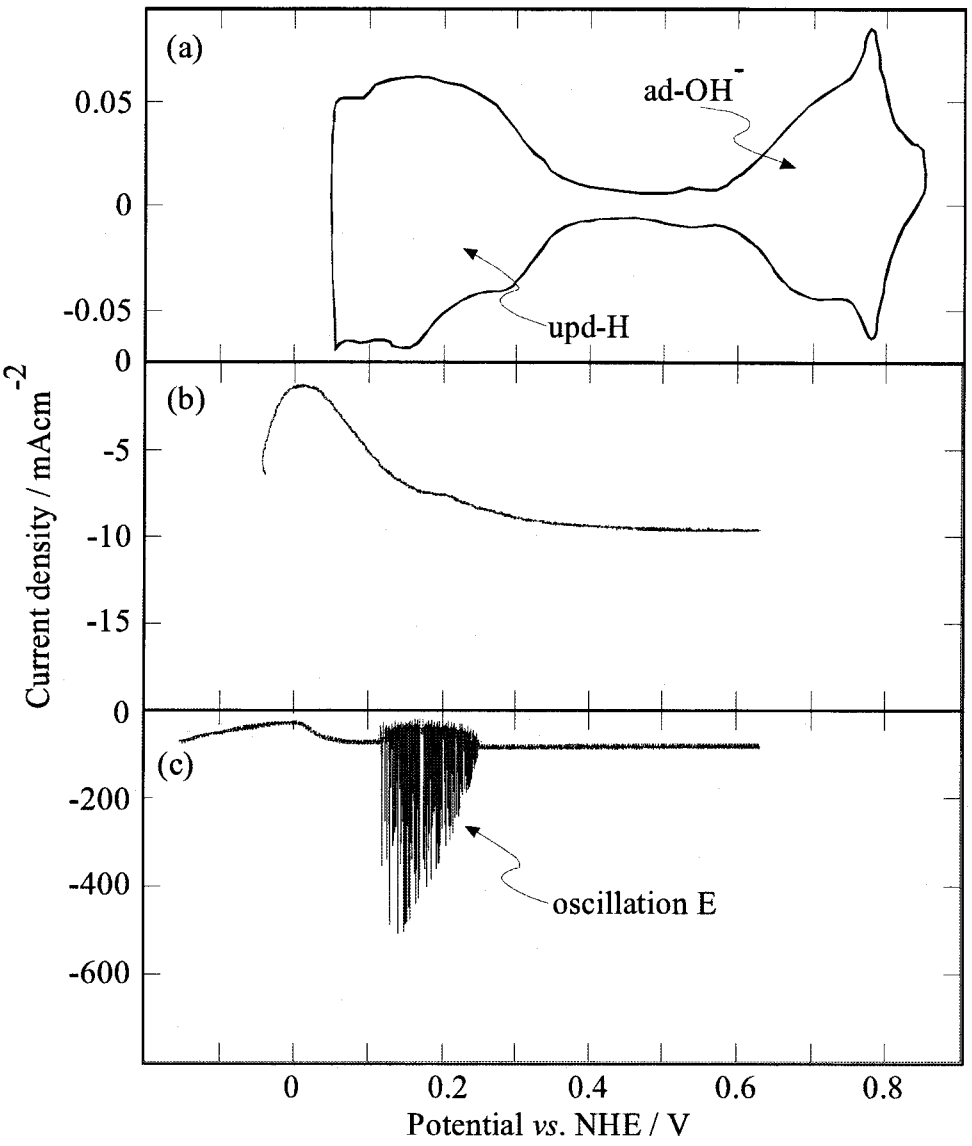

Fig. 9 *j-U* curves for an atomically *flat* Pt(111) electrode, drawn in the same way as Fig. 2. Electrolyte: (a) 0.3 M $HClO_4$, (b) 0.2 M H_2O_2 + 0.3 M $HClO_4$, and (c) 0.7 M H_2O_2 + 0.3 M $HClO_4$. Scan rate: (a) 100 mV/s, and (b) and (c) 10 mV/s.

Figure 10 shows, comparatively, the H_2O_2-reduction currents and the negative resistances for various Pt electrodes in 0.3 M H_2SO_4 containing low-concentration (0.2 M) H_2O_2. The H_2O_2-reduction current in 0.65 to 0.35 V for atomically *flat* Pt(111) is higher in the absolute value than that for atomically *non-flat* Pt(111) even in the same H_2O_2 concentration (Fig. 10a). Also, the H_2O_2-reduction current in this potential region decreases in the order of atomically *flat* Pt(111), Pt(110), Pt(100), and *non-flat* poly-Pt (Fig. 10b). The differences in the H_2O_2-reduction current become more prominent with the increasing scanning rate. It is also to be noted that the aforementioned "new" negative resistance in 0.35 to 0.10 V is observed prominently only for atomically *flat* Pt(111), which shows the highest H_2O_2-reduction current in 0.65 to 0.35 V. This result indicates that the increase in the H_2O_2-reduction current in 0.65 to 0.35 V for atomically *flat* Pt(111) has a close relation with the appearances of the "new" negative resistance and oscillation E.

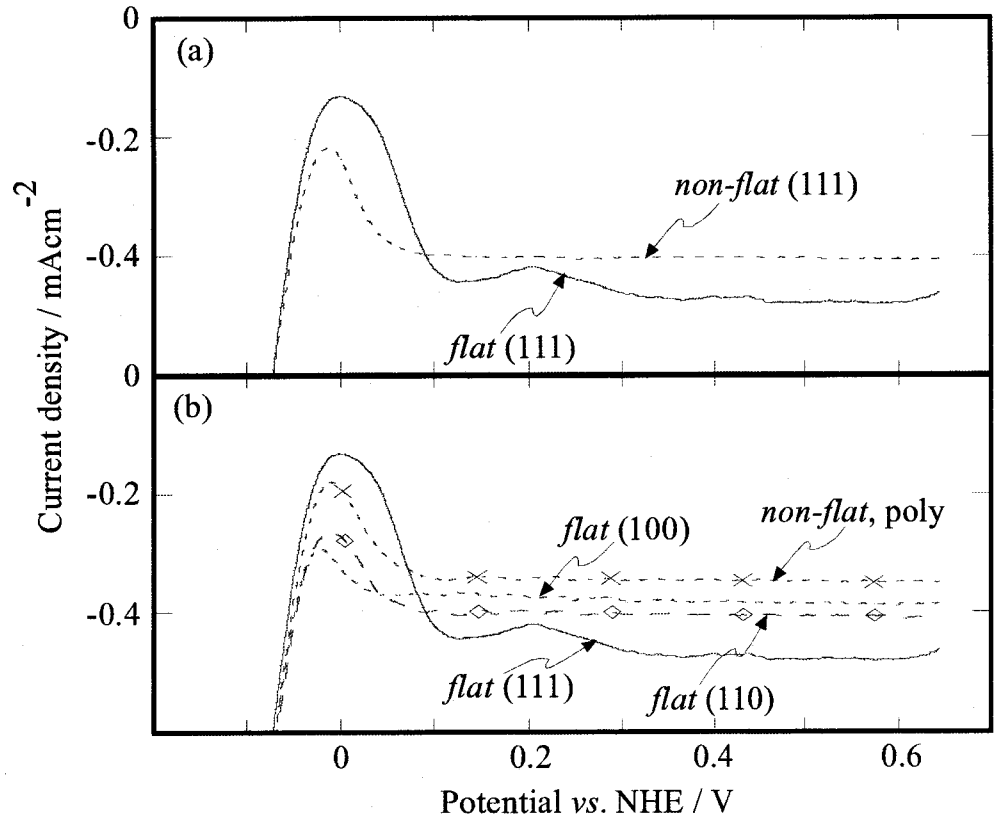

Fig. 10 (a) *j-U* curves for atomically *flat* and *non-flat* Pt(111) electrodes, (b) those for atomically *flat* Pt(111), Pt(100), Pt(110), and *non-flat* poly-Pt electrodes. Electrolyte: 0.2 M H_2O_2 + 0.3 M H_2SO_4. Scan rate: 10 mV/s.

Figure 11 shows a phase diagram for the appearance of oscillations A and E in case of atomically *flat* Pt(111) with respect to the H_2O_2 and H_2SO_4 concentrations. It seems that not only the H_2O_2 and H_2SO_4 concentrations but also their ratio are important for the appearance of these oscillations.

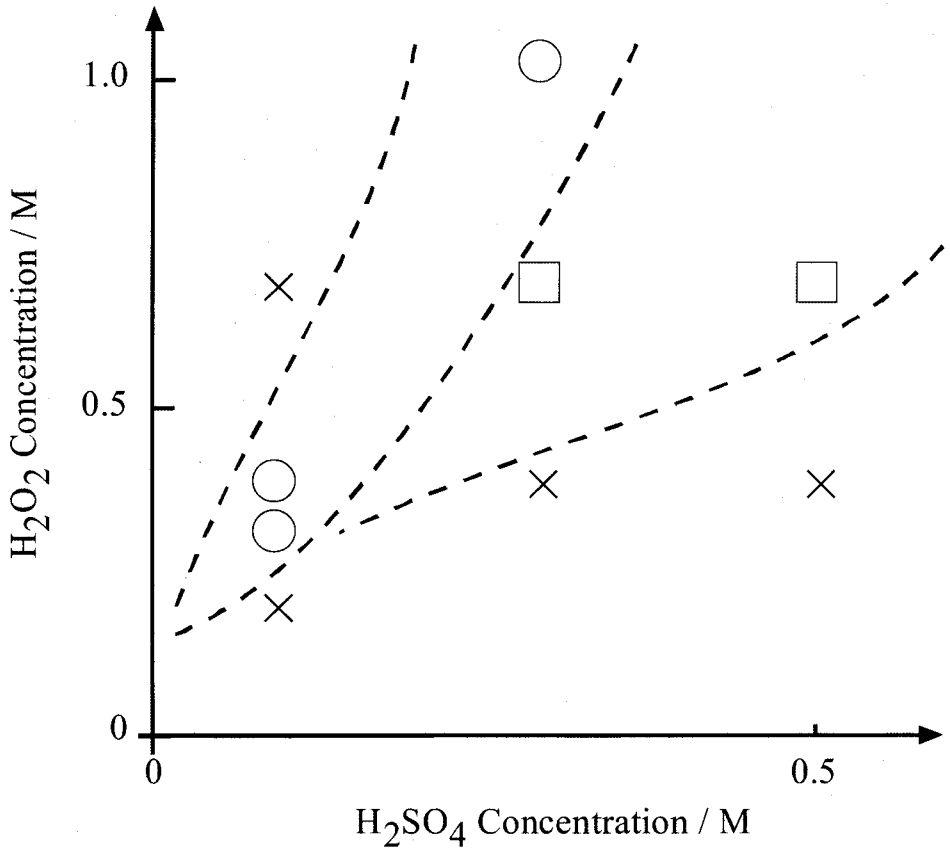

Fig. 11 A phase diagram with respect to the H_2O_2 and H_2SO_4 concentrations. □: Only oscillation E appears, ○: Both oscillations A and E appear, ×: No oscillation appears. Electrode: atomically *flat* Pt(111).

Mathematical simulation

The author reported in previous papers[12,14,15] that oscillations C and D appearing in 0.40 to 0.00 V in the presence of a small amount of halide ions, such as Cl^-, Br^-, and I^-, could be explained by taking account of a catalytic effect of adsorbed halogen (Pt-X) and an autocatalytic effect of adsorbed OH (Pt-OH) for the dissociative adsorption of H_2O_2. Namely, the appearance of oscillations C and D could be explained by expressing the rate constant (k_1) for reaction (1) in the preceding section as follows:

$$k_1 = k_{10} + \gamma' \theta_X \theta_{OH} \quad (3)$$

where k_{10} was a normal rate constant for reaction (1), γ' a proportional constant, and θ_X and θ_{OH} the surface coverages of Pt-X and Pt-OH, respectively. The appearance of oscillation E in 0.2 to 0.1 V for atomically *flat* Pt(111) in the present work may be explained by taking account of a similar autocatalytic effect of Pt-OH on the Pt(111) surface, i.e., by expressing k_1 as follows:

$$k_1 = k_{10} + \gamma \theta_{OH} \quad (4)$$

Thus the author has made mathematical simulation on the basis of this idea.

The following reactions were considered in addition to reactions (1) and (2), in the same way as in our previous paper[15]:

$$\mathrm{Pt + H^+ + e^- \underset{k_{-5}}{\overset{k_5}{\leftrightarrow}} Pt\text{-}H\ (upd\text{-}H)} \quad (5)$$

$$\mathrm{2Pt\text{-}OH \xrightarrow{k_6} 2Pt + O_2 + 2H^+ + 2e^-} \quad (6)$$

$$\mathrm{Pt + H^+ + e^- \underset{k_{-7}}{\overset{k_7}{\leftrightarrow}} Pt\text{-}H\ (on\text{-}top\text{-}H)} \quad (7)$$

$$\mathrm{Pt\text{-}H\ (on\text{-}top\text{-}H) + Pt\text{-}H\ (on\text{-}top\text{-}H) \xrightarrow{k_8} H_2} \quad (8)$$

where Pt represents schematically surface site(s) at the Pt electrode.

The differential equations were also expressed in the same way as in our previous work.[13] From the conservation of the current, we obtain[24,25]

$$I = jA = (U - E)/R_\Omega = I_C + I_F = AC_{DL}(dE/dt) + I_F \quad (9)$$

where I is the total current, A the electrode area, j the current density, U the (external or applied) electrode potential, E the true electrode potential, $(U\text{-}E)$ the ohmic drop between the electrode surface and the position of the reference electrode (RE), R_Ω the solution resistance in the same place as above, $I_C = AC_{DL}(dE/dt)$ is the charging current,

C_{DL} the double-layer capacitance, and I_F the Faradaic current. Equation (9) can be rewritten as

$$dE/dt = (U - E)/AC_{DL}R_{\Omega} - I_F/AC_{DL} \quad (10)$$

I_F is expressed, from reactions (2) and (5) - (7), as follows:

$$I_F = AF\{- k_5 C_{H+}{}^S(1 - \theta_H - \theta_{OH}) + k_{-5}\theta_H - k_2 C_{H+}{}^s\theta_{OH} + k_6\theta_{OH}{}^2 - k_7 C_{H+}{}^s(1 - \Theta_H) + k_{-7}\Theta_H\} \quad (11)$$

where $C_{H+}{}^s$ is the concentration of H^+ ions at the electrode surface, and θ_{OH}, θ_H, and Θ_H are the surface coverages of Pt-OH, upd-H, and on-top-H, respectively. The quantities, k_2, k_5, k_{-5}, k_6, k_7, and k_{-7} are the rate constants for the i-th reactions (i = 2, 5, -5, 6, 7, and –7), which can be expressed by the Butler-Volmer equations,

$$k_i = k_{i0}\exp[-\alpha_i n_i F(E-E_{i0})/RT] \quad \text{for i = 2, 5 and 7} \quad (12)$$

$$k_i = k_{i0}\exp[(1-\alpha_i)n_i F(E-E_{i0})/RT] \quad \text{for i = -5, 6 and –7} \quad (13)$$

where k_{i0} is the rate constant at $E = E_{i0}$, E_{i0} the equilibrium redox potential for the i-th reaction, α_i the transfer coefficient, n_i the number of transferred electrons, F the Faraday constant, R the gas constant, and T the temperature. Because reaction 5 and –5 (and 7 and –7) are reverse reactions to each other, we obtain $E_{50} = E_{-50}$ and $E_{70} = E_{-70}$.

The time dependences of $C_{H+}{}^s$, $C_{HO}{}^s$ (the surface concentration of H_2O_2), θ_{OH}, θ_H, and Θ_H are expressed as follows:

$$(\delta_{HO}/2)\, dC_{HO}{}^s/dt = (D_{HO}/\delta_{HO})(C_{HO}{}^b - C_{HO}{}^s) - k_1 C_{HO}{}^s(1 - \theta_H - \theta_{OH})^2 \quad (14)$$

$$(\delta_{H+}/2)\, dC_{H+}{}^s/dt = (D_{H+}/\delta_{H+})(C_{H+}{}^b - C_{H+}{}^s) + \{- k_2 C_{H+}{}^s\theta_{OH} - k_5 C_{H+}{}^s(1 - \theta_H - \theta_{OH}) + k_{-5}\theta_H + k_6\theta_{OH}{}^2 - k_7 C_{H+}{}^s(1- \Theta_H) + k_{-7}\Theta_H\} \quad (15)$$

$$N_0 d\theta_{OH}/dt = k_1 C_{HO}{}^s(1 - \theta_H - \theta_{OH})^2 - k_5 C_{H+}{}^s\theta_{OH} - k_6\theta_{OH}{}^2 \quad (16)$$

$$N_0 d\theta_H/dt = k_5 C_{H+}{}^s(1 - \theta_H - \theta_{OH}) - k_{-5}\theta_H \quad (17)$$

$$N_0 d\Theta_H/dt = k_7 C_{H+}{}^s(1 - \Theta_H) - k_{-7}\Theta_H - 2k_8\Theta_H{}^2 \quad (18)$$

where D_{HO} and D_{H+} are the diffusion coefficients for H_2O_2 and H^+, respectively, δ_{HO} and δ_{H+} the thicknesses of the diffusion layers for H_2O_2 and H^+, respectively, and $C_{HO}{}^b$ and $C_{H+}{}^b$ the concentrations of H_2O_2 and H^+ in the solution bulk, respectively. A small contribution of the drift motion of H^+ was neglected. N_0 schematically represents the total amount of surface Pt sites per unit area.

Figure 12 shows *j-U* curves obtained by mathematical calculations. With no or a small autocatalytic effect ($\gamma \lesssim 7$), only a one-step negative resistance was reproduced for low-concentration (0.2 M) H_2O_2 (Fig. 12a) and only oscillation A was reproduced for high-concentration (0.7 M) H_2O_2 (Fig. 12b). On the other hand, with a large autocatalytic effect ($\gamma \gtrsim 8$), the appearance of oscillation E was reproduced together with the increase in the H_2O_2-reduction current in 0.60 to 0.40 V and the appearance of

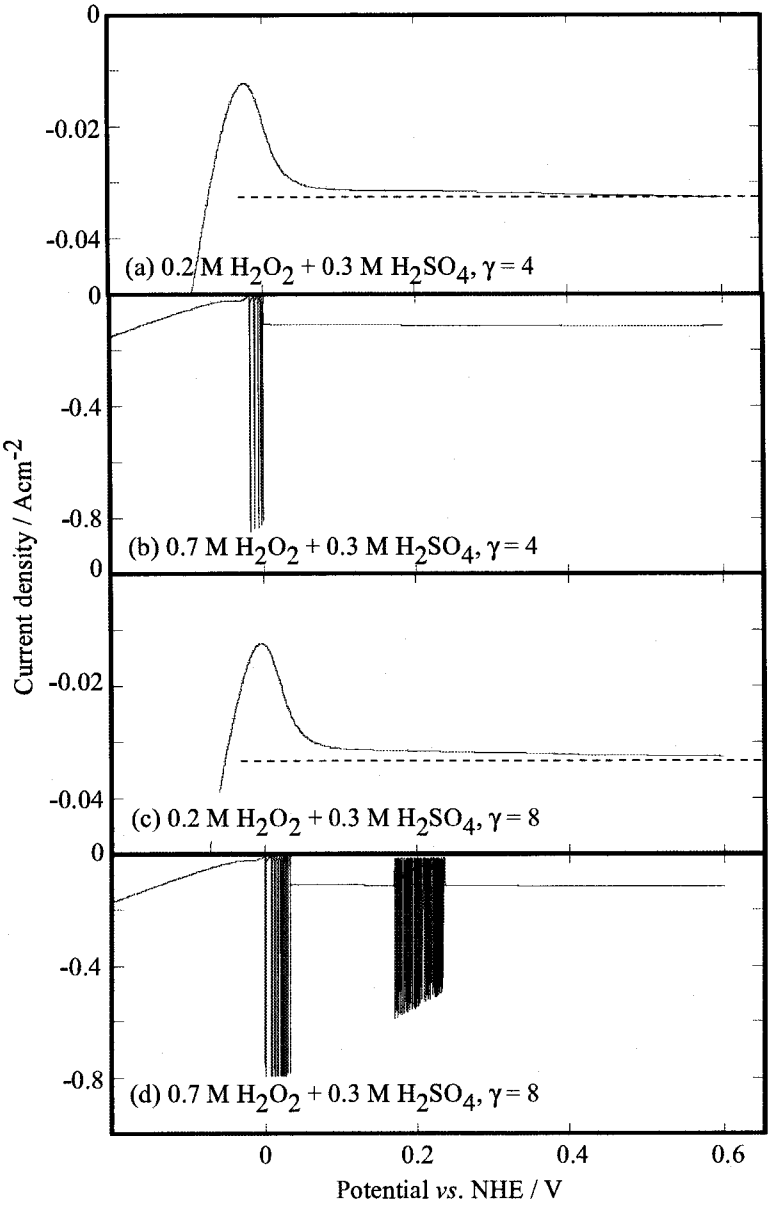

Fig. 12 Calculated *j-U* curves with U scanned at a rate of 0.01 V/s. Parameter values used are as follows: $C_{HO}^{b} = 0.2 \times 10^{-3}$ mol cm^{-3} for (a) and (c), and 0.7×10^{-3} mol cm^{-3} for (b) and (d), $\delta_{HO} = 0.01$ cm, $D_{HO} = 1.7 \times 10^{-5}$ cm^2 s^{-1}, $C_{H+}^{b} = 0.3 \times 10^{-3}$ mol cm^{-3}, $\delta_{H+} = 0.004$ cm, $D_{H+} = 9.3 \times 10^{-5}$ cm^2 s^{-1}, $A = 0.01$ cm^2, $C_{DL} = 2.0 \times 10^{-5}$ F cm^{-2}, $N_0 = 2.2 \times 10^{-9}$ mol cm^{-2}, $R_\Omega = 60\ \Omega$, $T = 300$ K, $\alpha_i = 0.25$ (i = 2) and 0.50 (i ≠ 2), $n = 1$, $k_{10} = 4 \times 10^{-2}$ cm s^{-1}, $k_{20} = 1 \times 10^{-5}$ cm s^{-1}, $k_{50} = 1 \times 10^{-2}$ cm s^{-1}, $k_{-50} = 1 \times 10^{-5}$ mol cm^{-2} s^{-1}, $k_{60} = 1 \times 10^{-8}$ mol cm^{-2} s^{-1}, $k_{70} = 5 \times 10^{-3}$ cm s^{-1}, $k_{-70} = 5 \times 10^{-6}$ mol cm^{-2} s^{-1}, $k_8 = 5 \times 10^{-6}$ mol cm^{-2} s^{-1}, $E_{20} = 1.37$ V vs. NHE, $E_{50} = E_{-50} = 0.08$ V, $E_{60} = 0.67$ V, and $E_{70} = E_{-70} = -0.03$ V, γ = 4 for (a) and (b) and 8 for (c) and (d).

the "new" negative resistance in 0.35 to 0.10 V (Fig. 12c and d). Figure 13 shows a time course of oscillation E, calculated with $\gamma = 8$. Compared with the observed oscillation (Fig. 8(a)), the oscillation period is well reproduced, but there is a difference in wave shape, which may be due to the adoption of the Nernst's diffusion-layer model with a constant thickness in equations (14) and (15).

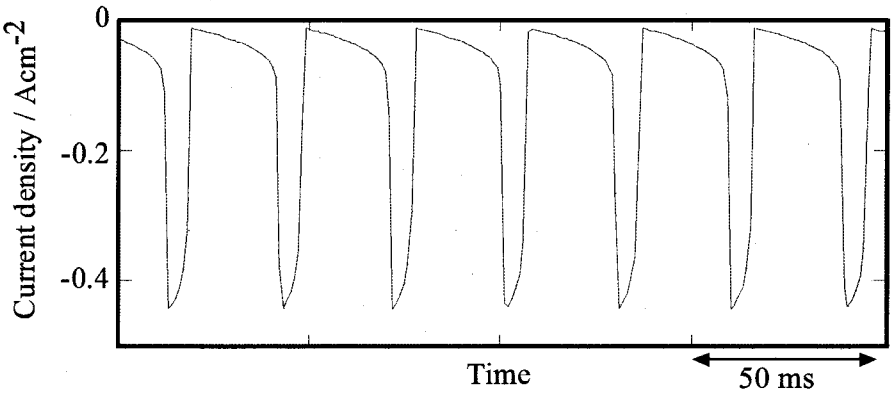

Fig. 13 Time course of oscillation E, calculated with $\gamma = 8$ and $U = 0.24$ V. The other parameters are the same as Fig. 12.

Discussion

The experimental results have shown that the atomically *flat* Pt(111) electrodes show the electrochemical behavior for the H_2O_2 reduction, quite different from that of other Pt electrodes, such as atomically *flat* Pt(100) and (110), atomically *non-flat* Pt(111), and poly-Pt. The behavior of the latter electrodes, i.e., the appearance of the one-step negative resistance in a narrow potential region from 0.10 to –0.02 V and the appearance of only oscillation A in this potential region, can be explained by taking account of the suppression of the H_2O_2 reduction by the formation of upd-H as reported previously.[11-13] On the other hand, the behavior of the atomically *flat* Pt(111) electrode cannot be explained by this model and a new model has to be taken into account.

As already mentioned in the preceding section, the appearance of oscillation E, together with the appearance of the new negative resistance in a potential region from 0.35 to 0.10 V and the increase in the H_2O_2-reduction current in 0.65 to 0.35 V, can be explained by taking account of the autocatalytic effect of adsorbed OH (Pt-OH) for the dissociative adsorption of H_2O_2. This effect is not considered for our previous model for polycrystalline Pt.[13] Mathematical simulation based on this model has reproduced well the essential behavior of the atomically *flat* Pt(111). According to this model, the increase in the H_2O_2-reduction current in 0.65 to 0.35 V for Pt(111) is attributed to the autocatalytic effect of surface Pt-OH for the dissociative adsorption of H_2O_2 and the appearance of the new negative resistance in 0.35 to 0.20 V is attributed to a decrease of the Pt-OH concentration with a negative shift of the electrode potential. Oscillation E appears on the basis of this new negative resistance.

The difference in the electrochemical behavior between the atomically *flat* Pt(111) and other Pt electrodes can thus be attributed to be a difference in the efficiency of the autocatalytic mechanism (i.e., the γ value in equation (4)) between these electrodes. In other words, the γ value is expected to decrease in the following order, Pt(111) $>$ (100) $\approx$ (110) $\geq$ poly-Pt, as estimated from the magnitude of the H_2O_2-reduction current in 0.65 to 0.35 V (Fig. 10). How can this order be explained? The author tentatively assumes that, as shown in Fig. 14A, adsorbed OH (Pt-OH) is present at hollow sites of surface Pt atoms and that H_2O_2 is adsorbed with negatively polarized oxygen atoms of H_2O_2 directed to surface Pt atoms. Under this assumption, it is expected that the adsorption of H_2O_2 is accelerated on surface Pt atoms in the neighborhood of adsorbed OH (Pt-OH) because they are more or less positively polarized by an electronegativity difference between Pt atom and OH-group (Fig. 14A). This can be responsible for the autocatalytic effect. The differences in the γ value among

various Pt electrodes can be attributed, in the first approximation, to the differences in the number of "pairs of Pt atoms" for the accelerated adsorption of H_2O_2. Figure 14B illustrates possible examples of such "pairs of Pt atoms" by arrows with two heads. The number of the "pairs of Pt atoms" is 15, 12, and 6 for atomically *flat* Pt(111), (100), and (110) surfaces, respectively. Accordingly, the author can expect that the autocatalytic effect of Pt-OH is the most efficient for Pt(111) and decreases in the order of Pt(111), (100), and (110), in agreement with the experiment. The corresponding number for atomically *non-flat* Pt surfaces is estimated to be in a range of 6 to 12, because the current peaks for upd-H for atomically *non-flat* Pt is given by a simple sum of those for Pt(100) and (110).

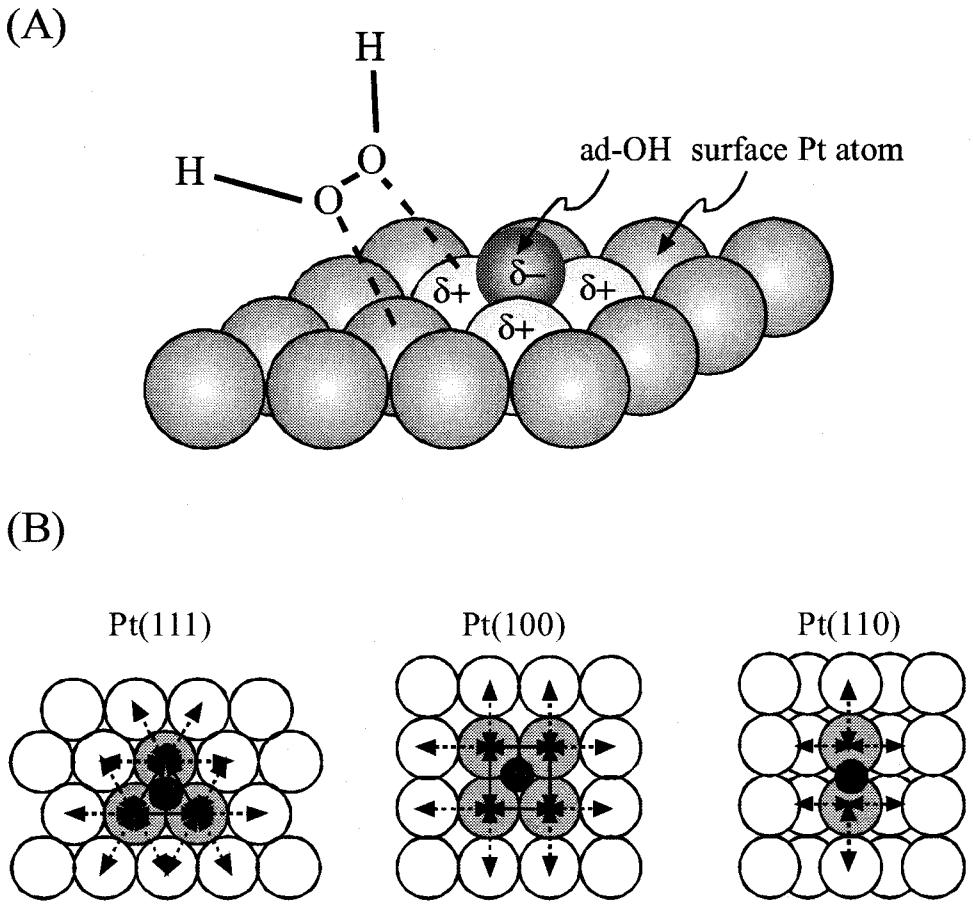

Fig. 14 Schematic illustration of an autocatalytic mechanism in which the dissociative adsorption of H_2O_2 is accelerated on surface Pt atoms in the

Finally it should be mentioned that Ross et al.[26] reported that the H_2O_2-reduction currents on low-index single crystal Pt electrodes showed the negative resistance in a potential region from 0.1 to –0.3 V vs. SCE, which was more prominent in the order of Pt(110), (100), and (111), in agreement with the new negative resistance in the present work. Ross et al. explained their negative resistance to be due to the suppression of the H_2O_2 reduction by the formation of upd-H, contrary to an explanation in the present work. However, the atomically *flat* Pt(111) electrodes show the negative resistance of a two-step structure (Fig. 3b), and, in harmony with this result, the Pt(111) (and sometimes Pt(100)) electrodes show two-type oscillations (i.e., oscillations A and E). This strongly suggests that the negative resistance for Pt(111) is composed of two components.

In conclusion, the present work has revealed that the current oscillations in the "H_2O_2-acid-Pt electrode" system strongly depend on the atomic-level structure of the Pt electrode surface. The detailed analyses of the behavior, combined with mathematical simulation, have suggested the presence of an autocatalytic mechanism of adsorbed OH (Pt-OH) for the dissociative adsorption of H_2O_2, which depends in efficiency on the atomic-level structure of the Pt surface. Further studies will serve for deeper understanding of oscillation mechanisms and mechanisms of electrochemical reactions themselves.

This work was partly supported by a Grant-in-Aid for Scientific Research on Priority Area of "Electrochemistry of Ordered Interfaces" (No. 09237105) from the Ministry of Education, Science, Sports and Culture, Japan. The authors thank Prof. K. Itaya and his coworkers in Tohoku University for their kind instruction of detailed techniques of STM measurements.

References

1. J. L. Hudson and T. T. Tsotsis, *Chem. Eng. Sci.*, **49**, 1493 (1994).
2. T. Z. Fahiday and Z. H. Gu, "Modern Aspects of Electrochemistry Vol. 27", ed by R. E. White, J. O'M. Bockris, and R. E. Conway, Plenum, New York (1995), p.383.
3. M. T. M. Koper, "Advances in Chemical Physics Vol. 92", ed by I. Prigogine and S. A. Rice, John Willey & Sons, New York (1996), p.161.
4. K. Krischer, M. Luebke, W. Wolf, M. Eiswirth, G. Ertl, *Electrochim. Acta,* **40**, 69 (1995).
5. F. Raspel, M. Eiswirth, *J. Phys. Chem.*, **98**, 7613 (1994).
6. M. Eiswirth, M. Luebke, K. Krischer, W. Wolf, J. L. Hudson, G. Ertl, *Chem. Phys. Lett.*, **192**, 254 (1992).
7. F. Raspel, R. J. Nichols, D. M. Kolb, *J. Electroanal. Chem.*, **286**, 279 (1990).
8. P. Strasser, M. Luebke, F. Raspel, M. Eiswirth, G. Ertl, *J. Chem. Phys.*, **107**, 979 (1997).
9. N. Markovic, P. N. Ross, *J. Phys. Chem.*, **97**, 9771 (1993).
   A. Tripkovic, K. Popvic, R. R. Adzic, *J. Chim. Phys.*, 88, 1635 (1991).
10. H. Hommura, Y. Mukouyama, T. Matsuda, S. Yae, Y. Nakato, *Chem. Lett.*, 391 (1996).; T. Matsuda, H. Hommura, Y. Mukouyama, S. Yae, Y. Nakato, *J. Electrochem. Soc.*, **144**, 1988 (1997).
11. Y. Mukouyama, S. Nakanishi, Y. Nakato, *Bull. Chem. Soc. Jpn.*, **72**, 2573 (1999).
12. Y. Mukouyama, H. Hommura, S. Nakanishi, T. Nishimura, H. Konishi, Y. Nakato, *Bull. Chem. Soc. Jpn.*, **72**, 1247 (1999).
13. Y. Mukouyama, H. Konishi, S. Nakanishi, Y. Nakato, *Chem. Lett.*, 1009 (1998).
14. Y. Mukouyama, S. Nakanishi, H. Konishi, and Y. Nakato, *J. Electroanal. Chem.*, **473**, 156 (1999).
15. S. Nakanishi, H. Hommura, Y. Mukouyama, T. Matsuda, Y. Nakato, *Chem. Lett.*, 977 (1998).
16. J. Clavilier, R. Faure, G. Guinet, D. Durand, *J. Electrochem. Soc.*, **107**, 205 (1980).
    A. J. Bard, L. R. Faulkner, *Electrochemical Methods: Fundamentals and Applications*, John-Wiley & Sons, Inc., New York (1980), p.540.
17. R. J. Nichols, A. Bewick, *J. Electroanal. Chem.*, 243, 445 (1988).
    A. Wieckowski, P. Zelenav, K. Varga, *J. Chim. Phys.*, 88, 1247 (1991).
18. T. Wagner, P. N. Ross, *J. Electroanal. Chem.*, 250, 301 (1988).
19. K. Itaya, S. Sugawara, K. Sashikata, N. Furuya, *J. Vac. Sci. Technol.*, **A8(1)**, 515 (1990).

20. N. Furuya, S. Koide, *Surf. Sci.*, 220, 18 (1989).
21. M. T. M. Koper, J. H. Sluyters, *J. Electroanal. Chem.*, **303**, 73 (1991).
22. M. T. M. Koper, J. H. Sluyters, *J. Electroanal. Chem.*, **347**, 31 (1993).
23. N. N. Markovic, H. A. Gasteiger, P. N. Ross, Jr., *J. Phys. Chem.*, 99, 3411 (1995).

Chapter 2

Observation of Two Stationary States of Low and High H_2O_2-Reduciton Currents at a Pt Electrode, Arising from the Occurrence of a Positive Feedback Mechanism including Solution-Stirring by Gas Evolution

Introduction

Chemical and electrochemical oscillations are of much interest from the point of view of dynamic self-organization of molecular systems. Elucidation of the mechanisms will give new insights into understanding of highly organized molecular systems such as living bodies. For these twenty years, electrochemical oscillations have been reported for a variety of systems, as summarized in recent reviews. [1-4] Mechanistic studies have also made rapid progress recently, especially since the work of Koper and Sluyters. [5,6] It is now well established[4,7,8] that the negative differential resistance (NDR) plays a crucial role in the appearance of electrochemical oscillations, thus most of them being classified into NDR or hidden NDR (HNDR) oscillators.[8]

The author reported previously[9-13] that H_2O_2 reduction on Pt electrodes in acidic solutions showed five electrochemical oscillations of different types, called oscillation A, B, C, D, and E. Oscillation A is observed in a potential region just before hydrogen evolution,[9-11] whereas oscillation B is observed in a potential region of hydrogen evolution.[9-11] Oscillations C and D are observed when small amounts of halide ions are added to the solution.[11,12] Oscillation E is observed only for single-crystal Pt (111) electrodes.[11,13] With respect to the oscillation mechanisms, oscillations A[10,11] and E [13] are classified into NDR oscillators, whereas oscillations C and D are classified into HNDR oscillators.[12,14] On the other hand, recent studies[15] have revealed that oscillation B is caused by electrode-surface inhomogeneity (the presence of active and non-active areas) as well as electrical-coupling effect and solution-stirring effect of hydrogen-gas evolution, and classified into a new-type oscillator, which may be called a coupled NDR (CNDR) oscillator.

Electrochemical oscillations are also interesting from a point of view of investigation of mechanisms of electrochemical reactions themselves, because their studies sometimes reveal new mechanisms that will otherwise not be clarified. In fact, in the course of studies on the above oscillations, the author found the autocatalytic effect[12,13] of adsorbed OH on the dissociative adsorption of H_2O_2 and the catalytic effect[16] of adsorbed halogen on the same reaction, together with the important role of solution stirring by gas-evolution reactions.[15] A similar autocatalytic effect of adsorbed OH was reported for Ag electrodes.[17]

In connection with the above findings, the author further found that the H_2O_2 reduction on Pt sometimes showed unusually high current densities, never observed thus far. In the present paper, the author reports the behavior and the mechanism of such a high-current state. The appearance of the high-current state gives confirmative support

to the autocatalytic effect of adsorbed OH as well as the important role of solution-stirring effect by gas-evolution reaction. The appearance of the high-current state is also of much interest as an appearance of a new state by a positive feedback mechanism including solution stirring near the electrode surface.

Experimental

Polycrystalline Pt (poly-Pt) discs and single-crystal Pt (111), (100), and (110) discs of about 1.0 to 2.0 mm in diameter, having *atomically flat* surfaces, were used as the working electrode.[13] The discs were obtained by the method of Clavilier et al.[18] or a modified one. Namely, they were obtained by heating Pt wires (99.97% in purity, 0.3 or 0.8 mm in diameter) in a hydrogen flame to prepare poly- or single-crystal Pt spheres, followed by cutting and polishing with diamond slurry. The discs were then annealed in a hydrogen flame for 30 s in order to obtain atomically flat surfaces, followed by immediate quenching in Ar-bubbled pure water for 5 to 120 s.

Poly-Pt and single-crystal Pt (111), (100), and (110) discs, having *atomically roughened* surfaces,[13] were also used. Itaya et al. reported[19] by in-situ STM experiments that surface roughening of the order of a few atomic layers was caused by a procedure of electrochemical oxidation and re-reduction for atomically flat Pt (111) surfaces. In the present work, cyclic potential scans were repeated for atomically flat Pt between –0.35 and +1.60 V vs. SCE at a rate of 0.1 V/s in 0.3 M H_2SO_4 (M = mol/dm^3) for a few minutes because the Pt surface should be oxidized in potentials above 0.55 V and the resulting surface Pt-oxide should be reduced below 0.45 V. It is to be noted that the atomically roughened Pt has still flat surfaces on a scale of 5 nanometers.

In addition, poly-Pt discs having just *cut and polished* surfaces[9] were also used as the working electrode. In this case, the Pt electrodes were immersed in 60% HNO_3 for about one day to remove surface contamination. Just before measurements, cyclic potential scans were repeated between -0.35 and +1.60 V vs. SCE in 0.3 M H_2SO_4 for about 30 min to clean the electrode surface.

Electrochemical measurements were done using a cell with two arms for the reference and counter electrodes, as reported previously.[13] A Pt disc as the working electrode was held such that only the flat surface was in contact with the electrolyte by use of its meniscus.[13] A gold plate was used as the counter electrode (CE). A saturated calomel electrode (SCE) or a hydrogen electrode (HE) was used as the reference electrode. For polished poly-Pt, a beaker-type cell was also used, together with a Pt plate (10×10 mm^2) as the counter electrode, and a saturated calomel electrode (SCE) or an Ag/AgCl electrode as the reference electrode.

Current density (j) vs. potential (U) curves were measured with a potentiogalvanostat (Hokuto-Denko, HA501) and a potential programmer (Nikko-Keisoku NPS-2), and recorded with a data-storing system (instruNET, GW Instruments) with a sampling frequency of 1 or 10 kHz. The electrolyte solutions were

kept stagnant in all measurements. The solutions were prepared using special grade chemicals and pure water, the latter of which was obtained by purification of deionised water with a Milli-Q water purification system. The ohmic drops in the solution between the Pt electrode and the reference electrode were not corrected in the present work.

Results

Let us first explain, for reference in later discussion, two reported *j-U* curves of different types, shown in Fig. 1 and Fig. 2(a), for Pt electrodes in 0.3 M H_2SO_4 + 0.7 M H_2O_2 under potential-controlled conditions. Figure 1 is for a polished poly-Pt electrode with a rough surface.[9-12] The H_2O_2-reduction (cathodic) current starts at about 0.83 V vs. NHE, and is independent of the potential between about –0.02 and 0.65 V. The potential-independent current is explained[11-13] by assuming that the H_2O_2 reduction is initiated by the dissociative adsorption of H_2O_2

$$2\,Pt + H_2O_2 \xrightarrow{k_1} 2\,Pt\text{-}OH \qquad (1)$$

followed by electrochemical reduction of the resultant Pt-OH

$$Pt\text{-}OH + H^+ + e^- \xrightarrow{k_2} Pt + H_2O \qquad (2)$$

and that the former (reaction (1)) is the rate-determining step. (The explanation in terms of the diffusion limit of H_2O_2 reported in our early papers[9,10] was revised in later papers.[11-13]) A "negative differential resistance (NDR)" appears in a potential region of about –0.05 to –0.02 V vs. NHE (just before hydrogen evolution) owing to suppression of the dissociative adsorption of H_2O_2 (reaction (1)) by formation of under-potential deposited hydrogen (upd-H) of a nearly full coverage.[9-13] In the potential region of this NDR, oscillation A appears. Hydrogen evolution starts at about –0.05 V, and oscillation B appears in the region of hydrogen evolution.[9-11,15]

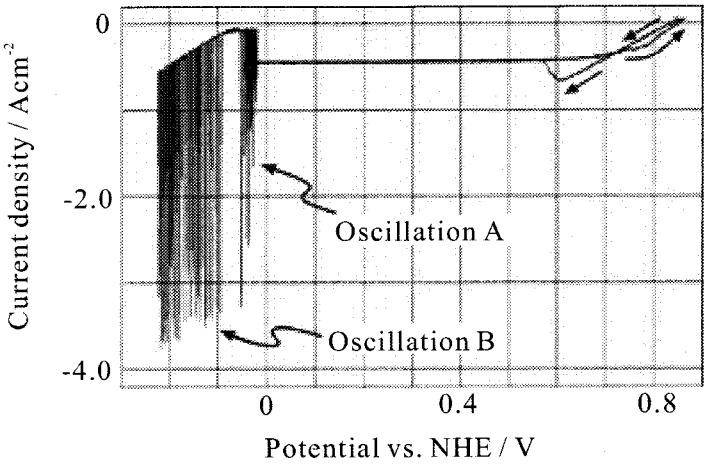

Fig. 1 A typical *j-U* curve for polished poly-Pt in 0.3 M H_2SO_4+ 0.7 M H_2O_2 under a potential-controlled condition. The scan rate is 0.01 V s^{-1}.

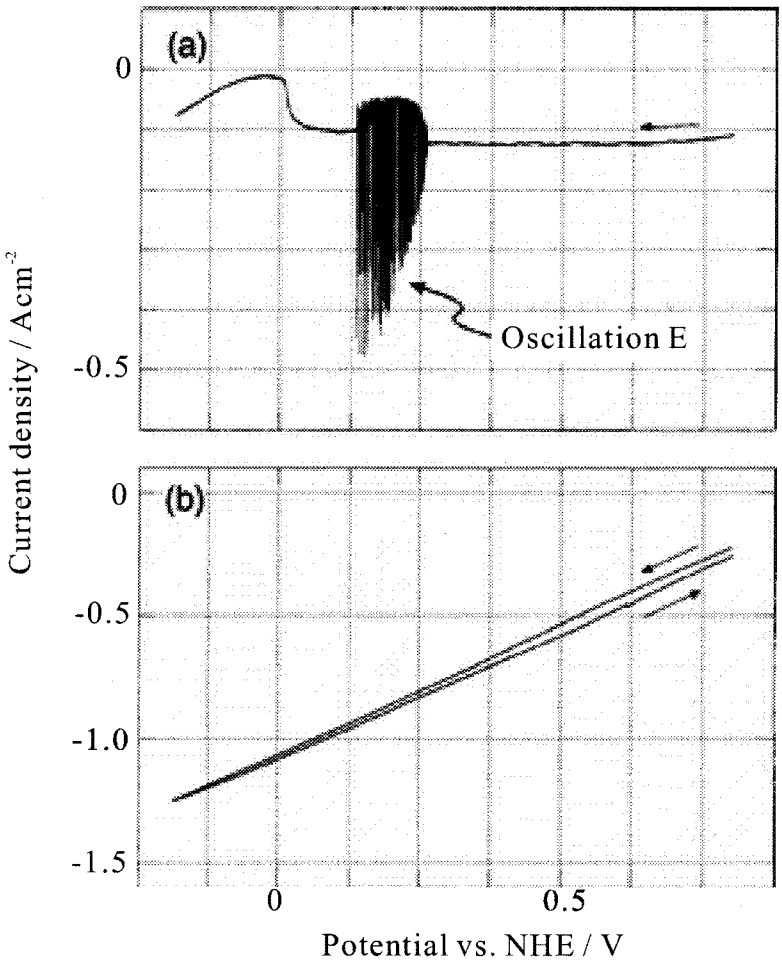

Fig. 2 (a) A typical *j-U* curve for atomically flat Pt (111) in 0.3 M H_2SO_4+ 0.7 M H_2O_2 under potential-controlled conditions. The scan rate is 0.01 V s^{-1}. (b) Another *j-U* curve observed under the same experimental conditions as (a). See text for details.

Figure 2(a) is for an atomically flat Pt (111) meniscus electrode. The *j-U* curve in Fig. 2(a) is similar to that in Fig. 1, in that it shows the potential-independent current between about 0.02 and 0.75 V. There are, however, some differences between Figs. 1 and 2(a). First, the NDR due to upd-H appears similarly, but oscillation A for atomically flat Pt (111) is observed only in higher H_2O_2 concentrations[13] probably because of effective suppression of the H_2O_2 reduction by upd-H on Pt(111). Second, oscillation B does not appear for atomically flat Pt owing to lack of the surface inhomogeneity.[13,15] The third important difference is the appearance of oscillation E for atomically flat Pt (111). This is explained[13] by taking account of another NDR arising from the

autocatalytic effect of adsorbed OH. Namely, adsorbed OH, formed by the dissociative adsorption of H_2O_2 (reaction (1)), acts as an autocatalyst for the reaction itself. Thus, a decrease in the surface coverage (θ_{OH}) of adsorbed OH with a negative potential shift, caused by an increase in the rate of electrochemical reduction of adsorbed OH (reaction (2)), leads to a decrease in the rate of reaction (1) (as the rate-determining step) and hence to a decrease in the H_2O_2-reduction current (j). Oscillation E appears from this NDR.[13] The autocatalytic effect of adsorbed OH is most prominent for Pt (111), which is the reason why oscillation E is observed only for Pt (111).[13]

Recently the author has found that atomically flat Pt (111) meniscus electrodes sometimes show another-type j-U curve, such as shown in Fig. 2(b). The curve is quite different from that in Fig. 1 or 2(a), in that the j increases monotonously (in the absolute value) with a negative potential shift and reaches a high negative value at a potential on the negative side, say, 0.00 V. It is to be noted that both the j-U curves in Figs. 2(a) and (b) are observed under the common experimental conditions, depending on experiments. This implies that the H_2O_2 reduction on Pt in acidic solutions has two stationary states of low and high current densities, called LC- and HC-mechanism states, respectively. Figure 2(a) and Fig. 1 are examples of the j-U curves of the LC-mechanism state, and Fig. 2(b) is an example of the HC-mechanism state.

Careful experiments showed that which of Figs. 2(a) and (b) was observed depended on the initial state of the potential scan. In Figs. 2(a) and (b), the potential scan was started from a positive potential (~0.65 V) near the rest potential (lying at about 0.83 V), toward the negative. The j-U curves of the HC-mechanism state, such as shown in Fig. 2(b), were often observed in case where the potential scan was started as soon as the Pt electrode was immersed in the solution, i.e., the potential scan was started from a state of a high H_2O_2 concentration at the electrode surface, accompanied by fairly vigorous oxygen gas evolution by catalytic H_2O_2 decomposition on Pt. On the other hand, the j-U curves of the LC-mechanism state, such as shown in Fig. 2(a), were often observed in case where the potential scan was started several minutes after the Pt electrode was immersed, especially after the electrode was kept at, say, 0.65 V with the flow of the H_2O_2-reduction current, i.e., the potential scan was started from a state of a low H_2O_2 concentration at the electrode surface, accompanied by weak or no oxygen gas evolution.

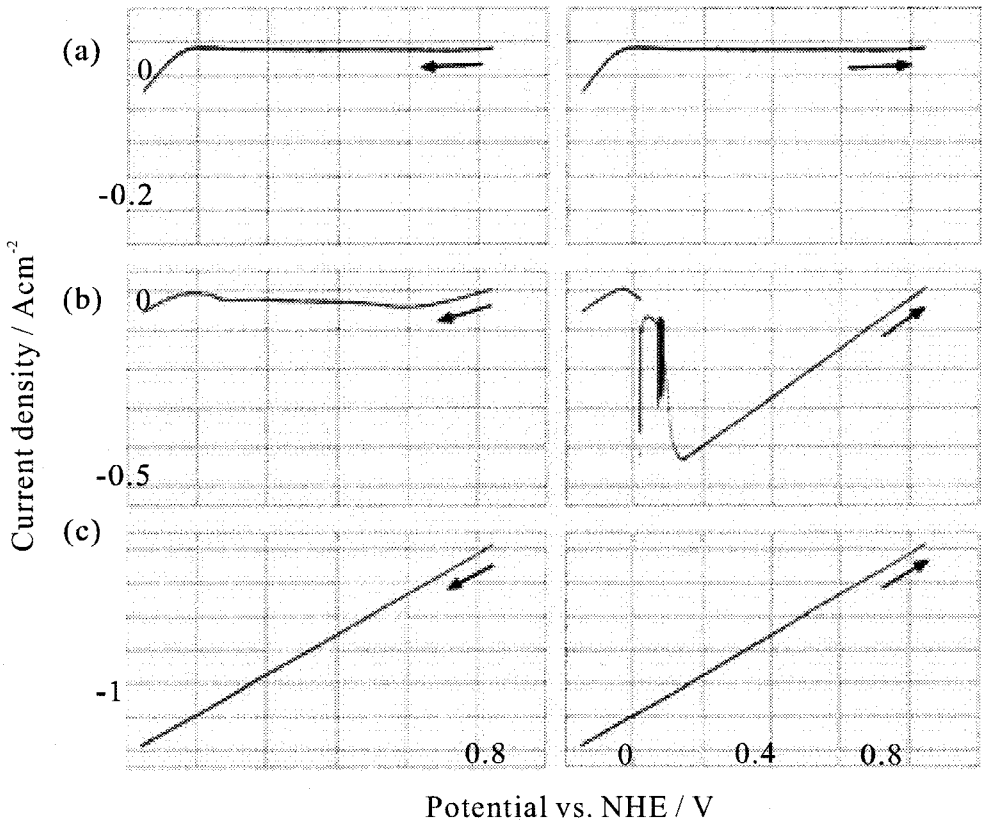

Fig. 3 The effect of the H_2O_2 concentration on the *j-U* curves for atomically flat Pt (111) under potential-controlled conditions. The left-hand side: negative potential scans, and the right-hand side: positive potential scans. The electrolyte: 0.3 M H_2SO_4 containing (a) 0.1 M H_2O_2, (b) 0.7 M H_2O_2 and (c) 1.4 M H_2O_2. The scan rate is 0.01 V s^{-1}.

Figure 3 shows the influence of the H_2O_2 (bulk) concentration on the *j-U* curve for atomically flat Pt (111) meniscus electrodes. In a low H_2O_2 concentration (0.3 M H_2SO_4 + 0.1 M H_2O_2), the *j-U* curve of the LC-mechanism state (Fig. 3(a)) was observed, whereas in a high H_2O_2 concentration (0.3 M H_2SO_4 + 1.4 M H_2O_2), the *j-U* curve of the HC-mechanism state (Fig. 3(c)) was observed. The result is in harmony with the aforementioned result that the HC-mechanism state was observed for the potential scans from high H_2O_2 concentrations at the electrode surface.

Figure 3(b) is another example of the *j-U* curves observed in an intermediate

H_2O_2 concentration (0.3 M H_2SO_4 + 0.7 M H_2O_2). Note that the *j-U* curve upon the negative potential scan is of the LC-mechanism state, whereas that upon the positive potential scan is a mixture of both the states, showing a transition from the LC-mechanism state to the HC-mechanism one at about 0.0 to 0.1 V. The *j-U* curve such as shown in Fig. 3(b) was observed only rarely (about once in twenty or thirty experiments), but it was included in Fig. 3 to demonstrate an example of the transition from the LC- to HC-mechanism states. On the left side of Fig. 3(b), oscillation E is absent, contrary to Fig. 2(a). The absence of oscillation E was also observed rarely, depending on electrodes, probably owing to a slight increase in the surface roughness on an atomic level for Pt (111) electrodes.

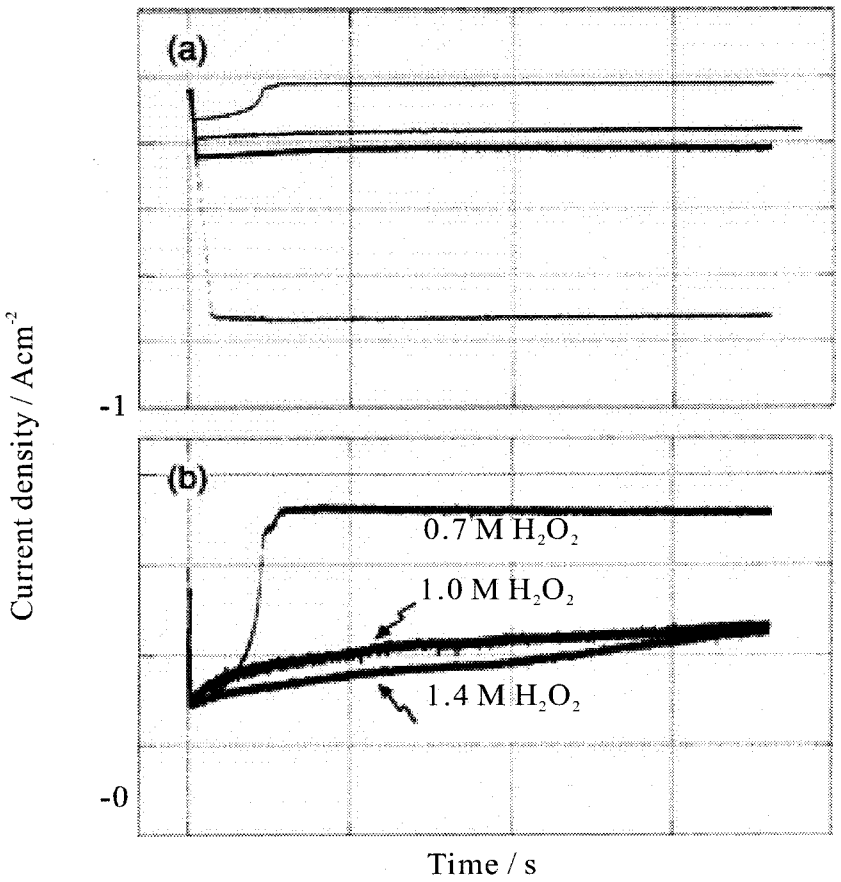

Fig.4 The *j-t* curves for an atomically flat Pt (111) meniscus electrode, obtained (a) in 0.3 M H_2SO_4+ 0.7 M H_2O_2 and (b) in 0.3 M H_2SO_4 containing 0.7 M, 1.0 M and 1.4 M H_2O_2. See text for further details.

Figure 4(a) shows j vs. time (t) curves for an atomically flat Pt (111) meniscus electrode in an intermediate H_2O_2 concentration (0.3 M H_2SO_4 + 0.7 M H_2O_2), which can be compared with the results of Fig. 2. The j-t curves were obtained by scanning the electrode potential at a rate of 0.01 Vs^{-1} immediately after the meniscus electrode was formed, from the rest potential (~0.83 V) toward the negative, followed by the stop of the potential scan when the current density (j) reached certain values. The j increased (in the absolute value) initially with the potential scan, as shown in Fig. 2(b), and then stopped increasing after the stop of the potential scan. When the potential scan was stopped at a low j of about -0.12 Acm^{-2}, the j decreased (in the absolute value) gradually and suddenly in about 200 s, indicating the occurrence of a transition from the HC- to LC-mechanism states. However, when the potential scan was stopped at a higher j of about -0.2 Acm^{-2}, the j was kept constant for a long time (>1800 s) except an initial slight decrease. For a much higher j of about -0.72 Acm^{-2}, the j was entirely constant for a long time (>1800 s), indicating that the HC-mechanism state is really a stationary state.

Figure 4(b) shows the effect of the H_2O_2 concentration on the j-t curves in the region of low j. The curves in this case were obtained after rapid changes of the electrode potential from the rest potential toward the negative. Contrary to the case of an intermediate H_2O_2 concentration (0.7 M H_2O_2), in high H_2O_2 concentrations (1.0 or 1.4 M H_2O_2), the j kept the high values for long times, showing no transition from the HC- to LC-mechanism states. Naturally, the j was entirely constant for a long time in the region of high j in high H_2O_2 concentrations (1.0 or 1.4 M H_2O_2).

The author mentioned before that which of Figs. 2(a) and (b) were observed in an intermediate H_2O_2 concentration (0.7 M H_2O_2) depended on the initial condition of the potential scan. It also depended on other factors. The polished poly-Pt electrodes having morphologically rough surfaces tended to show the j-U curves of the LC-mechanism state (see Fig. 1). On the other hand, poly-Pt and single crystal Pt (111), (100), and (110) electrodes, having atomically flat surfaces, were apt to show the j-U curves of the HC-mechanism state. Besides, the time of quenching of Pt discs in pure water, after they were annealed in a hydrogen flame (see the experimental section), and the diameter of Pt wires, from which Pt-disc electrodes were prepared, affected the j-U curves. The HC-mechanism state was measured more often for shorter-time quenching and for thinner Pt wires. In addition, Pt-disc electrodes with larger diameters tended to show the HC-mechanism state.

Mathematical Simulation

The *j-U* curves of the LC-mechanism state, such as shown in Figs. 1 and 2(a), were all reproduced by mathematical simulation in our previous papers.[10-13,15] The *j-U* curve in Fig. 1, except oscillation B, was reproduced[10-12] by taking account of reactions (1) and (2) together with the NDR arising from upd-H. Oscillation B was reproduced[15] by adding the effect of electrode-surface inhomogeneity (the presence of active and non-active areas) as well as electrical-coupling effect and solution-stirring effect of hydrogen-gas evolution.

The *j-U* curve such as shown in Fig. 2(a), including the appearance of oscillation E, was also reproduced[13] by taking into account the autocatalytic effect of adsorbed OH (Pt-OH) on the dissociative adsorption of H_2O_2 (reaction (1)). The rate constant of reaction (1), k_1, was expressed as follows:

$$k_1 = k_{10} + \gamma\theta_{OH} \qquad (3)$$

where k_{10} was a normal rate constant, γ a proportional constant, and θ_{OH} the surface coverage of adsorbed OH. The NDR giving rise to oscillation E arose from a decrease in k_1 by a decrease in θ_{OH} with a negative potential shift, the decrease in θ_{OH} being caused by an increase in the rate of reaction (2).

The appearance of the HC-mechanism state can be explained by a simple extension of the above model. It is to be noted first that the *j-U* curves for the LC-mechanism state, such as Figs. 1 and 2(a), are explained under the assumption that reaction (1) is the rate-determining step.[10-13] In high H_2O_2 concentrations, however, the rate of reaction (1) can become higher than that of reaction (2), as explained below. First, fairly vigorous gas-bubble evolution occurs at the Pt surface by catalytic decomposition of H_2O_2 on Pt, as really seen by eyes. The gas-bubble evolution causes solution stirring near the electrode surface, which keeps the surface H_2O_2 concentration (C_{HO}^{s}) high. The rate of reaction (1) can thus become very high, because the high C_{HO}^{s} leads to a high surface coverage (θ_{OH}), which in turn leads to a high k_1 value (equation (3)) and to a further high θ_{OH}. The shift of the rate-determining step from reaction (1) to reaction (2) leads to the appearance of the HC-mechanism state.

Mathematical simulation based on the above model reproduced the observed *j-U* curves, as shown in Fig. 5. The author assumed essentially the same reactions and equivalent circuit as those reported.[11-13] The following reactions were assumed, in addition to reactions (1) and (2).

$$2\ \text{Pt-OH} \xrightarrow{k_4} 2\ \text{Pt} + O_2 + 2\ H^+ + 2\ e^- \qquad (4)$$

$$4\ \text{Pt-OH} \xrightarrow{k_5} 4\ \text{Pt} + \text{O}_2 + 2\ \text{H}_2\text{O} \quad (5)$$

$$\text{Pt} + \text{H}^+ + \text{e}^- \underset{k_{-6}}{\overset{k_6}{=}} \text{Pt-H (upd-H)} \quad (6)$$

$$\text{Pt} + \text{H}^+ + \text{e}^- \underset{k_{-7}}{\overset{k_7}{=}} \text{Pt-H (on-top-H)} \quad (7)$$

$$\text{Pt-H (on-top-H)} + \text{Pt-H (on-top-H)} \xrightarrow{k_8} 2\ \text{Pt} + \text{H}_2 \quad (8)$$

Reactions (1) and (5) represent catalytic decomposition of H_2O_2 (or catalytic oxygen gas evolution) on Pt

Under potential-controlled conditions, the following differential equations can be derived for mass balances, a current balance, and reaction rates:

$$(\delta_{HO}/2)\, dC_{HO}^s/dt = (D_{HO}/\delta_{HO})(C_{HO}^b - C_{HO}^s) - k_1 C_{HO}^s (1 - \theta_H - \theta_{OH})^2 + s\,(C_{HO}^b - C_{HO}^s)/C_{HO}^b \quad (9)$$

$$(\delta_{H+}/2)\, dC_{H+}^s/dt = (D_{H+}/\delta_{H+})(C_{H+}^b - C_{H+}^s) - k_2 C_{H+}^s \theta_{OH} + k_4 \theta_{OH}^2 - k_6 C_{H+}^s \times(1 - \theta_H - \theta_{OH}) + k_{-6}\theta_H - k_7 C_{H+}^s (1 - \Theta_H) + k_{-7}\Theta_H + s\,(C_{H+}^b - C_{H+}^s)/C_{H+}^b \quad (10)$$

$$dE/dt = I/AC_d - I_F/AC_d \quad (11)$$

$$I_F = AF\{- k_2 C_{H+}^s \theta_{OH} + k_4 \theta_{OH}^2 - k_6 C_{H+}^s (1 - \theta_H - \theta_{OH}) + k_{-6}\theta_H - k_7 C_{H+}^s \times(1 - \Theta_H) + k_{-7}\Theta_H\} \quad (11')$$

$$N_0\, d\theta_{OH}/dt = k_1 C_{HO}^s (1 - \theta_H - \theta_{OH})^2 - k_2 C_{H+}^s \theta_{OH} - k_4 \theta_{OH}^2 - k_5 \theta_{OH}^2 \quad (12)$$

$$N_0\, d\theta_H/dt = k_6 C_{H+}^s (1 - \theta_H - \theta_{OH}) - k_{-6}\theta_H \quad (13)$$

$$N_0\, d\Theta_H/dt = k_7 C_{H+}^s (1 - \Theta_H) - k_{-7}\Theta_H - 2\, k_8 \Theta_H^2 \quad (14)$$

where C_{HO}^s and C_{H+}^s are the surface concentrations of H_2O_2 and H^+, respectively, and C_{HO}^b and C_{H+}^b are the bulk concentrations of H_2O_2 and H^+, respectively. θ_{OH}, θ_H, and Θ_H are the surface coverages of adsorbed OH (Pt-OH), upd-H, and on-top H, respectively. E is the true electrode potential, U the externally applied potential ($U = E + IR$, where IR is the ohmic drop between the electrode surface and the reference electrode, I being negative for a cathodic current), I_F the Faradaic current, A the electrode area, C_d the electrode capacity. N_0 is the total amount of surface sites per unit area, and D_{HO} and D_{H+} the diffusion coefficients of H_2O_2 and H^+, respectively.

The rate constants (k_i) for electrochemical reactions were expressed by the conventional Butler-Volmer equations:

$$k_i(E) = k_{i0} \exp\,[-\alpha n F(E - E_{i0})/RT] \quad \text{for reduction reactions} \quad (15)$$

$$k_i(E) = k_{i0} \exp [(1-\alpha)nF(E-E_{i0})/RT] \quad \text{for oxidation reactions} \quad (16)$$

where k_{i0} is the rate constant at $E = E_{i0}$ for the i-th reaction, E_{i0} the equilibrium redox potential, α the transfer coefficient, and n the number of transferred electrons. In the present work $\alpha = 0.5$ was assumed for all reactions.

The effect of solution stirring by oxygen-gas evolution was simply taken into account by introducing terms of s (C_{HO}^{b} - C_{HO}^{s}) / C_{HO}^{b} and s (C_{H+}^{b} - C_{H+}^{s}) / C_{H+}^{b} into equations (9) and (10). Under an assumption that the stirring effect is in proportion to the rate of oxygen-gas evolution, s is expressed as follows:

$$s = s_0 \{ k_4\theta_{OH}^{2} + k_5\theta_{OH}^{4} \} \quad (17)$$

where s_0 is a proportional constant, taken as a parameter.

Calculations showed that only oscillation A was reproduced with no autocatalytic effect ($\gamma = 0$) and no solution-stirring effect ($s_0 = 0$), as shown in Fig. 5(a).[11,12] If the autocatalytic effect ($\gamma = 50$) was taken into account, oscillation E was reproduced (Fig. 5(b)).[13] If both the autocatalytic effect ($\gamma = 50$) and the solution-stirring effect ($s_0 = 1.0\times10^{3}$) were taken into account, the j-U curve of the HC-mechanism state was reproduced (Fig. 5(c)), in agreement with the experiment (Fig. 3(c)).

Calculations of the j-t curves with the same parameter values as those for Fig. 5(c) showed that the j at a constant potential was kept entirely constant for a very long time of 1×10^{20} s or more at any potential, supporting the aforementioned conclusion that the HC-mechanism state is really a stationary state. Similarly, the j at a constant potential, calculated with the same parameter values as those for Figs. 5(a) and (b), was kept entirely constant, except the potential regions of oscillations A and E.

Interestingly, a calculated j-U curve for a positive potential scan with appropriate parameter values (the same s_0 and γ values as Fig. 5(c) but a little smaller k_5 value than Fig. 5(c)) showed a transition from the LC- to the HC-mechanism states, as shown in Fig. 5(d), indicating that such a transition can occur under an appropriate condition. This can be regarded as a reproduction of the observed j-U curve shown on the right side of Fig. 3(b).

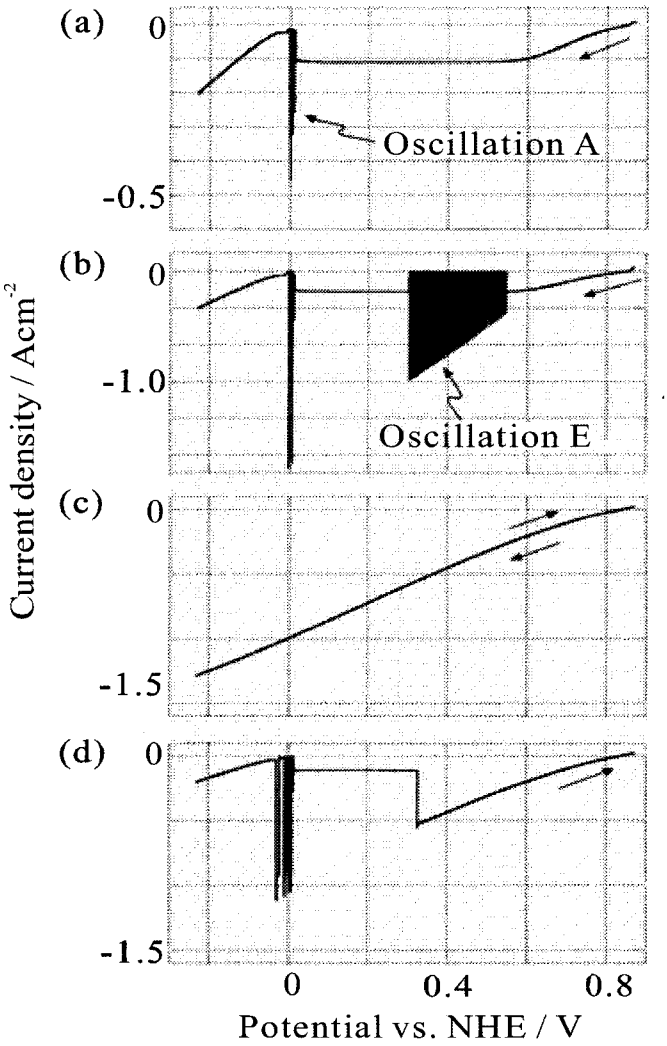

Fig. 5 Calculated *j-U* curves under potential-controlled conditions, (a) with no solution-stirring effect ($s_0 = 0$) and no autocatalytic effect ($\gamma = 0$), (b) with $s_0 = 0$ and autocatalytic effect ($\gamma = 50$), and (c) with solution-stirring effect ($s_0 = 1.0\times10^3$) and $\gamma = 50$, all for negative potential scans. Curve (d) was calculated with the same s_0 and γ as (c) but a little smaller k_5 (see below) for a positive potential scan. The other parameter values are as follows: $C_{HO}^{b} = 0.7 \times 10^{-3}$ mol cm^{-3}, $\delta_{HO} = 0.01$ cm, $D_{HO} = 1.7 \times 10^{-5}$ cm^2 s^{-1}, $C_{H+}^{b} = 0.3 \times 10^{-3}$ mol cm^{-3}, $\delta_{H+} = 0.004$ cm, $D_{H+} = 9.3 \times 10^{-5}$ cm^2 s^{-1}, $A = 0.01$ cm^2, $C_{DL} = 2.0 \times 10^{-5}$ F cm^{-2}, $N_0 = 2.2 \times 10^{-9}$ mol cm^{-2}, $R_\Omega = 60\ \Omega$, $T = 300$ K, $\alpha = 0.5$, $n = 1$, $k_{10} = 4.0 \times 10^{-2}$ cm s^{-1}, $k_{20} = 1.0 \times 10^{-5}$ cm s^{-1}, $k_{40} = 1.0 \times 10^{-8}$ mol cm^{-2} s^{-1}, $k_5 = 5.0 \times 10^{-6}$ mol cm^{-2} s^{-1}, except $k_5 = 2.0 \times 10^{-6}$ mol cm^{-2} s^{-1} for (d), $k_{60} = 1.0 \times 10^{-2}$ cm s^{-1}, $k_{-60} = 1.0 \times 10^{-5}$ mol cm^{-2} s^{-1}, $k_{70} = 5.0 \times 10^{-3}$ cm s^{-1}, $k_{-70} = 5.0 \times 10^{-6}$ mol cm^{-2} s^{-1}, $k_8 = 5.0 \times 10^{-6}$ mol cm^{-2} s^{-1}, $E_{20} = +1070$ mV vs. NHE, $E_{40} = +670$ mV, $E_{60} = E_{-60} = 80$ mV, and $E_{70} = E_{-70} = -30$ mV. The scan rate is

Discussion

It is evident from the experiments and mathematical simulation that both the LC- and HC-mechanism states can be regarded as stationary states, though transitions between these states sometimes occur under intermediate experimental conditions. The LC-mechanism state is stable in case where the surface H_2O_2 concentration (C_{HO}^s) is low, determined by the diffusion limitation, with almost no solution stirring by oxygen gas evolution reaction. On the other hand, the HC-mechanism state is stable in case where the C_{HO}^s is high, accompanied by efficient supply of H_2O_2 from the solution bulk through vigorous solution stirring near the electrode surface by oxygen gas evolution due to catalytic H_2O_2 decomposition on Pt.

It is also evident from the experiments and simulation that the appearance of the HC-mechanism state is due to a shift of the rate-determining step for the H_2O_2 reduction from reaction (1) to reaction (2) by a large increase in the rate of reaction (1). The *j-U* curves for the HC-mechanism state, shown in Figs. 2(b) and 3(c), show linear increases in *j* with negative potential shifts, contrary to exponential increases expected from the Butler-Volmer equation for the rate of reaction (2). This is because of the large ohmic drop in the solution, which determines the curve shape. The resistance of the solution estimated from the slope of the *j-U* curves is about 15 Ω, which is in agreement with the value measured by an impedance analyzer. (A value of 60 Ω was used in the present calculation, as shown in the caption of Fig. 5, to have a consistency with our previous calculation.[10-13])

The LC- and HC-mechanism states are clearly distinguished from each other because the latter is characterized by the occurrence of a positive feedback mechanism including solution stirring by gas evolution reaction. Namely, vigorous gas evolution leads to vigorous solution stirring and hence to the high C_{HO}^s, which in turn leads to the high surface coverage (θ_{OH}) of adsorbed OH and hence to vigorous oxygen gas evolution (equation (5)). On the contrary, in the LC-mechanism state, almost no solution stirring occurs near the electrode surface. The author can also say that the HC-mechanism state is characterized by the occurrence of doubled positive feedback mechanisms including solution stirring, because the adsorbed OH, formed by the dissociative adsorption of H_2O_2 (reaction (1)), acted as an autocatalyst for the reaction itself[13]. The presence of such positive feedback mechanisms (and the shift of the rate-determining step for the H_2O_2 reduction) lead to a clear difference in θ_{OH} between the LC- and HC-mechanism states, that is, $\theta_{OH} \cong 0$ in the former state and $\theta_{OH} \cong 1$ in the latter state, as confirmed by calculation.

It is not unreasonable that some scattered results are observed with respect to which of the LC- and HC-mechanism states are observed under intermediate experimental conditions, e.g., in intermediate H_2O_2 concentrations such as 0.3 M H_2SO_4 + 0.7 M H_2O_2 for flat-surface Pt (Figs. 2 and 3(b)). This is because which of the LC- and HC-mechanism states are observed is determined by whether the above-mentioned doubled positive feedback mechanisms effectively work or not, which in turn depends on slight differences in experimental parameters (near boundaries in phase diagrams) such as the C_{HO}^{s}, the atomic-level roughness of the electrode surface, and the height of the meniscus (the distance between the Pt surface and the uppermost surface of the electrolyte other than the meniscus part) which strongly affected the H_2O_2 diffusion in the meniscus and hence the C_{HO}^{s}.

The author mentioned in the Results section that the HC-mechanism state was often observed for atomically flat Pt electrodes. This can be explained easily by the effective autocatalytic effect of adsorbed OH on such flat Pt surfaces.[13] The solution stirring by gas-bubble evolution may also be effective on such flat surfaces.

The HC-mechanism state was measured more often for shorter-time quenching an for thinner Pt wires, as also mentioned in the Results section. In the present work, the measurements of *j*-*U* curves were in most cases started soon after Pt disc electrodes were annealed at high temperatures and quenched. Therefore, it is likely that Pt-disc electrodes of shorter-time quenching and with thinner Pt wires were still in somewhat higher temperatures than the electrolyte solution upon the measurements of the *j*-*U* curves, especially for meniscus electrodes, which led to fast surface H_2O_2 reactions and high H_2O_2 diffusion, namely, to the higher k_1 and higher C_{HO}^{s}.

The HC-mechanism state was also observed more often for Pt disc electrodes with larger diameters. This can be attributed to a higher current and hence a higher ohmic drop in the solution, which leads to a more positive true electrode potential (E) and hence to a higher value in θ_{OH} due to the lower rate of reaction (2).

Figure 4(a) shows that, when the potential scan is stopped at a low j of about -0.12 Acm^{-2}, the j decreases (in the absolute value) gradually and suddenly in about 200 s, indicating that the HC-mechanism state with a low j is not stable in an intermediate H_2O_2 concentration, though the HC-mechanism state with a high j is stable enough. The sudden decrease in j for the low j is probably caused by a decrease in C_{HO}^{s} with time by slow H_2O_2 diffusion, leading to the disappearance of the aforementioned positive feedback mechanisms. The detailed reason for the above j-dependence of the stability is not clear at present. The mathematical simulation has shown that all the HC-mechanism states of Fig. 5(c) are stable, independent of j. A possible explanation for the stability

difference between the low and high j in Fig. 4(a) may be given by taking into account a slight temperature increase at the electrode surface for high j owing to a large Joule heat, which leads to sufficiently fast H_2O_2 reactions and high H_2O_2 diffusion to maintain the positive feedback mechanisms.

An inverse transition from the LC- to HC-mechanism states is observed on the right side of Fig. 3(b). The transition is certainly induced by the initial appearance of oscillation E, followed by a transition from the high-current state of oscillation E to the HC-mechanism state. It is to be noted that the θ_{OH} in the high-current state of oscillation E is fairly high owing to the autocatalytic effect of adsorbed OH. Thus, the transition from this state to the HC-mechanism state can occur if a sufficient amount of catalytic oxygen-gas evolution occurs.

In conclusion, the present studies have revealed that the H_2O_2 reduction at Pt electrodes in acidic solutions has two stationary states of the LC- and HC-mechanism states. For flat-surface Pt, the LC-mechanism state is observed in low H_2O_2 concentrations, whereas the HC-mechanism state is observed in high H_2O_2 concentrations. In intermediate H_2O_2 concentrations, both the states are observed, depending on slight differences in experimental parameters which affect the occurrence of the doubled positive feedback mechanisms. The observation of the HC-mechanism state gives confirmative evidence to the presence of the autocatalytic effect of adsorbed OH on the dissociative adsorption of H_2O_2 reported previously[12-14]. The observation of the LC- and HC-mechanism states is also of much interest from a point of view of chemical dynamics, because they are, to our knowledge, the first and unique example of two stationary states arising from a difference in the self-sustaining solution dynamics (or solution stirring) near the electrode surface.

This work was partly supported by a Grant-in-Aid for Scientific Research on Priority Area of "Electrochemistry of Ordered Interfaces" (No.09237105) from the Ministry of Education, Culture, Sports, Science and Technology, Japan.

References

1. J. L. Hudson and T. T. Tsotsis, *Chem. Eng. Sci.*, **49**, 1493 (1994).
2. T. Z. Fahiday and Z. H. Gu, "Modern Aspects of Electrochemistry Vol. 27", ed by R. E. White, J. O'M. Bockris, and R. E. Conway, Plenum, New York (1995), p.383.
3. M. T. M. Koper, "Advances in Chemical Physics Vol. 92", ed by I. Prigogine and S. A. Rice, John Willey & Sons, New York (1996), p.161.
4. K. Krischer, "Modern Aspects of Electrochemistry Vol. 32", ed by R. E. White, J. O'M. Bockris, and R. E. Conway, Plenum, New York (1995), p.1.
5. M. T. M. Koper and J. H. Sluyter, *J. Electroanal. Chem.*, **303**, 73 (1991).
6. M. T. M. Koper and J. H. Sluyter, *J. Electroanal. Chem.*, **347**, 31 (1993).
7. M. T. M. Koper, *J. Electroanal. Chem.*, **409**, 175 (1996).
8. P. Strasser, M. Eiswirth and M. T. M. Koper, *J. Electroanal. Chem.*, **478**, 50 (1999).
9. T. Matsuda, H. Hommura, Y. Mukouyama, S. Yae and Y. Nakato, *J. Electrochem. Soc.*, **144**, 1988 (1997).
10. Y. Mukouyama, H. Hommura, S. Nakanishi, T. Nishimura, H. Konishi and Y. Nakato, *Bull. Chem. Soc. Jpn.*, **72**, 1247 (1999).
11. Y. Mukouyama, S. Nakanishi and Y. Nakato, *Bull. Chem. Soc. Jpn.*, **72**, 2573 (1999).
12. Y. Mukouyama, S. Nakanishi, H. Konishi and Y. Nakato, *J. Electroanal. Chem.*, **473**, 156 (1999).
13. S. Nakanishi, Y. Mukouyama, K. Karasumi, A. Imanishi, N. Furuya and Y. Nakato, *J. Phys. Chem. B*, **104**, 4181 (2000).
14. Y. Mukouyama, S. Nakanishi, T. Chiba, K. Murakoshi and Y. Nakato, *J. Phys. Chem. B*, **105**, 7246 (2001).
15. Y. Mukouyama, S. Nakanishi, H. Konishi, Y. Ikeshima, and Y. Nakato, *J. Phys. Chem. B*, **105**, 10905 (2000).
16. S. Nakanishi, Y. Mukouyama, Y. Nakato, *J. Phys. Chem. B*, **105**, 5751 (2001).
17. G. Flätgen, S. Wasle, M. Lűbke, C. Eickes, G. Radhakrishnan, K. Doblhofer and G. Ertl, *Electrochim. Acta*, **44**, 4499 (1999).
18. J. Clavilier, R. Faure, G. Guinet and D. Durand, *J. Electroanal. Chem.*, **107**, 205 (1980).
19. K. Itaya, S. Sugawara, K. Sashikata and N. Furuya, *J. Vac. Sci. Technol.*, **A8** (1), 515 (1990).

Chapter 3

Catalytic Effect of Adsorbed Iodine Atoms on Hydrogen Peroxide Reduction at Single Crystal Pt Electrodes, Causing Enhanced Current Oscillations

Introduction

Chemical and electrochemical oscillations are quite attractive phenomena as typical examples of dynamic self-organization of molecular systems. Much work has recently been done on oscillations in electrochemical systems[1-4] especially from points of views of exploration of new-type oscillations,[5] observation of spatio-temporal patterns,[6-9] and investigations of their mechanisms.[8-10]

Electrochemical oscillations are also interesting from a point of view of investigation of mechanisms of electrochemical reactions themselves, because their studies sometimes reveal new mechanisms that might otherwise not be discovered. The author reported previously[11-19] that hydrogen peroxide (H_2O_2) reduction on Pt electrodes showed five oscillations of different types, named oscillation A, B, C, D and E, depending on the electrode potential, the electrode-surface structure, and the presence or absence of halide ions in electrolytes. Of these, oscillation E, which is observed only for atomically flat Pt(111) electrodes[19], and oscillation C[13,14] are interesting, in that they show the presence of autocatalytic effect of adsorbed OH (Pt-OH) on dissociative adsorption of H_2O_2 (the first step of the H_2O_2 reduction). A similar autocatalytic effect of adsorbed OH was reported for Ag electrodes.[20]

In the present paper, the author reports that oscillation E is enhanced much by the presence of adsorbed iodine atoms. Detailed studies including mathematical simulation have revealed that adsorbed iodine atoms have catalytic effect on the dissociative adsorption of H_2O_2, which leads to the enhancement of oscillation E.

Experimental

Single-crystal Pt(111), (100), and (110) electrodes with atomically flat surfaces were prepared by the method of Clavilier et al,[21] using Pt(99.97% pure) wires heated in a hydrogen flame. The details of electrode preparation were described in a previous paper.[19] Just before measurements, all the electrodes were annealed in a hydrogen flame for 60 s and immediately quenched in Ar-bubbled pure water in order to obtain atomically flat surfaces.

Iodine-modified Pt electrodes were obtained by immersing the above Pt electrodes in aqueous 10 μM KI (M=mol/dm^3) for a certain period of time, the amount of adsorbed iodine being regulated by a change in the immersion time. The adsorption of iodine on Pt was confirmed by X-ray photoelectron spectroscopy (Shimadzu ESCA-1000). Once iodine atoms were adsorbed on Pt, it was not desorbed at all during electrochemical measurements.

An electrochemical cell, having two arms for the reference and the counter electrodes, was used in the present work, in the same way as reported in a previous paper.[19] A Pt plate was used as the counter electrode (CE), and a hydrogen electrode, composed of platinized Pt, 1.0 M H_2SO_4, and 1 atm of hydrogen gas, was used as the reference electrode (RE). The electrolyte was 0.3 M H_2SO_4 (pH 0.55) with or without H_2O_2. They were prepared using special grade chemicals and pure water, the latter of which was obtained by purification of de-ionized water with a Milli-Q water purification system.

Current density (j) vs. potential (U) curves, and j vs. time (t) curves were measured with a potentio-galvanostat (Nikko-Keisoku NPGS-301) and a potential programmer (Nikko-Keisoku NPS-2). They were either recorded with an X-Y recorder (Riken-Denshi F-35C) or stored digitally at 1 or 10 kHz with a Mac ADIOS II/16 (GW Instruments). Ohmic drops in the solution are not corrected in the present work.

Results

Figures 1(a) and (b) show, for reference, reported *j-U* curves for atomically flat Pt(111) in relatively low and high H_2O_2 concentrations (0.2 M H_2O_2 and 1.0 M H_2O_2 + 0.3 M H_2SO_4) under potential-controlled conditions. In Fig. 1(a), a cathodic current in a potential region from about +0.50 to +0.02 V vs. NHE is attributed to H_2O_2 reduction, which starts at about +0.80 V. A hydrogen evolution current flows in a potential region more negative than ca. +0.02 V. It is to be noted in Fig. 1(a) that the H_2O_2 reduction current, which is nearly independent of the electrode potential in 0.50 to 0.30 V, shows two negative differential resistances (NDR's) in a regions from +0.30 to +0.15 V and +0.10 to +0.02 V.[19] The potential-independent H_2O_2 reduction current is explained by assuming that the H_2O_2 reduction is initiated by dissociative adsorption of H_2O_2

$$2Pt + H_2O_2 \xrightarrow{k_1} 2Pt\text{-}OH \qquad (1)$$

followed by electrochemical reduction of the resultant Pt-OH

$$Pt\text{-}OH + H^+ + e^- \xrightarrow{k_2} Pt + H_2O \qquad (2)$$

and that reaction (1) is the rate-determining step.[13,16,19] The NDR in +0.10 to +0.02 V is caused by suppression of the dissociative adsorption of H_2O_2 (reaction (1)) by formation of under-potential deposited hydrogen (upd-H) of a nearly full coverage.[13,16,19] On the other hand, the NDR in +0.30 to +0.15 V is caused by a decrease in the coverage (θ_{OH}) of adsorbed OH (acting as an autocatalyst for the dissociative adsorption of H_2O_2) with a negative potential shift.[19] In a higher H_2O_2 concentration (1.0 M H_2O_2 + 0.3 M H_2SO_4), two oscillations, called oscillation A and E, appear in the potential regions of the above-mentioned NDR's, respectively, as shown in Fig. 1(b).[19] Slight shifts of the potential regions of the NDR's between Figs. 1(a) and (b) are due to the ohmic drops in the solution between the working and reference electrodes.

Figures 1(c) and 1(d) show *j-U* curves for an iodine-modified Pt(111) electrode prepared by 30-s immersion in 10 μM KI, drawn in the same way as Figs. 1(a) and 1(b), respectively. The coverage (θ_I) of adsorbed iodine is about 0.4 as estimated from a decrease in the current peaks of the upd-H formation in 0.3 M H_2SO_4. The potential region of the NDR due to adsorbed OH in Fig. 1(c) is extended to more positive potentials, up to about +0.5 V, than that in Fig. 1(a), and the magnitude (or the slope) of the NDR also becomes higher, though the exact shape of the *j-U* curve in this region is somewhat scattered from experiment to experiment. In accordance with the changes of the NDR, the potential region where oscillation E appears is also extended to the

positive (Fig. 1(d)). Oscillation A for the iodine-modified electrode is not observed in Fig. 1(d) owing to its long oscillation period compared with the speed of the potential scan.

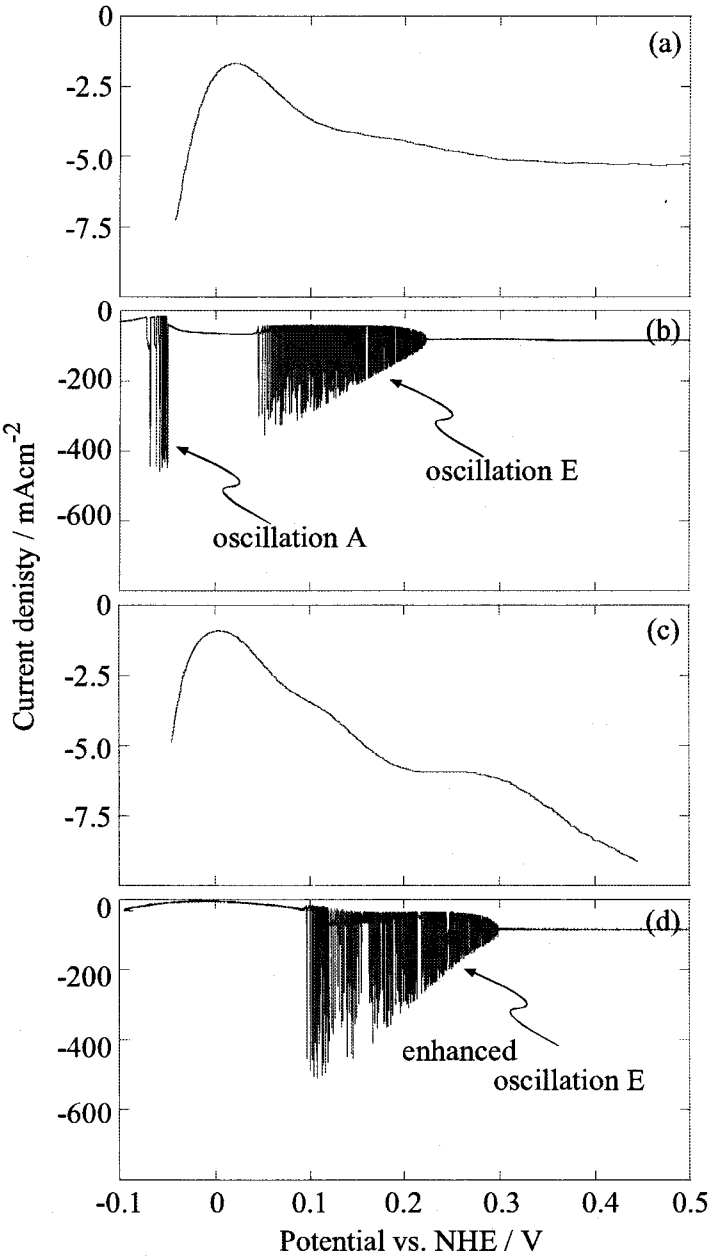

Fig. 1 Effect of iodine adsorption on *j-U* curves for Pt(111) under potential-controlled conditions. Electrode: (a) and (b) naked Pt(111), and (c) and (d) iodine-modified Pt(111). Electrolyte: (a) and (c) 0.2 M H_2O_2 + 0.3 M H_2SO_4, and (b) and (d) 1.0 M H_2O_2 + 0.3 M H_2SO_4. Scan rate: 10 mV/s. The shape of the *j-U* curve in (c) is somewhat scattered in a region from 0.1 to 0.3 V.

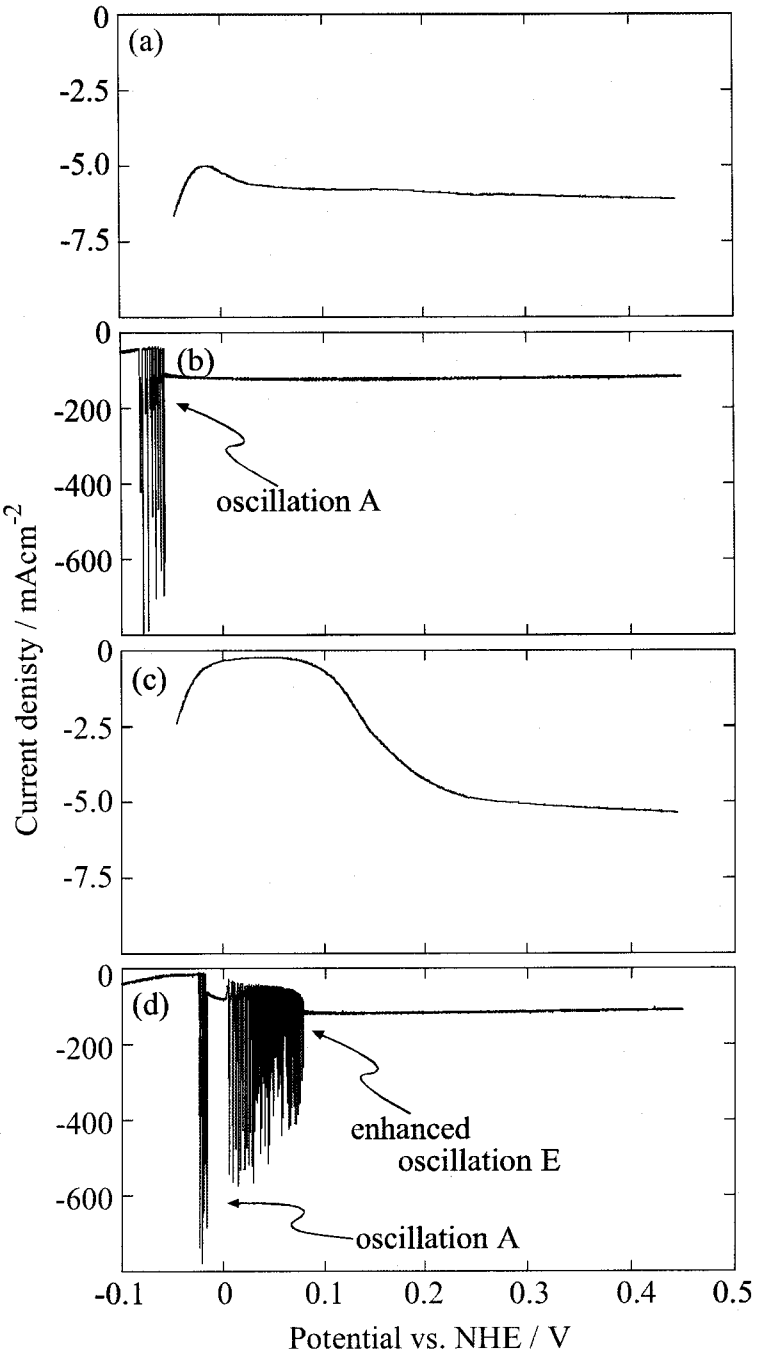

Fig. 2 The same as Fig. 1, except that the electrodes are changed to naked and iodine-modified Pt(100). The shape of the *j-U* curve in (c) is somewhat scattered in a region from 0.1 to 0.3 V.

A similar result was obtained for atomically flat Pt(100) electrodes, as shown in Fig. 2. The NDR due to adsorbed OH is weak for Pt(100) in a low H_2O_2 concentration (Fig. 2(a)), and no oscillation E, except oscillation A, appears in a high H_2O_2 concentration (Fig. 2(b)). The result is explained by the weak autocatalytic effect of adsorbed OH on Pt(100).[19] For iodine-modified Pt(100) prepared by 30-s immersion in 10 μM KI, however, the NDR due to adsorbed OH becomes higher in magnitude and is extended to the positive potentials (Fig.2(c)). In harmony with the NDR change, oscillation E appears for iodine-modified Pt(100) in a higher H_2O_2 concentration (Fig. 2(d)).

Figure 3 shows *j-U* curves for atomically flat Pt(110), drawn in the same way as Figs. 1 and 2. Contrary to the cases of Pt(111) and (100), no extension of the potential region of the NDR nor appearance of oscillation E was observed by iodine adsorption for Pt(110), independent of the immersion time in 10 μM KI.

Figure 4 shows in detail the NDR's changes by changes in the coverage (θ_I) of adsorbed iodine, for (a) Pt(111), (b) Pt(100), and (c) Pt(110), in a low H_2O_2 concentration (0.2 M H_2O_2 + 0.3 M H_2SO_4). Curves 1, 2, and 3 are for Pt electrodes which were beforehand immersed in 10 μM KI for 0, 30, and 300 s, respectively. The coverages θ_I for these curves are estimated to be 0, 0.4, and 1.0, respectively. For Pt(111) in Fig. 4(a), the H_2O_2-reduction current in curve 3 is nearly zero throughout the potential, clearly showing the site-blocking effect of adsorbed iodine. On the other hand, the current in curve 2 is low (in the absolute value) in potentials from 0.00 to 0.05 V, whereas it is high in positive potentials from +0.2 to +0.4 V, even higher than that for a naked (no-iodine adsorbed) electrode (curve 1). The latter result clearly indicates that the adsorbed iodine has catalytic effect on the dissociative adsorption of H_2O_2, in addition to the site-blocking effect, as discussed in more detail in the discussion section. A similar result is obtained for Pt(100) in Fig. 4(b). Namely, the H_2O_2-reduction current in curve 2 is low on the negative-potential side, whereas it is high on the positive-potential side. For Pt(110) in Fig. 4(c), however, the current is decreased by the iodine adsorption uniformly throughout the potentials between 0.0 and 0.5 V, suggesting that almost no catalytic effect of adsorbed iodine is present for this surface, only the site-blocking effect playing a role.

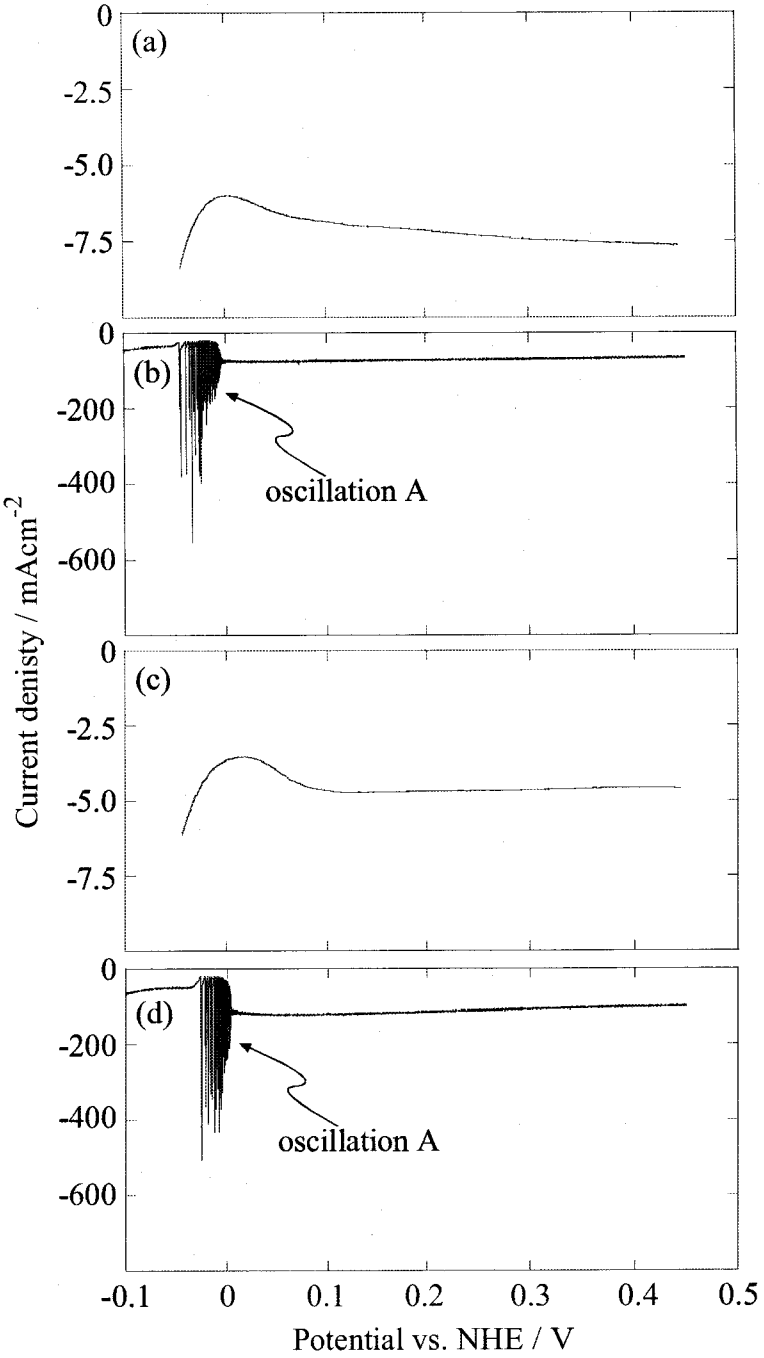

Fig. 3 **The same as Fig. 1, except that the electrodes are changed to naked and iodine-modified Pt(110).**

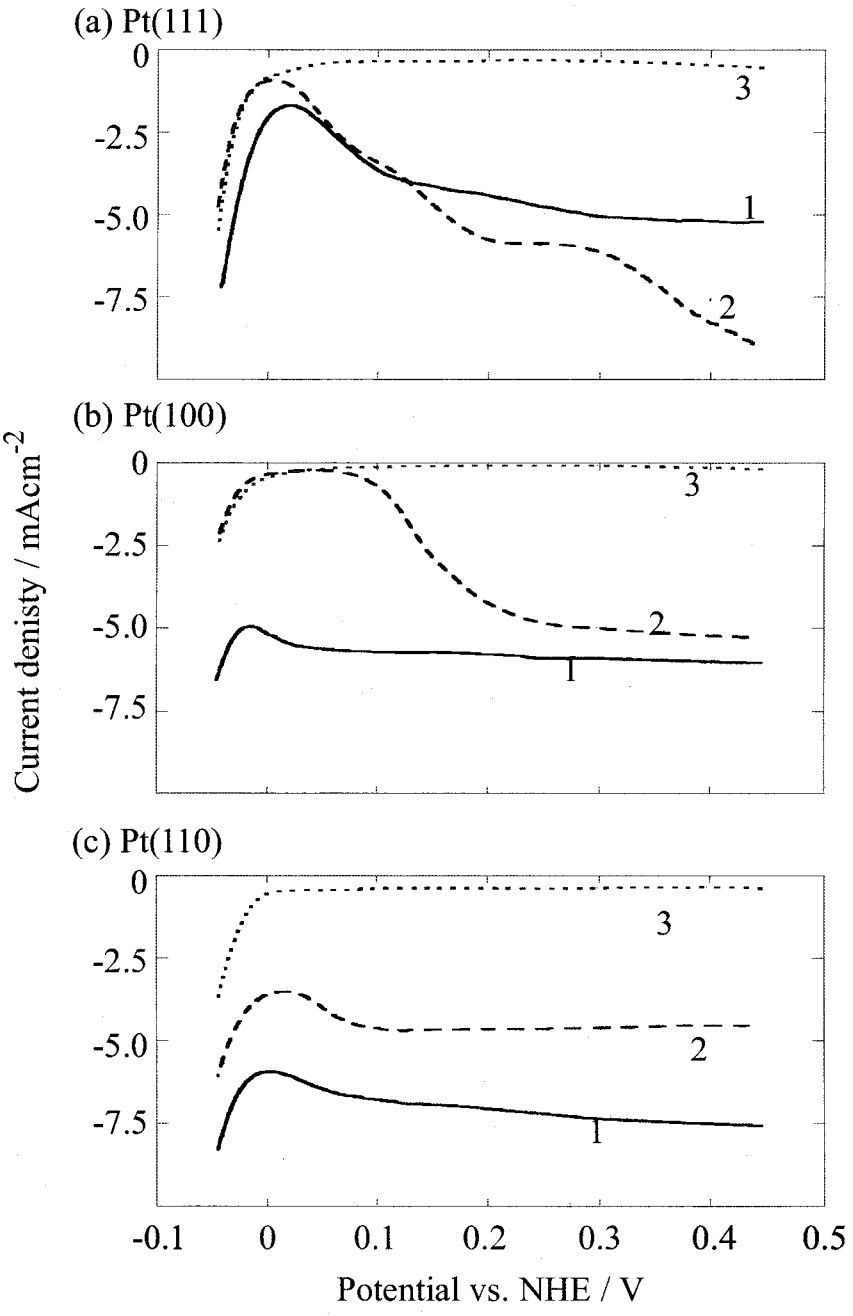

Fig. 4 Dependence of *j-U* curves for (a) Pt(111), (b) Pt(100), and (c) Pt(110) on the coverage (θ_I) of adsorbed iodine. Curve 1 is for naked Pt (θ_I=0), curve 2 for iodine-modified Pt (θ_I≈0.4), and curve 3 for iodine-modified Pt (θ_I≈1). Electrolyte: 0.2 M H_2O_2 + 0.3 M H_2SO_4. Scan rate: 10 mV/s. The exact shapes of the *j-U* curves in curve 2 for Pt(111) and (100) are somewhat scattered, depending on experiments.

Figure 5 shows time courses of oscillation E in 1.0 M H_2O_2 + 0.3 M H_2SO_4, (a) and (b) for naked Pt(111), and (c) to (e) for iodine modified Pt(111) with $\theta_I \approx 0.4$. No notable change is caused in the wave shape by iodine adsorption.

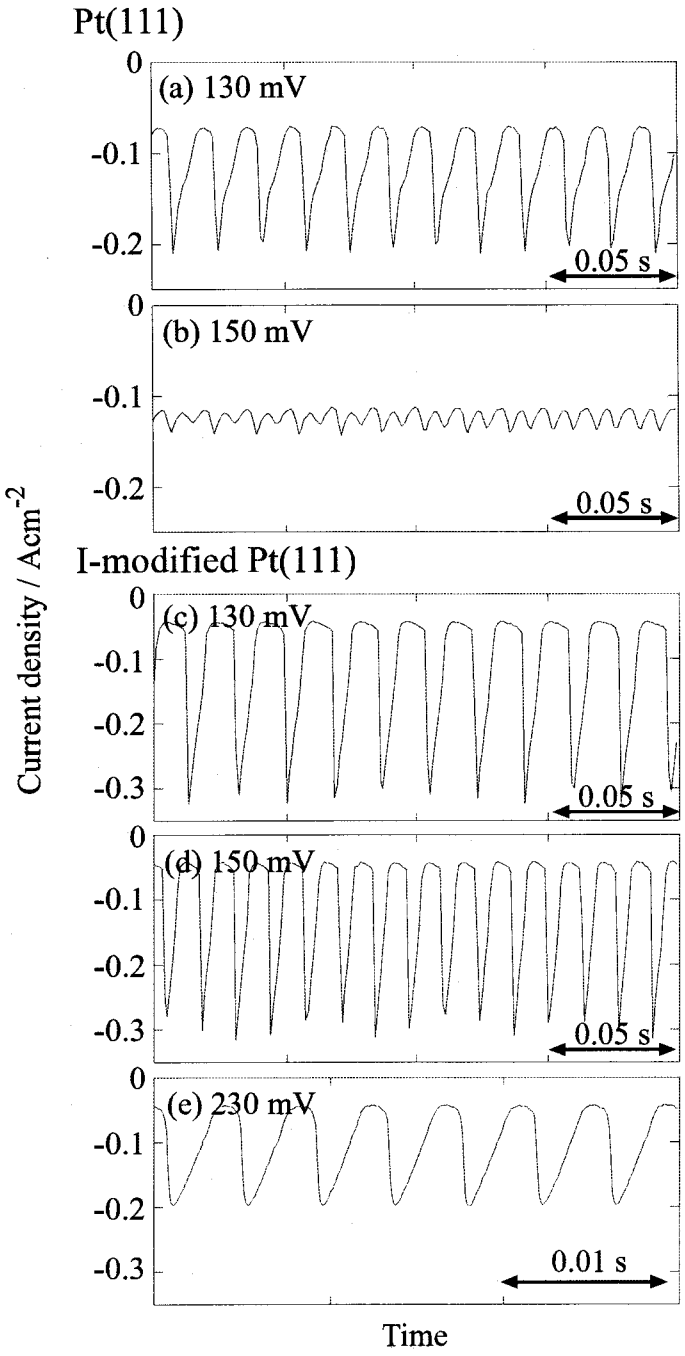

Fig. 5 Time courses of oscillation E, (a) and (b) for Pt(111), and (c)~(e) for iodine-modified Pt(111) with $\theta_I \approx 0.4$, at the electrode potential given in the figure (vs. NHE). Electrolyte: 0.2 M H_2O_2 + 0.3 M H_2SO_4.

Mathematical Simulation

The results of Fig. 4 show that adsorbed iodine on Pt has the catalytic effect on the dissociative adsorption of H_2O_2, in addition to the site-blocking effect. The author reported previously[19] that the appearance of oscillation E for naked Pt(111) was explained by taking account of the autocatalytic effect of adsorbed OH on the same reaction. The catalytic effect of adsorbed iodine for iodine-modified Pt(111) will thus co-operate with the autocatalytic effect of adsorbed OH on a naked-Pt(111) part. The enhancement of oscillation E can be reproduced by mathematical simulation on the basis of this model, as explained below.

In addition to reactions (1) and (2), the following reactions on Pt sites were considered in the same way as in our previous papers.[13,16,19]

$$\mathrm{Pt} + \mathrm{H^+} + \mathrm{e^-} \underset{k_{-3}}{\overset{k_3}{\leftrightarrow}} \mathrm{Pt\text{-}H\ (upd\text{-}H)} \tag{3}$$

$$2\mathrm{Pt\text{-}OH} \xrightarrow{k_4} 2\mathrm{Pt} + \mathrm{O_2} + 2\mathrm{H^+} + 2\mathrm{e^-} \tag{4}$$

$$\mathrm{Pt} + \mathrm{H^+} + \mathrm{e^-} \underset{k_{-5}}{\overset{k_5}{\leftrightarrow}} \mathrm{Pt\text{-}H\ (on\text{-}top\text{-}H)} \tag{5}$$

$$\mathrm{Pt\text{-}H\ (on\text{-}top\text{-}H)} + \mathrm{Pt\text{-}H\ (on\text{-}top\text{-}H)} \xrightarrow{k_6} \mathrm{H_2} \tag{6}$$

where Pt represents schematically surface Pt site(s). The coverage (θ_I) of adsorbed iodine was taken to be constant, independent of oscillating reactions.

The differential equations for a current balance, mass balances, and rate equations, were also obtained in the same way as in our previous work,[13,16,19]

$$I = jA = (U - E)/R_\Omega = I_C + I_F = AC_{DL}(dE/dt) + I_F \tag{7}$$

$$I_F = AF\{- k_3 C_{H^+}{}^S(1 - \theta_H - \theta_{OH} - \theta_I) + k_{-3}\theta_H - k_2 C_{H^+}{}^s\theta_{OH} + k_4\theta_{OH}{}^2 - k_5 C_{H^+}{}^s(1 - \Theta_H) + k_{-5}\Theta_H\} \tag{8}$$

$$(\delta_{HO}/2)\, dC_{HO}{}^s/dt = (D_{HO}/\delta_{HO})(C_{HO}{}^b - C_{HO}{}^s) - k_1 C_{HO}{}^s (1 - \theta_H - \theta_{OH} - \theta_I)^2 \tag{9}$$

$$N_0 d\theta_{OH}/dt = k_1 C_{HO}{}^s(1 - \theta_H - \theta_{OH} - \theta_I)^2 - k_3 C_{H^+}{}^s\theta_{OH} - k_4\theta_{OH}{}^2 \tag{10}$$

$$N_0 d\theta_H/dt = k_3 C_{H^+}{}^s(1 - \theta_H - \theta_{OH} - \theta_I) - k_{-3}\theta_H \tag{11}$$

$$N_0 d\Theta_H/dt = k_5 C_{H^+}{}^s(1 - \Theta_H - \theta_I) - k_{-5}\Theta_H - 2k_6\Theta_H{}^2 \tag{12}$$

where I is the total current, A the electrode area, j the current density, U the external (or

applied) electrode potential, E the true electrode potential, (U-E) the ohmic drop between the electrode surface and the position of the reference electrode, R_Ω the solution resistance in the same place as above, $I_C = AC_{DL}(dE/dt)$ the charging current, C_{DL} the double-layer capacitance, and I_F the Faradaic current. C_{HO}^{s} and C_{H+}^{s} are the concentrations of H_2O_2 and H^+ ions at the electrode surface, respectively, C_{HO}^{b} and C_{H+}^{b} the concentrations of H_2O_2 and H^+ in the solution bulk, respectively, and θ_{OH}, θ_H, and Θ_H are the surface coverages of Pt-OH, upd-H, and on-top-H, respectively. D_{HO} and D_{H+} are the diffusion coefficients for H_2O_2 and H^+, respectively, δ_{HO} and δ_{H+} the thickness of the diffusion layers for H_2O_2 and H^+, respectively. N_0 schematically represents the total amount of surface Pt sites per unit area. In the present work $C_{H+}^{s} = C_{H+}^{b}$ was assumed owing to a high mobility (high diffusion rate) of H^+ compared with H_2O_2.

The rate constants, k_2, k_3, k_{-3}, k_4, k_5, and k_{-5}, were expressed by the Butler-Volmer equations,

$$k_i = k_{i0}\exp[-\alpha_i n_i F(E-E_{i0})/RT] \quad \text{for i = 2, 3 and 5} \quad (13)$$

$$k_i = k_{i0}\exp[(1-\alpha_i) n_i F(E-E_{i0})/RT] \quad \text{for i = -3, 4 and –5} \quad (14)$$

where k_{i0} is the rate constant at $E = E_{i0}$, E_{i0} the equilibrium redox potential for the i-th reaction, α_i the transfer coefficient, n_i the number of transferred electrons.

The site-blocking effect of adsorbed iodine, namely, that the dissociative adsorption of H_2O_2 could not occur on adsorbed iodine, was taken into account by introducing such terms as $(1-\theta_H-\theta_{OH}-\theta_I)$. The autocatalytic effect of adsorbed OH (Pt-OH) and the catalytic effect of adsorbed iodine on the dissociative adsorption of H_2O_2 were taken into account by expressing k_1 as follows

$$k_1 = k_{10} + \gamma_1\theta_{OH} + \gamma_2\theta_I \quad (15)$$

where k_{10} is a normal rate constant for reaction (1), and γ_1 and γ_2 are proportional constants expressing the strength of the autocatalytic effect and the catalytic effect, respectively.

Figures 6(a) and (b) show calculated j-U curves with γ_1=8 and $\theta_I = 0$ (no iodine adsorption) and with $\gamma_1 = 8$, $\gamma_2 = 0.01$, and $\theta_I = 0.3$, respectively. The result of Fig. 6(a) is essentially the same as reported,[19] reproducing the appearance of oscillation E. In Fig. 6(b), enhanced oscillation E is reproduced, in agreement with the experiments. Figure 6(c) shows a calculated time course (j-t curve) at U=+0.30 V with the same γ_1, γ_2, and θ_I values as Fig. 6(b). The calculated wave shape and period are namely the same as the experimental result (Fig. 5). In addition, the calculated amplitude of oscillation E showed a tendency to become larger from zero with negative potential shifts, similar to the experimental results (see Figs. 1(b) and 1(d)), as the rate of the potential scan was made lower.

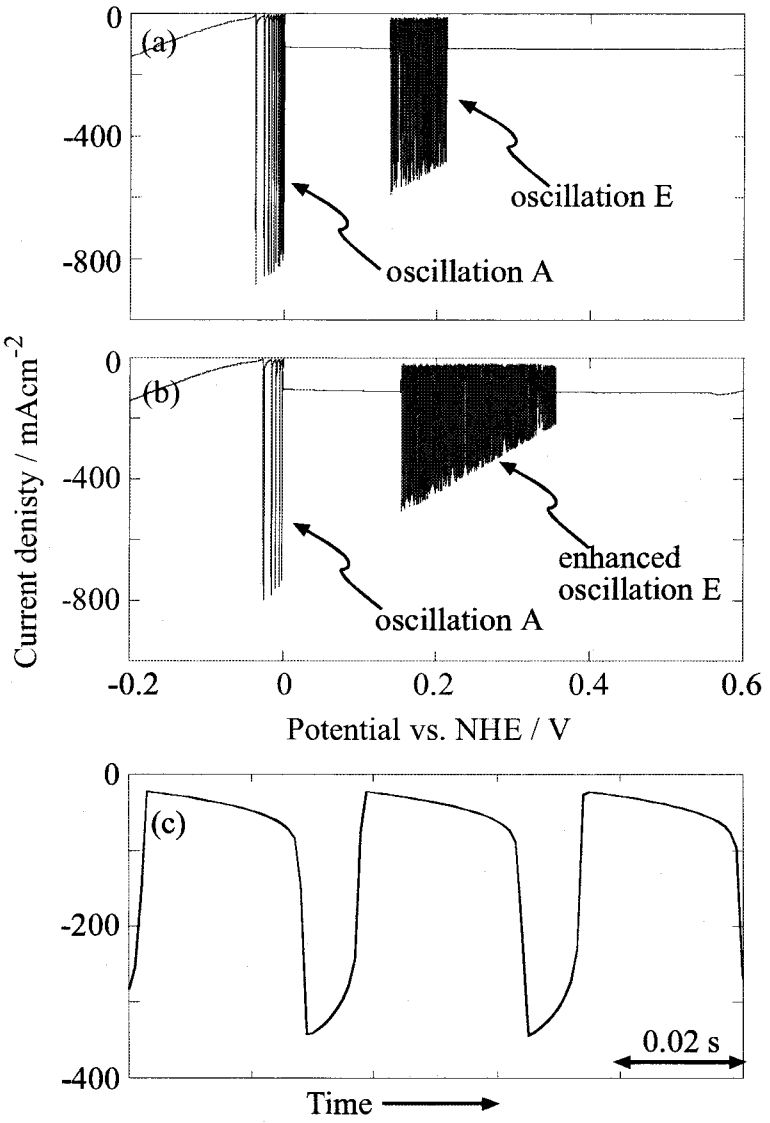

Fig. 6 (a) and (b): Calculated *j-U* curves with (a) γ_1=8 and θ_I=0, and (b) γ_1=8, γ_2=0.01, and θ_I=0.3. *U* was scanned at a rate of 0.01 V/s. (c): Calculated *j-t* curve at *U*=+0.30 V with γ_1=8, γ_2=0.01, and θ_I=0.3. Other parameter values are as follows: C_{HO}^{b} = 0.7 × 10^{-3} mol cm^{-3}, δ_{HO} = 0.01 cm, D_{HO} = 1.7 × 10^{-5} cm^2 s^{-1}, C_{H+}^{b} = 0.3 × 10^{-3} mol cm^{-3}, δ_{H+} = 0.004 cm, D_{H+} = 9.3 × 10^{-5} cm^2 s^{-1}, A = 0.01 cm^2, C_{DL} = 2.0 × 10^{-5} F cm^{-2}, N_0 = 2.2 × 10^{-9} mol cm^{-2}, R_Ω = 60 Ω, T = 300 K, α_i = 0.25 (i = 2) and 0.50 (i ≠ 2), n = 1, k_{10} = 4 × 10^{-2} cm s^{-1}, k_{20} = 1 × 10^{-5} cm s^{-1}, k_{30} = 1 × 10^{-2} cm s^{-1}, k_{-30} = 1 × 10^{-5} mol cm^{-2} s^{-1}, k_{40} = 1 × 10^{-8} mol cm^{-2} s^{-1}, k_{50} = 5 × 10^{-3} cm s^{-1}, k_{-50} = 5 × 10^{-6} mol cm^{-2} s^{-1}, k_6 = 5 × 10^{-6} mol cm^{-2} s^{-1}, E_{20} = 1.37 V vs. NHE, E_{50} = E_{-50} = 0.08 V, E_{60} = 0.67 V, and E_{70} = E_{-70} = -0.03 V.

Discussion

The experiments and mathematical simulation have clearly shown that adsorbed iodine has the catalytic effect on the dissociative adsorption of H_2O_2, in addition to the site-blocking effect. Experimentally, the site-blocking effect is clearly observed in the *j-U* curve for Pt(110) in Fig. 4(c), in which the H_2O_2-reduction current is decreased by (in the absolute value) iodine adsorption uniformly throughout the potentials between 0.00 and 0.45 V. Similar decreases in the H_2O_2-reduction current by iodine adsorption are observed for Pt(111) and (100) throughout the potentials in curve 3 ($\theta_I \approx 1$) of Figs. 4(a) and (b) and also in potentials of about 0.00 to 0.05 V in curve 2 ($\theta_I \approx 0.4$) of Figs. 4(a) and (b). On the other hand, in curve 2 of Figs. 4(a) and (b), the H_2O_2-reduction current in positive potentials from +0.2 to +0.4 V does not show such a decrease, remaining only slightly lower or even higher than that for naked Pt (curve 1) in the same potentials. This high H_2O_2-reduction current in the positive potentials can be attributed to the catalytic effect of adsorbed iodine. The result indicates that the catalytic effect is comparable to or even exceeds the site-blocking effect in a region of moderate θ_I.

The reason why the catalytic effect of adsorbed iodine appears prominently in the positive potentials from 0.2 to 0.4 V can be explained by taking account of its co-operation with the autocatalytic effect of Pt-OH. In a previous paper,[19] the autocatalytic effect of Pt-OH was explained as follows: Pt-OH is present at hollow sites of surface Pt lattice and H_2O_2 is adsorbed with negatively polarized oxygen atoms of H_2O_2 directed to surface Pt atoms, as shown in Fig. 7A. Thus, the adsorption of H_2O_2 is accelerated on surface Pt sites in the neighborhood of adsorbed OH because they are more or less positively polarized by an electronegativity difference between Pt atom and OH-group (Fig. 7A). The catalytic effect of adsorbed iodine can be understood in the same way, because iodine atoms have a fairly large electronegativity than Pt, similarly to OH group. Thus, the co-operation occurs such that the increased adsorbed OH, formed by the catalytic effect of adsorbed iodine, further increases the adsorbed OH by its autocatalytic effect. The coverage of adsorbed OH (θ_{OH}) can be significant only in the positive potentials from +0.2 to +0.4 V, as the rate of its electrochemical reduction (reaction (2)) becomes high in more negative potentials. The extension of the potential region where oscillation E appears toward the positive can be explained by the same reasoning.

The catalytic effect of adsorbed iodine is more prominent in the order, Pt(111)>Pt(100)>>Pt(110). This can be explained by considering the differences in the

values of γ_1 and γ_2 in equation (15). The author reported previously[19] that the γ_1 value decreased in the order, Pt(111)>(100)>(110), owing to the difference in the number of Pt pairs on which accelerated H_2O_2 adsorption occurred, as shown in Fig. 7B. The same ordering is expected for the catalytic effect of adsorbed iodine (Fig. 7B).

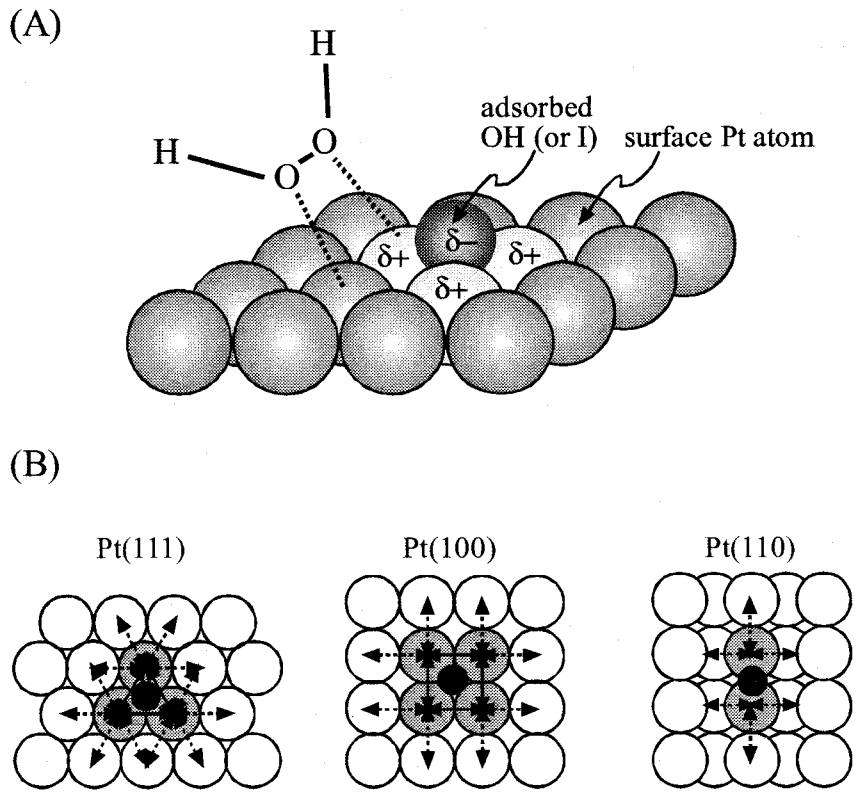

Fig. 7 Schematic illustration of the autocatalytic effect of adsorbed OH and the catalytic effect of adsorbed iodine. (A) The dissociative adsorption of H_2O_2 is accelerated on positively polarized surface Pt atoms in the neighborhood of adsorbed OH and iodine. (B) The difference in the number of Pt pairs on which accelerated adsorption of H_2O_2 can occur, among Pt(111), (100), and (110).

In conclusion, the present work has revealed that adsorbed iodine has the catalytic effect on the dissociative adsorption of H_2O_2, causing the enhancement of oscillation E. The presence of the catalytic effect of adsorbed iodine, as well as the autocatalytic effect of Pt-OH, and their strong dependence on the atomic-level structure of the Pt surface, are of much interest, showing new mechanisms (or aspects) of electrochemical reactions.

This work was partly supported by a Grant-in-Aid for Scientific Research on Priority Area of "Electrochemistry of Ordered Interfaces" (No. 09237105) from the Ministry of Education, Culture, Sports, Science and Technology, Japan.

References

1. J. L. Hudson and T. T. Tsotsis, *Chem. Eng. Sci.*, **49**, 1493 (1994).
2. T. Z. Fahiday and Z. H. Gu, "Modern Aspects of Electrochemistry Vol. 27", ed by R. E. White, J. O'M. Bockris, and R. E. Conway, Plenum, New York (1995), p.383.
3. M. T. M. Koper, "Advances in Chemical Physics Vol. 92", ed by I. Prigogine and S. A. Rice, John Willey & Sons, New York (1996), p.161.
4. K. Krischer, "Modern Aspects of Electrochemistry Vol. 32", ed by R. E. White, J. O'M. Bockris, and R. E. Conway, Plenum, New York (1995), p.1.
5. B. H. Erné, F. Ozanam, M. Stchakovsky, D. Vanmaekelbergh, J. N. Chazalviel, *J. Phys. Chem. B,* **104**, 5961 (2000).
6. G. Flätgen, K. Krischer, B. Pettinger, K. Doblhofer, H. Junkes, G. Ertl, *Science*, **269**, 668 (1995).
7. I. Z. Kiss, V. Gaspar, J. L. Hudson, *J. Phys. Chem. B*, **104**, 7554 (2000).
8. J. Christoph, R. D. Otterstedt, M. Eiswirth, N. I. Jaeger, J. L. Hudson, *J. Chem. Phys.* **110**, 8614 (1999).
9. P. Strasser, J. Christoph, W. F. Lin, M. Eiswirth, J. L. Hudson, *J. Phys. Chem. A*, **104**, 1854 (2000).
10. N. Mazouz, K. Krischer, G. Flätgen, G. Ertl, *J. Phys. Chem. B*, **101**, 2403 (1997).
11. T. Matsuda, H. Hommura, Y. Mukouyama, S. Yae, Y. Nakato, *J. Electrochem. Soc.*, **144**, 1988 (1997).
12. Y. Mukouayama, H. Hommura, S. Nakanishi, T. Nishimura, H. Konishi, Y. Nakato, *Bull. Chem. Soc. Jpn.* **72**, 1247 (1999).
13. Y. Mukouyama, S. Nakanishi, H. Konishi, and Y. Nakato, *J. Electroanal. Chem.*, **473**, 156 (1999).
14. Y. Mukouyama, S. Nakanishi, T. Chiba, K. Murakoshi, Y. Nakato, *J. Phys. Chem. B*, **105**, 7246 (2001).
15. Y. Mukouyama, S. Nakanishi, H. Konishi, Y. Ikeshima, Y. Nakato, *J. Phys. Chem. B*, **105**, 10905 (2001).
16. Y. Mukouyama, S. Nakanishi, Y. Nakato, *Bull. Chem. Soc. Jpn.*, **72**, 2573 (1999).
17. S. Nakanishi, H. Hommura, Y. Mukouyama, T. Matsuda, Y. Nakato, *Chem. Lett.*, 977 (1998).
18. Y. Mukouyama, T, Nishimura, S. Nakanishi, Y. Nakato, *J. Phys. Chem. B,* 104, 11186 (2000).
19. S. Nakanishi, Y. Mukouayma, K. Karasumi, A. Imanishi, N. Furuya, Y. Nakato, *J. Phys. Chem. B*, **104**, 4181 (2000).

20. G. Flätgen, S. Wasle, M. Lübke, C. Eickes, G. Radhakirishnan, K. Doblhofer, G. Ertl, *Electrochim. Acta*, **44**, 4499 (1999).
21. J. Clavilier, R. Faure, G. Guinet, D. Durand, *J. Electrochem. Soc.*, **107**, 205 (1980).

Chapter 4

Oscillatory Peroxodisulfate Reduction on Pt and Au Electrodes under High Ionic Strength Conditions, Caused by Catalytic Effect of Adsorbed OH

Introduction

Electrochemical reactions with nonlinear kinetics show a variety of interesting dynamic behavior such as periodic and chaotic oscillations.[1-4] Mechanistic studies of electrochemical oscillations have made rapid progress recently, resulting in the classification on the basis of the oscillation mechanisms.[4,5] Very recently, growing attention has been paid to the observation and understanding of spatiotemporal patterns arising from nonlinear kinetics, such as traveling chemical waves[6-10] and Turing patterns.[11]

The author has reported thus far[12-19] that H_2O_2 reduction on Pt electrodes in acidic solution shows at least five oscillations of different types, depending on the electrode potential and the current density, the atomic-level flatness of the electrode surface, and the presence or absence of halogen ions in solution. The finding of such new oscillations led to the improvement of the classification of electrochemical oscillations.[15,16] Moreover, the studies have revealed new mechanisms for electrochemical reactions themselves, such as an autocatalytic effect of adsorbed OH on the dissociative adsorption of H_2O_2[12,17] and a catalytic effect of adsorbed halogen on the same reaction,[16,19] which will be important not only for oscillation studies but also for exploration of new active electrode materials for fuel cells. A similar autocatalytic effect of adsorbed OH is reported for an oscillation in H_2O_2 reduction on Ag electrodes.[20]

Unfortunately, modern atomic-level techniques for further confirmation of the above new mechanisms, such as electrochemical quartz crystal microbalance (EQCM) and FTIR techniques, are difficult to apply to adsorbed OH that is the key intermediate of the H_2O_2 reduction. Thus, the author started studies on electrochemical oscillations in $S_2O_8^{2-}$ reduction, to which the EQCM and FTIR techniques will be applicable because of the large mass of adsorbed $S_2O_8^{2-}$ and SO_4^{2-} and strong IR absorption of adsorbed SO_4^{2-} at 1100 to 1200 cm^{-1}. The purpose of the present paper is to find an oscillation mechanism in the $S_2O_8^{2-}$-reduction system, similar to that found in the H_2O_2-reduction system, which enables to use the above atomic level techniques for the further confirmation of the mechanism.

The electrochemical oscillation in the $S_2O_8^{2-}$ reduction was first reported by Frumkin et al,[21] and since then, a lot of investigations have been done on this system.[22-27] However, most studies have been made using electrolytes of low ionic strength, in which the origin of the oscillations (or the negative differential resistances) comes from the electrostatic repulsion of a negatively charged electrode to electroactive anions, $S_2O_8^{2-}$ (so called the Frumkin effect). In the present work, the author used

electrolytes of high ionic strength, in which the Frumkin effect is neglected, and found that the $S_2O_8^{2-}$ reduction on Pt or Au electrodes show four oscillations of different types (named oscillation α, β, γ, and δ). Detailed studies have revealed that oscillation γ, appearing in the most positive potentials, arises from the catalytic effect of adsorbed OH on the dissociative adsorption of $S_2O_8^{2-}$, similarly to oscillations C and E in the H_2O_2-reduction system.

Experimental

Polycrystalline Pt (99.9 % in purity) and Au (99.99 %) discs of about 6.0 mm in diameter, and single crystal Au (99.999 %) discs of about 2~3 mm in diameter, were used as the working electrode. The poly-Pt and Au discs were polished with 0.06 μm alumina slurry, and immersed in a hot (HNO_3 + H_2O_2) solution for 10 min to remove surface contamination. Just before measurements, cyclic potential scans were repeated between -0.50 and +1.50 V vs. SCE in 0.5 M $HClO_4$ (M = mol/dm^3) for about 30 min for further cleaning of the electrode surface. Single-crystal Au(111), (100), and (110) electrodes with atomically flat surfaces were prepared by the method of Clavilier et al.[28] The details of the preparation method were described in a previous paper.[17]

Current density (j) vs. potential (U) curves and j vs. time (t) curves were measured with a potentiogalvanostat (Nikko-Keisoku, NPGS-301) and a potential programmer (Nikko-Keisoku NPS-2), using a Pt plate (10×10 mm^2) as the counter electrode, and a saturated calomel electrode (SCE) as the reference electrode. The data were recorded with an X-Y recorder (Riken-Denshi F-35C) or a data-storing system (instruNET, GW Instruments) with a sampling frequency of 1 kHz. The electrolyte solutions were prepared using special grade chemicals and pure water, the latter of which was obtained by purification of deionised water with a Milli-Q water purification system. The electrolyte solutions were kept stagnant during measurements. The ohmic drops in the solution between the working electrode and the reference electrode were not corrected in the present work.

Impedance measurements were carried out with a Solartron 1260 impedance analyzer combined with a Solartron 1287 electrochemical interface potentiostat. The amplitude of modulation potential was 10 mV. Just before the measurements, the electrode potential was held at a potential at which the measurement was done, for about 180 s, in order to accomplish a steady distribution of the $S_2O_8^{2-}$ concentration.

Results

Figures 1 and 2 summarize four electrochemical oscillations, named oscillation α, β, γ, and δ, observed for the $S_2O_8^{2-}$ reduction on poly-Au (Fig. 1) and poly-Pt (Fig. 2) electrodes. Figure 3 summarizes, for reference in later discussion, reported oscillations for the H_2O_2 reduction on Pt.[15,17]

Figure 1(a) is a *j-U* curve for poly-Au in 0.5 M $HClO_4$ without $S_2O_8^{2-}$, which is included to show the potential region of formation and disappearance of surface Au-oxide. No current peaks corresponding to hydrogen adsorption and desorption are observed for Au, contrary to the case of Pt (cf. Fig. 2a). When 0.5 M $Na_2S_2O_8$ is added to the solution (Fig. 1b), a cathodic current due to the $S_2O_8^{2-}$ reduction starts at about 0.4 V vs. SCE, just a potential at which the reduction of surface Au-oxide is nearly completed (Fig. 1a). According to the work by Müller et al.[29,30] and Samec et al.[26,31] using rotating Au electrodes, the $S_2O_8^{2-}$ reduction on Au proceeds via two pathways. The first one is initiated by the dissociative adsorption of $S_2O_8^{2-}$, probably followed by immediate reduction of adsorbed $SO_4^{\cdot -}$ radicals,

$$S_2O_8^{2-} \rightarrow 2\ SO_4^{\cdot -}{}_{ad} \qquad (1a)$$

$$SO_4^{\cdot -}{}_{ad} + e^- \rightarrow SO_4^{2-}{}_{ad} \qquad (1b)$$

This pathway gives a current near the onset of the $S_2O_8^{2-}$ reduction in a region from + 0.4 to 0 V (see Fig. 1b). The other pathway is a direct reduction of $S_2O_8^{2-}$ via no adsorption

$$S_2O_8^{2-}{}_{aq} + e^- \rightarrow SO_4^{\cdot -}{}_{aq} + SO_4^{2-}{}_{aq} \qquad (2a)$$

$$SO_4^{\cdot -}{}_{aq} + e^- \rightarrow SO_4^{2-}{}_{aq} \qquad (2b)$$

and the corresponding current is observed in a region of more negative potentials from 0 to –0.6 V or further negative potentials. Hydrogen evolution starts at about –0.8 V in Fig. 1(b).

Under current-controlled conditions for Au electrodes, three oscillations (oscillations β, γ, and δ) appear, as shown in Figs. 1(c) and (d). It is to be noted that oscillation γ appears in a region of the most positive potentials, i.e., in a potential region of reaction (1). On the other hand, oscillation β appears in a potential region of reaction (2) and hydrogen evolution, similarly to oscillation B in the H_2O_2-reduction system which also appears in a region of hydrogen evolution (Fig. 3).[12,13,16] Zelin et al.[32] reported an oscillation for the $S_2O_8^{2-}$ reduction on Ag in 1.0 M NaOH, which may correspond to oscillation β in the present work. Oscillation δ appears between oscillations γ and β when the scan rate of *j* is made high (Fig. 1d). Oscillation δ was unstable under a constant current density, weakened in the amplitude with time and

finally disappearing.

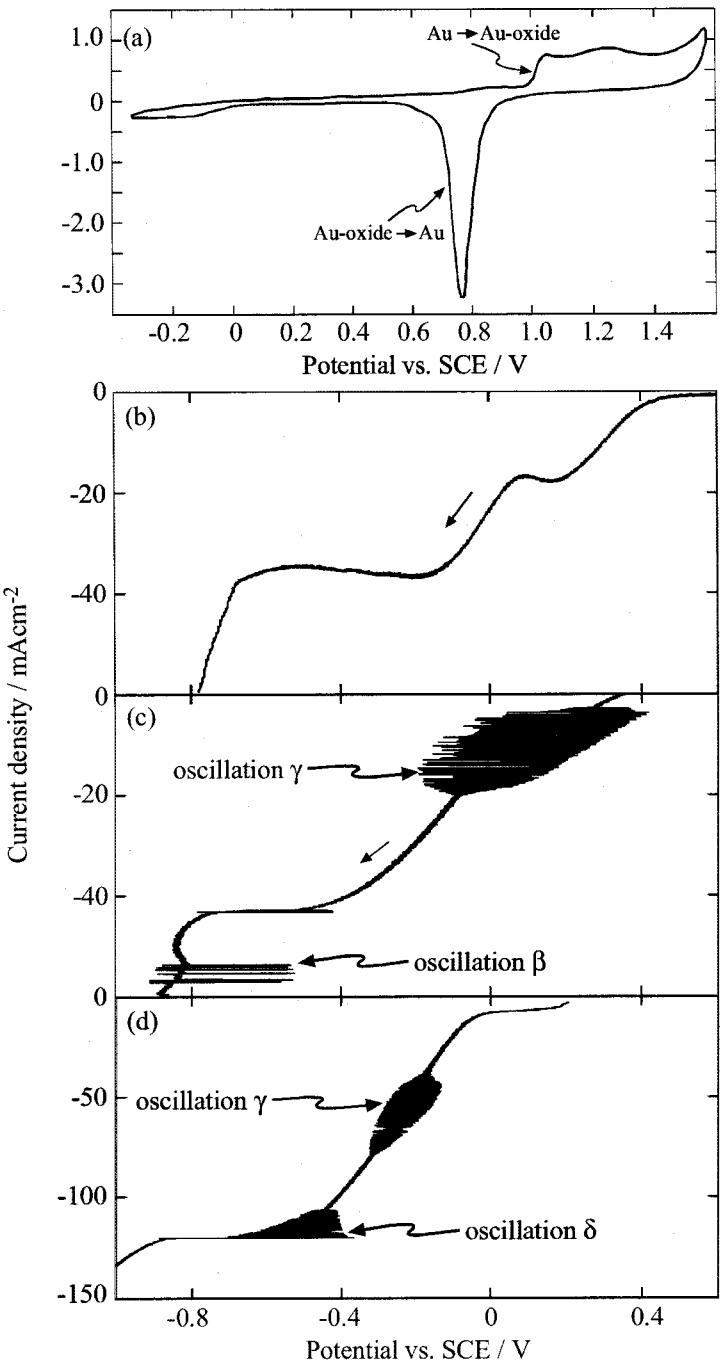

Fig. 1 Current density (j) vs. potential (U) curves for poly-Au under, (a) and (b), potential-controlled and, (c) and (d), current-controlled conditions. Electrolyte: (a) 0.5 M $HClO_4$, and (b), (c), and (d) 0.5 M $HClO_4$ + 0.5 M $Na_2S_2O_8$. Scan rate: (a) 100 mV/s, (b) 10 mV/s, (c) 1mA/s, and (d) 10 mA/s.

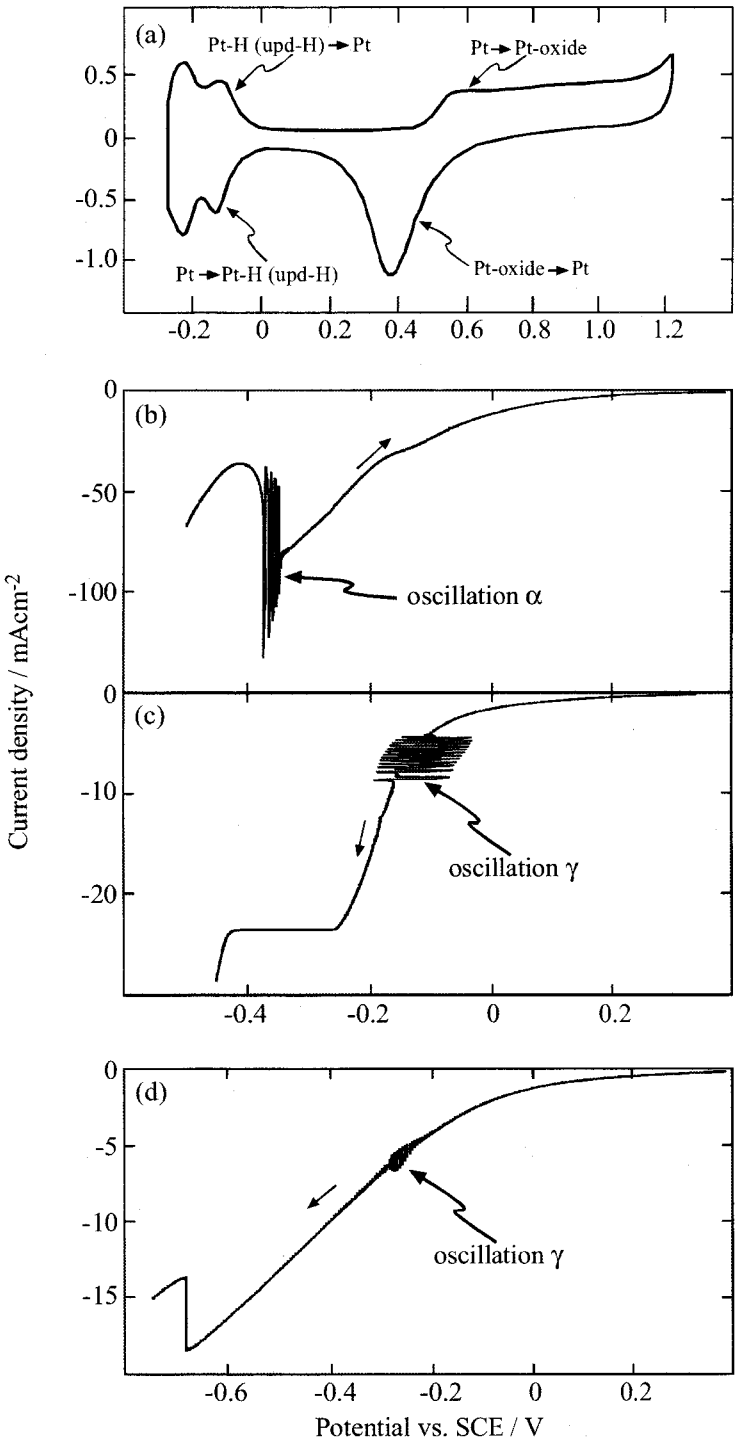

Fig. 2 *j-U* curves for poly-Pt under (a), (b), and (d) potential-controlled and (c) current-controlled conditions. Electrolyte: (a) 0.5 M $HClO_4$, (b) 0.5 M $HClO_4$ + 0.7 M $Na_2S_2O_8$, and (c) and (d) 0.5 M $HClO_4$ + 0.5 M $Na_2S_2O_8$. Scan rate: (a) 100 mV/s, (b) and (d) 10 mV/s, and (c) 1mA/s. An external resistance of 120 Ω is added for (d).

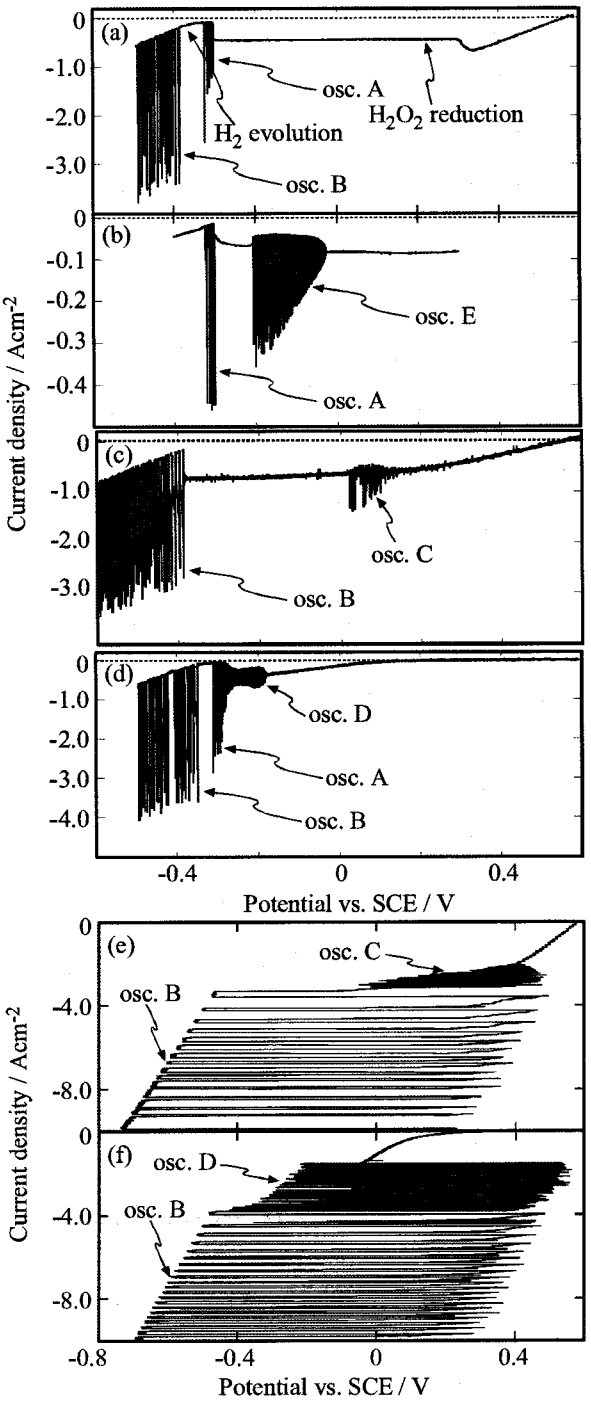

Fig. 3 Reported five oscillations, called oscillation A, B, C, D, and E, observed for the H_2O_2 reduction on Pt in an acidic solution under (a) ~ (d) potential-controlled and (e) and (f) current-controlled conditions. Electrode: poly-Pt except that single-crystal Pt (111) is used for (b). Oscillation E is observed only for Pt(111). Electrolyte: 0.3 M H_2SO_4 containing (a) 0.7 M H_2O_2, (b) 1.0 M H_2O_2, (c) and (e) 1.2 M H_2O_2 + 1.0×10^{-3} M KCl, and (d) and (f) 0.7 M H_2O_2 + 1.0×10^{-4} M KBr.

Figure 2 shows *j-U* curves for poly-Pt. When 0.7 M $S_2O_8^{2-}$ is added (Fig. 2b), the $S_2O_8^{2-}$-reduction current starts at about 0.2 V, at which the reduction of surface Pt-oxide is nearly completed (Fig. 2a), and increases (in the absolute value) with the decreasing potential, in a similar manner to the case of Au electrodes. (Note that the current peaks in Fig. 2(a) are not observed in Fig. 2(b) owing to a large difference in the current-density scale.) Hydrogen evolution starts at about –0.4 V, and in a narrow potential region just before it, oscillation α appears (Fig. 2b). This behavior of oscillation α is the same as that of oscillation A in the H_2O_2-reduction system (Fig. 3). The author reported previously[12,13] that oscillation A arises from an NDR due to the suppression of the H_2O_2 reduction by the formation of upd-H (under-potential deposited hydrogen) of a nearly full coverage. Oscillation α in Fig. 2(b) may thus appear by the same mechanism as oscillation A, a slight negative shift of the potential region of oscillation α from that of the upd-H in Fig. 2(a) being attributed to the ohmic drop in solution. This explanation is supported by the fact that oscillation α appears only for Pt electrodes on which upd-H is formed, not for Au.

Under current-controlled conditions for Pt electrodes, oscillation γ is observed, similar to the case of Au, though oscillations β and δ are not observed. Oscillation γ for Pt appears in the most positive potentials. In addition, oscillation γ appears under potential-controlled conditions if an external resistance of about 120 Ω is added (Fig. 2d). The author can thus say that oscillation γ is of a character similar to oscillation C in the H_2O_2-reduction system, which is also observed under both current- and potential-controlled conditions in a region of the most positive potentials (Fig. 3).

The author made detailed studies on oscillation γ because it appears initially and thus its mechanism may be understood most easily. Figure 4 shows a waveform of oscillation γ as a potential oscillation at -10 $mAcm^{-2}$ in 0.7 M $Na_2S_2O_8$ + 0.5 M $HClO_4$. The stable and periodic oscillation continued for about 10 min or more. Figure 5 shows an impedance diagram for poly-Au in 0.7 M $Na_2S_2O_8$ + 0.5 M $HClO_4$ at –0.16 V vs. SCE, near which oscillation γ appears (Fig. 1c). The diagram clearly shows the presence of an HNDR (i.e., negative differential resistances in a region of intermediate frequencies and positive differential resistances in low frequencies), indicating that oscillation γ is an HNDR oscillator. Oscillation C is also classified into HNDR oscillators.[15]

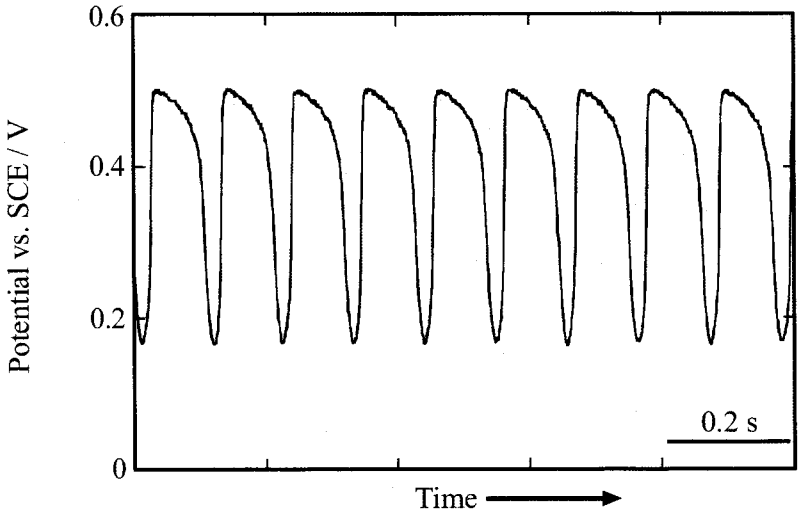

Fig. 4 Potential (U) vs. time (t) curve at -10 $mAcm^{-2}$ for poly-Au in 0.5 M $HClO_4$ + 0.7 M $Na_2S_2O_8$.

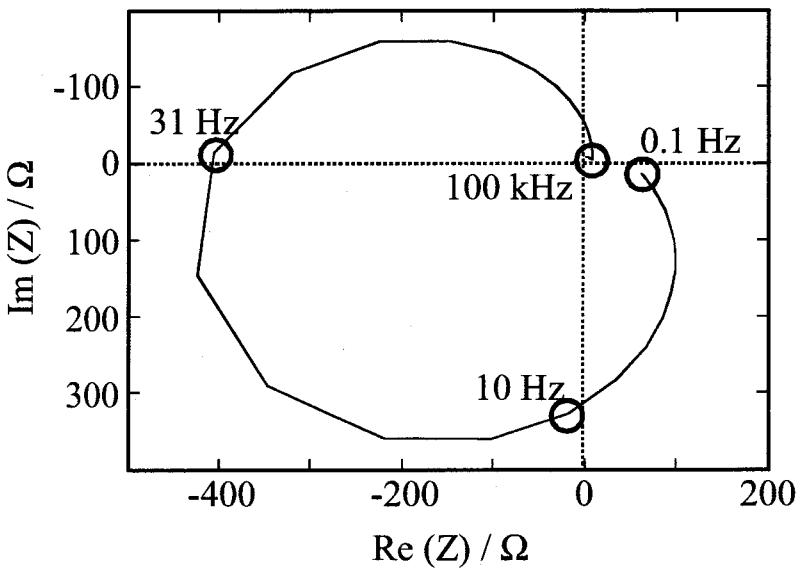

Fig. 5 Impedance diagram for poly-Au at –0.16 V vs. SCE in 0.5 M $HClO_4$ + 0.7 M $Na_2S_2O_8$.

In accordance with the above result, the *j-U* curves under potential-controlled conditions, measured at a high scan rate of 100 mV/s, showed an NDR in a region of 0.2 to 0.0 V (Fig. 6), though the NDR is not clear at a low scan rate (Fig. 1b). The NDR at a high scan rate was observed prominently for atomically flat Au(111), but not for Au(100) and Au(110) (Fig. 6a). The atomically roughened Au(111), prepared by repeated electrochemical oxidation and re-reduction[17,33], also showed no NDR (Fig. 6b). Quite the same behavior was observed for the NDR in the H_2O_2-reduction system, from which oscillation C as well as oscillation E appear. Namely, the NDR in the H_2O_2-reduction system, originating from an autocatalytic effect of adsorbed OH on the dissociative adsorption of H_2O_2, was prominent for atomically flat Pt(111), but not for Pt(100) and Pt(110) and atomically roughened Pt(111).[17] This fact strongly suggests that the NDR in Fig. 6 appears by a similar mechanism to the above NDR in the H_2O_2-reduction system, or in other words, oscillation γ appears by a similar mechanism to oscillation C. Why the NDR is observed only at high scan rates and for atomically flat Au (111) (Fig. 6) will be explained in the next section.

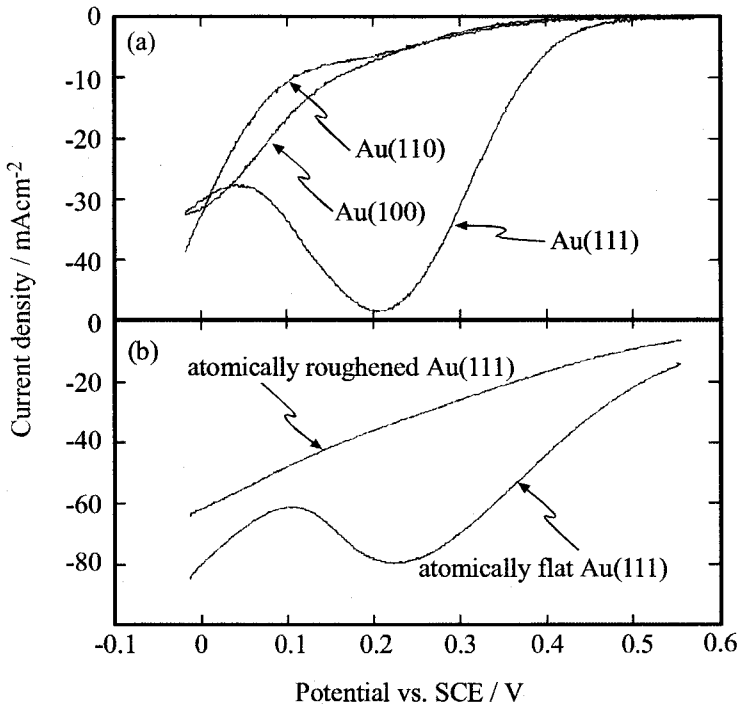

Fig. 6 Dependences of the *j-U* curves on (a) the crystal faces and (b) the surface atomic flatness for single-crystal Au electrodes under potential-controlled conditions. Electrolyte: 0.5 M $HClO_4$ + 0.7 M $Na_2S_2O_8$. The scan rate is 100 mV/s.

Oscillation γ is classified into an HNDR oscillator, as mentioned earlier (Fig. 5). In order to clarify what is the NDR-hiding species, the author investigated the effect of addition of SO_4^{2-} ions to the solution, which are a product of the $S_2O_8^{2-}$ reduction (reaction 1). Figure 7 shows that the NDR, observed in +0.05 to –0.05 V in the absence of SO_4^{2-}, is gradually hidden with the increasing concentrations of added SO_4^{2-}, accompanied by a decrease in the $S_2O_8^{2-}$-reduction current, which strongly suggests that adsorbed SO_4^{2-} is an NDR-hiding species.

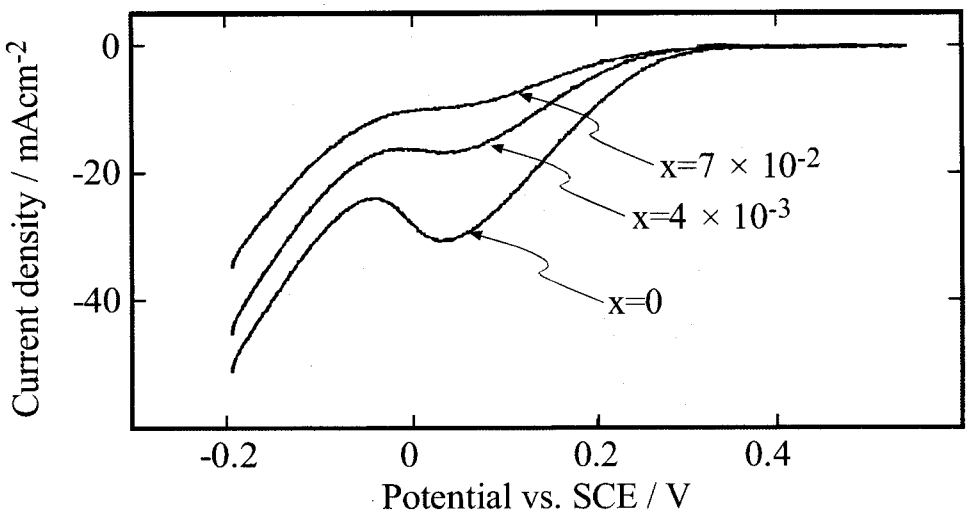

Fig. 7 Effect of addition of SO_4^{2-} to the solution on the *j-U* curves for poly-Au under potential-controlled conditions. Electrolyte: 0.5 M $HClO_4$ + 0.7 M $Na_2S_2O_8$ + *x* M Na_2SO_4, where *x* is indicated in the figure. The scan rate is 100 mV/s.

Mathematical Simulation

The experimental results indicate that (1) oscillation γ appears in a potential region where the $S_2O_8^{2-}$ reduction proceeds via its dissociative adsorption (reaction 1), (2) oscillation γ is an HNDR oscillator, (3) the NDR is likely to arise form a catalytic effect of adsorbed OH on the dissociative adsorption of $S_2O_8^{2-}$, and (4) the NDR-hiding species is most probably adsorbed SO_4^{2-} produced by reaction (1). Thus, there is a good parallelism between oscillation γ and previously reported oscillation C, which also appeared from the NDR due to the autocatalytic effect of adsorbed OH on the dissociative adsorption of H_2O_2, with adsorbed halogen as the NDR-hiding species.

The observation of the NDR for oscillation γ only at high scan rates and for atomically flat Au (111) (Fig. 6) can be explained, based on the reported mechanism[15,17] in the H_2O_2 reduction system, as follows: First, the surface coverage (θ_{OH}) of adsorbed OH, acting as a catalyst for reaction (1a), decreases with a negative potential scan, which leads to a decrease in the $S_2O_8^{2-}$-reduction current with the negative potential scan, i.e., the appearance of an NDR. The observation of the NDR only at high scan rates (or the disappearance of the NDR at low scan rates) can be attributed to *slow* desorption of adsorbed SO_4^{2-} produced by reaction (1). Namely, at low scan rates, the decrease in the amount of adsorbed OH due to the decrease in θ_{OH} is compensated by an increase in empty surface sites by desorption of adsorbed SO_4^{2-}. The observation of the NDR only for flat Au (111) can be attributed to the effective autocatalytic effect of adsorbed OH on this face[17,19], as explained in more detail later (Fig. 10).

The author made mathematical simulation for oscillation γ based on the above model. The author took into account the catalytic effect of adsorbed OH on reaction (1a) by expressing the rate constant k_{1a} as follows:

$$k_{1a} = k_{1a0} + \zeta \theta_{OH} \quad (3)$$

where k_{1a0} is a normal rate constant, and ζ is a proportional constant. The following reactions were considered in addition to the aforementioned reactions (1a) and (1b).

$$SO_4^{2-}{}_{ad} \rightarrow SO_4^{2-}{}_{aq} \quad (4)$$

$$OH_{ad} + H^+ + e^- \leftrightarrow H_2O \quad \text{(in the presence of } S_2O_8^{2-}\text{)} \quad (5)$$

The rate constant for electrochemical reaction (i), k_i, was given by the Butler-Volmer equation with the conventional notations.[12,14]

$$k_i = k_{i0} \exp[-\alpha n F(E-E_{i0})/RT] \quad (6)$$

The differential equations for a current balance, mass balances, and rate equations, were given in the same way as in previous work.[12,14-19]

$$I = jA = (U-E)/R_\Omega = I_C + I_F = AC_{DL}(dE/dt) + I_F \quad (7)$$

$$I_F = AF(-k_{1b}\theta_1) \quad (8)$$

$$(\delta/2)\, dC_{SO}^{s}/dt = (D/\delta)(C_{SO}^{b} - C_{SO}^{s}) - k_{1a}C_{SO}^{s}(1 - \theta_1 - \theta_2 - \theta_{OH})^2 \quad (9)$$

$$N_0 d\theta_1/dt = 2k_{1a}C_{SO}^{s}(1 - \theta_1 - \theta_2 - \theta_{OH})^2 - k_{1b}\theta_1 \quad (10)$$

$$N_0 d\theta_2/dt = k_{1b}\theta_1 - k_4\theta_2 \quad (11)$$

where θ_1 and θ_2 are the surface coverages of adsorbed $SO_4^{\cdot-}$ and SO_4^{2-}, respectively, and C_{SO}^{s} and C_{SO}^{b} the concentrations of $S_2O_8^{2-}$ at the electrode surface and in the solution bulk, respectively. D is the diffusion coefficient for $S_2O_8^{2-}$, δ the thickness of a diffusion layer for $S_2O_8^{2-}$, and N_0 the total amount of surface sites per unit area.

The site-blocking effect of adsorbed SO_4^{2-} (slow species), together with those of adsorbed $SO_4^{\cdot-}$ and OH, were taken into account by introducing such terms as $(1 - \theta_1 - \theta_2 - \theta_{OH})$ in the rate equations. The rate of reaction (5) was not explicitly considered in equation (8), because reaction (5) is actually a complex reaction, affected by a certain action of $S_2O_8^{2-}$ ions (as discussed later). The calculation of j-U curves with the neglect of reaction (5) reproduced well the observed curves, as mentioned later, indicating that reaction (5) makes no substantial contribution to the current.

The θ_{OH} vs. E relation can be expressed, if the author can assume that reaction (5) is in equilibrium at every (true) electrode potential (E), in the form[12],

$$\theta_{OH} = 1/[1 + \exp\{-a(E - E_{50}')\}] \quad (12)$$

where a equals (RT/nF) and E_{50}' refers to the apparent equilibrium potential for reaction (5) in the presence of $S_2O_8^{2-}$. The E_{50}' will be somewhat more negative than the (true) equilibrium potential, E_{50}, for reaction (5) in the absence of $S_2O_8^{2-}$. In the present work, E_{50}' was estimated from the reported experiment[34] discussed later, and a was taken as a parameter. Figure 8(a) shows a θ_{OH} vs. E relation calculated with $a = 45\ V^{-1}$ and $E_{50}' = +0.2$ V vs. SCE. The θ_{OH} changes from nearly one to nearly zero in a range of E from about 0.3 to 0.1 V.

Figure 8(b) shows a j-U curve calculated by use of equations (7) ~ (12) under the condition that the calculation is carried out within a range of j from zero to -10 $mAcm^{-2}$. The curve reproduces the appearance of oscillation γ as a potential oscillation. If the above condition is removed, computers cannot finish calculations, not giving any j-U curves, because reactions (1), (4), and (5) cannot give current densities higher (in the absolute value) than about 10 $mAcm^{-2}$. This is because, at more negative potentials than the calculated potential region in Fig. 8(b), θ_{OH} approaches zero and k_{1a} becomes quite small ($k_{1a} \approx k_{1a0}$), leading to small j.

Figure 8(c) shows an improved j-U curve obtained by adding contributions of reaction (2), the second pathway for the $S_2O_8^{2-}$ reduction, and hydrogen evolution

$$H^+ + e \leftrightarrow H_{ad} \quad (13)$$

$$2H_{ad} \rightarrow H_2 \qquad (14)$$

In this case, equations (8) ~ (10) are modified as follows, together with the addition of another differential equation (15) for the coverage (θ_H) of adsorbed hydrogen,

$$I_F = AF\{-k_{1b}\theta_1 - 2\,k_2\,C_{SO}^{s}\,(1-\theta_1-\theta_2-\theta_{OH}-\theta_H) - k_{13}\,C_H^{s}\,(1-\theta_1-\theta_2-\theta_{OH}-\theta_H) + k_{-13}\,\theta_H\} \qquad (8)'$$

$$(\delta/2)\,dC_{SO}^{s}/dt = (D/\delta)(C_{SO}^{b} - C_{SO}^{s}) - k_{1a}C_{SO}^{s}\,(1-\theta_1-\theta_2-\theta_{OH}-\theta_H)^2 - k_2\,C_{SO}^{s}\,(1-\theta_1-\theta_2-\theta_{OH}-\theta_H) \qquad (9)'$$

$$N_0 d\theta_1/dt = 2k_{1a}C_{SO}^{s}(1-\theta_1-\theta_2-\theta_{OH}-\theta_H)^2 - k_{1b}\theta_1 \qquad (10)'$$

$$N_0 d\theta_H/dt = k_{13}\,C_H^{s}\,(1-\theta_1-\theta_2-\theta_{OH}-\theta_H) - k_{-13}\,\theta_H - 2\,k_{14}\,\theta_H^2 \qquad (15)$$

where k_{13} and k_{-13} are the rate constants for the forward and backward processes of reaction (13), respectively, and C_H^{s} the surface concentration of H^+ ions. The *j-U* curve in Fig. 8(c) is in good agreement with the observed curves (Figs. 1c and 2c), except the appearance of oscillation β. Figure 9 shows a calculated *E-t* curve at a constant current density of -10 $mAcm^{-2}$, together with θ_1-*t*, and θ_2-*t* curves. The calculated *E-t* reproduces the essential feature of the waveform of oscillation γ as a potential oscillation (Fig. 4).

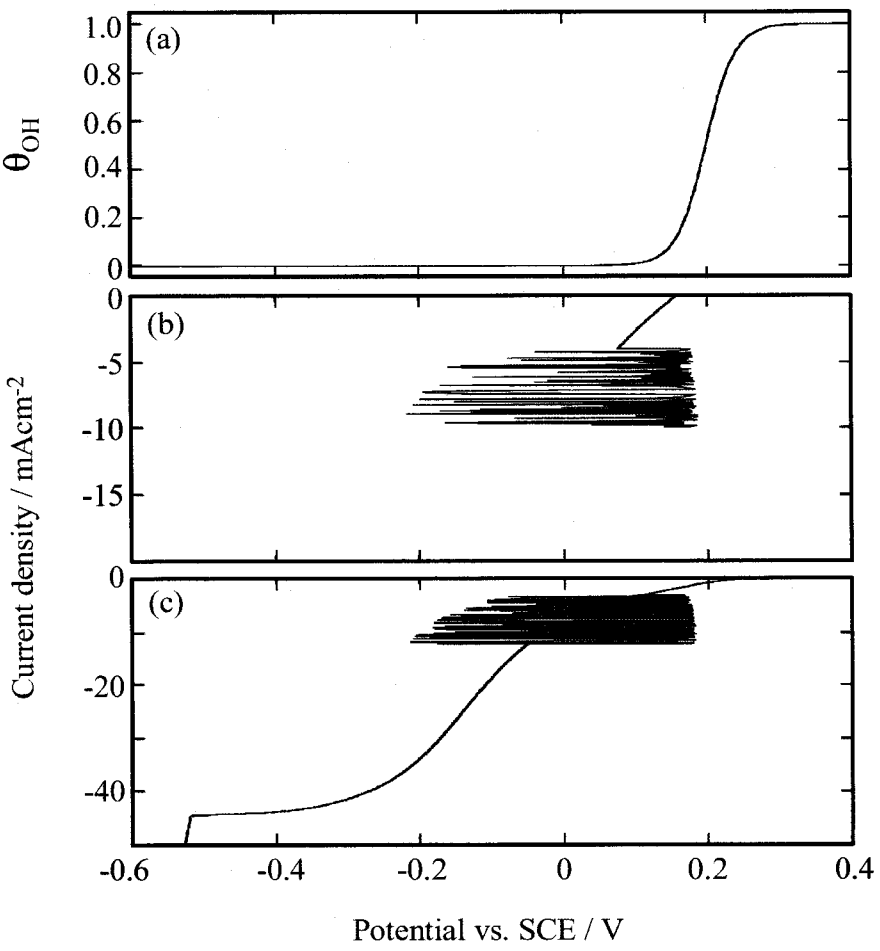

Fig. 8 (a) θ_{OH} vs. E, calculated by Eq. (12) with a = 45 V^{-1} and E_{50}' = +0.2 V vs. SCE. (b) j vs. U calculated by Eqs. (7) ~ (12) with k_{1a0} = 4.5 × 10^{-3} cm s^{-1}, ζ = 5, and a scan rate of 2 mA/s, under the condition that the calculation is carried out within a range of j from zero to −10 mAcm^{-2}. (c) Improved j vs. U calculated by adding contributions of reaction (2) and hydrogen evolution. Other parameter values are C_{SO}^{b} = 0.7 × 10^{-3} mol cm^{-3}, δ= 0.015 cm, D = 5.0 × 10^{-6} cm^2 s^{-1}, A = 0.28 cm^2, C_{DL} = 2.0 × 10^{-5} F cm^{-2}, N_0 = 2.2 × 10^{-9} mol cm^{-2}, R_Ω = 10 Ω, T = 300 K, α_i = 0.25 for i = 1b and 4 and 0.50 for others, n = 1, k_{1b0} = 6.5 × 10^{-4} mol cm^{-2} s^{-1}, E_{1b0} = 1.0 V vs. SCE, k_{20} = 1.0 × 10^{-8} cm s^{-1}, E_{20} = 0.4 V, k_{40} = 3.0 × 10^{-9} mol cm^{-2} s^{-1}, E_{40} = 0.5 V.

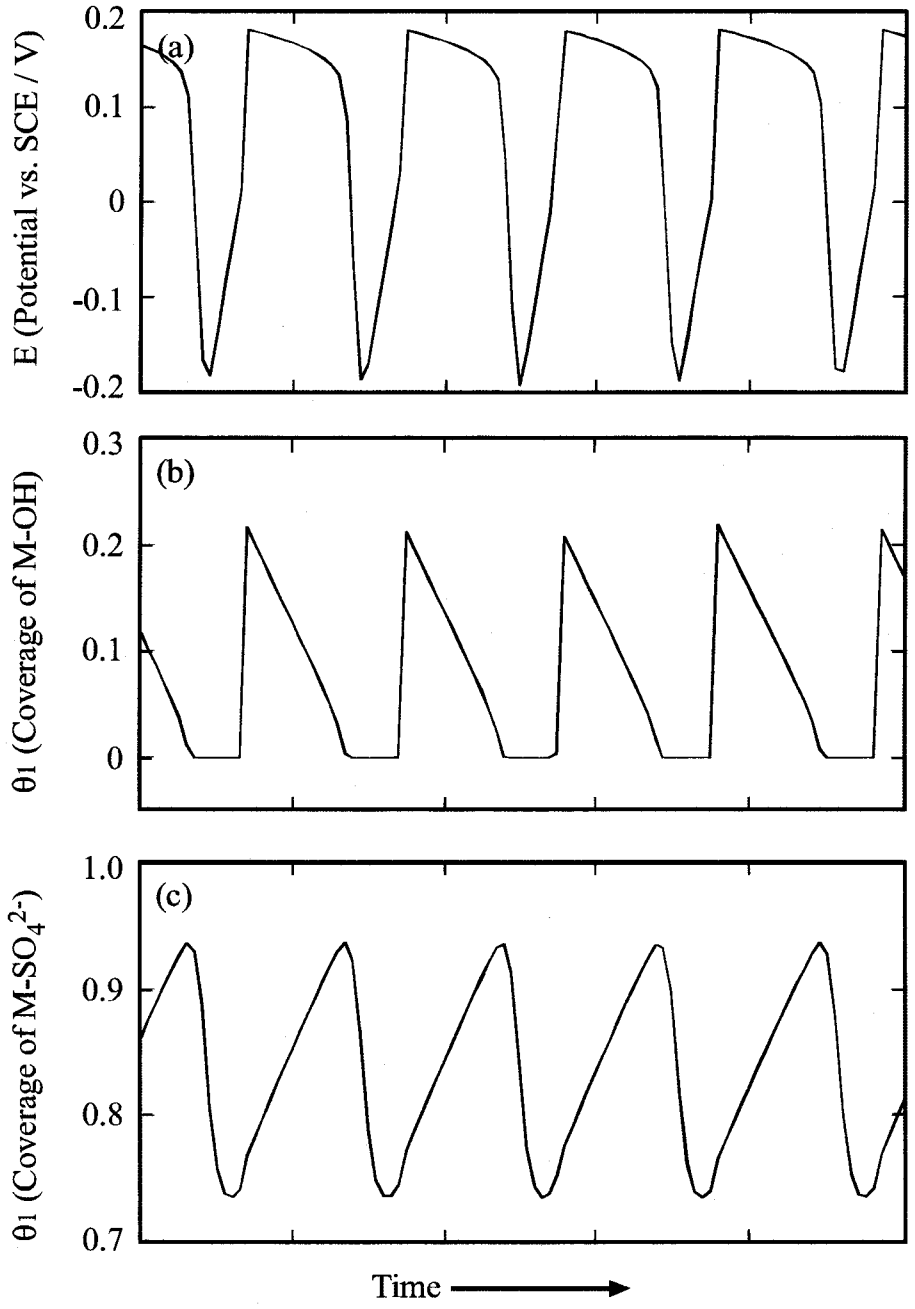

Fig. 9 Calculated E-t, θ_1-t, and θ_2-t curves at j = -10 mAcm^{-2}. The parameter values are the same as in Fig. 8.

Discussion

The experimental results and mathematical simulation have shown that oscillation γ is an HNDR oscillator and the NDR arises from the catalytic effect of adsorbed OH on the dissociative adsorption of $S_2O_8^{2-}$. Here arises a question whether the adsorbed OH can exist even in a potential region of oscillation γ, which is considerably more negative than the current peak for the reduction of surface Au- or Pt-oxide (Figs. 1a and 2a). It is reported by surface-enhanced Raman spectroscopy (SERS)[34] that, in the presence of 1~20 mM $S_2O_8^{2-}$, oxygen-containing adsorbed species (most probably attributable to adsorbed OH) survives on Au down to potentials 0.3 to 0.4 V more negative than the reduction peak of surface oxide. The strong oxidant, $S_2O_8^{2-}$, is likely to induce chemical (or electrochemical) oxidation of the Au surface leading to formation of adsorbed OH, though the detailed mechanism is unknown.

The effect of addition of SO_4^{2-} ions to the solution (Fig. 7) shows that adsorbed SO_4^{2-} acts as the NDR-hiding species. Oscillation γ appears without any addition of SO_4^{2-}, because adsorbed SO_4^{2-}, produced by the $S_2O_8^{2-}$ reduction (reaction 1b), can act as the NDR-hiding species, as mentioned before. This is an interesting example, for, in most cases, adsorbed species as the NDR-hiding species are supplied by the adsorption of solution species added.[5]

Based on the results of mathematical simulation (Figs. 8 and 9), oscillation γ can be explained as follows. In a high-potential state of a potential oscillation at a constant current density, the surface coverage of adsorbed OH (θ_{OH}) is large, and thus $k_{1a} \gg k_{1a0}$, i.e., the $S_2O_8^{2-}$ reduction occurs efficiently, which leads to an increase in the coverage (θ_2) of adsorbed SO_4^{2-} as a product of the $S_2O_8^{2-}$ reduction owing to slow desorption of adsorbed SO_4^{2-} (slow species). The increase in θ_2 leads to a decrease in vacant surface sites at which the dissociative adsorption of $S_2O_8^{2-}$ occurs, thus leading to a negative shift of the electrode potential (E) to promote the SO_4^{2-} desorption and keep a constant current density (j). The negative shift in E, in turn, leads to a decrease in θ_{OH} and hence a decrease in k_{1a} ($= k_{1a0} + \gamma\theta_{OH}$), which leads to a further negative shift in E to keep a constant j. Here is a positive feedback mechanism, and this causes a transition to a low-potential state.

In a low potential state, the desorption of adsorbed SO_4^{2-} becomes fast, which leads to an increase in vacant surface sites for the $S_2O_8^{2-}$ reduction and to a positive shift in E. The positive shift in E leads to an increase in θ_{OH} and k_{1a} and to a further positive shift in E to keep a constant j. Here is also a positive feedback mechanism, which leads to a transition to a high-potential state.

The NDR observed for the $S_2O_8^{2-}$ reduction strongly depends on the crystal faces of single crystal Au electrodes and the atomic flatness at the surface (Fig. 6). The NDR arising from the autocatalytic effect of adsorbed OH in the H_2O_2-reduction system showed quite the same behavior,[17] as already mentioned. The author can assum that the dissociative adsorption of negatively charged $S_2O_8^{2-}$ occurs fast on positively polarized metal atoms in the neighborhood of adsorbed OH (Fig. 10), similar to the case of dissociative adsorption of H_2O_2.[17] The difference in the ζ value in equation (3) among crystal faces of Au electrodes can be attributed to the difference in the number of the positively polarized metal atoms around adsorbed OH, as reported.[17,19]

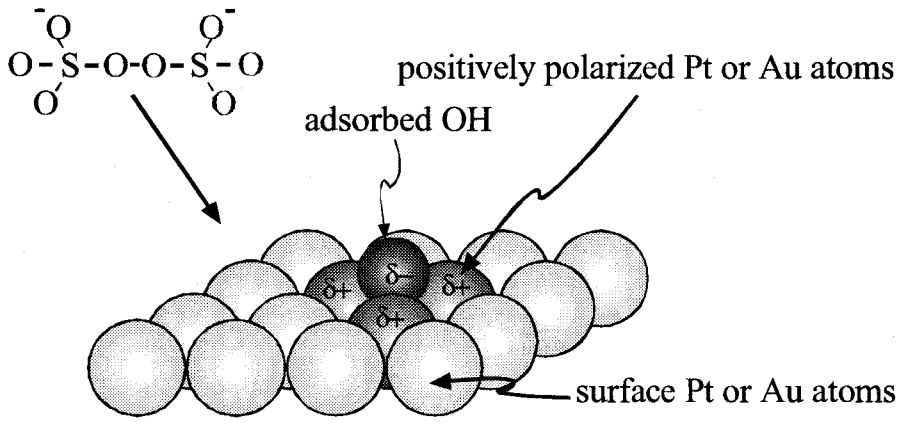

Fig. 10 Schematic illustration of a catalytic effect of adsorbed OH for the dissociative adsorption of $S_2O_8^{2-}$.

Finally, let us consider briefly oscillations other than oscillation γ. Oscillation α is of a character similar to oscillation A in the H_2O_2-reduction system, as mentioned before. This implies that the NDR for oscillation α arises from the suppression of the $S_2O_8^{2-}$ reduction by the formation of upd-H. However, a question remains on how the upd-H suppresses the $S_2O_8^{2-}$ reduction, because in a potential region of oscillation α, the $S_2O_8^{2-}$ reduction is reported to proceed via no adsorption.[31] For oscillations β and δ, impedance measurements revealed that they were of an HNDR-type, though further details are unclear at present. In solutions of high ionic strengths in the present work, oscillations due to the Frumkin effect[26,27] are not observed. On the other hand, oscillations α, β, γ, and δ will in principle be observed in solutions of low ionic strengths, though the appearance of oscillations depends on detailed conditions in various factors. In fact, oscillation α is observed even in 1.0 mM $Na_2S_2O_8$.

In conclusion, the present work has revealed that the $S_2O_8^{2-}$ reduction on Pt and Au in high ionic-strength electrolytes shows four oscillations of different kinds, named oscillation α, β, γ, and δ. Detailed studies on oscillation γ showed that adsorbed OH has a catalytic effect on the dissociative adsorption of $S_2O_8^{2-}$, leading to the appearance of oscillation γ. The present results as well as the reported ones on the H_2O_2 reduction[17,19] show the generality of an autocatalytic (or a catalytic) effect of adsorbed OH on electrochemical reactions.

References

1. J. L. Hudson and T. T. Tsotsis, *Chem. Eng. Sci.*, **49**, 1493 (1994).
2. T. Z. Fahiday and Z. H. Gu, "Modern Aspects of Electrochemistry Vol. 27", ed by R. E. White, J. O'M. Bockris, and R. E. Conway, Plenum, New York (1995), p.383.
3. M. T. M. Koper, "Advances in Chemical Physics Vol. 92", ed by I. Prigogine and S. A. Rice, John Willey & Sons, New York (1996), p.161.
4. K. Krischer, "Modern Aspects of Electrochemistry Vol. 32", ed by R. E. White, J. O'M. Bockris, and R. E. Conway, Plenum, New York (1995), p.1.
5. P. Strasser, M. Eiswirth, M. T. M. Koper, *J. Electroanal. Chem.*, **478**, 50 (1999).
6. G. Flätgen, K. Krischer, B. Pettinger, K. Doblhofer, H. Junkes, G. Ertl, *Science*, **269**, 668 (1995).
7. I. Z. Kiss, V. Gaspar, J. L. Hudson, *J. Phys. Chem. B*, **104**, 7554 (2000).
8. J. Christoph, R. D. Otterstedt, M. Eiswirth, N. I. Jaeger, J. L. Hudson, *J. Chem. Phys.* **110**, 8614 (1999).
9. P. Strasser, J. Christoph, W. F. Lin, M. Eiswirth, J. L. Hudson, *J. Phys. Chem. A*, **104**, 1854 (2000).
10. N. Mazouz, K. Krischer, G. Flätgen, G. Ertl, *J. Phys. Chem. B*, **101**, 2403 (1997).
11. Y. J. Li, J. Oslonovitch, N. Mazouz, F. Plenge, K. Krischer, G. Ertl, *Science*, **291**, 2395 (2001).
12. Y. Mukouyama, S. Nakanishi, Y. Nakato, *Bull. Chem. Soc. Jpn.*, **72**, 2573 (1999).
13. T. Matsuda, H. Hommura, Y. Mukouyama, S. Yae, Y. Nakato, *J. Electrochem. Soc.*, **144**, 1988 (1997).
14. Y. Mukouyama, S. Nakanishi, H. Konishi, and Y. Nakato, *J. Electroanal. Chem.*, **473**, 156 (1999).
15. Y. Mukouyama, S. Nakanishi, T. Chiba, K. Murakoshi, Y. Nakato, *J. Phys. Chem. B*, **105**, 7246 (2001).
16. Y. Mukouyama, S. Nakanishi, H. Konishi, Y. Ikeshima, Y. Nakato, *J. Phys. Chem. B*, **105**, 10905 (2001).
17. S. Nakanishi, Y. Mukouayma, K. Karasumi, A. Imanishi, N. Furuya, Y. Nakato, *J. Phys. Chem. B*, **104**, 4181 (2000).
18. S. Nakanishi, Y. Mukouyama, Y. Nakato, *J. Electrochem. Soc.*, **148**, E405 (2001).
19. S. Nakanishi, Y. Mukouyama, Y. Nakato, *J. Phys. Chem. B*, **105**, 5751 (2001).
20. G. Flätgen, S. Wasle, M. Lübke, C. Eickes, G. Radhakirishnan, K. Doblhofer, G. Ertl, *Electrochim. Acta*, **44**, 4499 (1999).

21. A. N. Frumkin, *Z. Electrochem.*, **59**, 807 (1955).
22. A. Y. Gokhshtein, A. N. Frumkin, *Dokl. Akad. Nauk. SSSR*, **132**, 388 (1960).
23. A. N. Frumkin, O. A. Petti, N. V. Nikolaeva-Fedorovich, *Dokl. Akad. Nauk. SSSR*, **136**, 1158 (1961).
24. M. T. M. Koper, *Ber. Bunsenges. Phys. Chem.*, **424**, 497 (1996).
25. G. Flätgen, K. Krischer, G. Ertl, *J. Electroanal. Chem.*, **409**, 183 (1996).
26. L. Treindl, K. Doblhofer, K. Krischer, Z. Samec, *Electrochim. Acta*, **44**, 3963 (1999).
27. W. Wolf, J. Ye, M. Purgand, M. Eiswirth, K. Doblhofer, *Ber. Bunsenges. Phys. Chem.*, **96**, 278 (1992).
28. J. Clavilier, R. Faure, G. Guinet, D. Durand, *J. Electrochem. Soc.*, **107**, 205 (1980).
29. L. Müller, *J. Electroanal. Chem.*, 13, 275 (1967).
30. L. Müller, W. Wetzel, H. Otto, *J. Electroanal. Chem.*, 24, 175 (1970).
31. Z. Samec, K. Doblhofer, *J. Electroanal. Chem.*, 141, 367 (1994).
32. L. Zelin, W. Tinghua, C. Ke, *Chinese Journal of Chemical Physics (in Chinese)*, 12, 251 (1999).
33. K. Itaya, S. Sugawara, K. Sashikata, N. Furuya, *J. Vac. Sci. Technol.*, **A8(1)**, 515 (1990).
34. J. Desilvestro, M. J. Weaver, *J. Electroanal. Chem.*, 234, 237 (1987).

Chapter 5

Promoted Dissociative Adsorption of Hydrogen Peroxide and Persulfate Ions by a Catalytic Effect of Adsorbed Bromine, Causing Electrochemical Oscillations

Introduction

Electrochemical oscillations in general appear in potential regions of negative differential resistances (NDR's) of current vs. potential curves,[1,2] though the NDR's are sometimes hidden by other electrochemical processes.[2,3] Electrochemical oscillations can also appear in potential regions of normal current vs. potential curves by coupling of electrochemical processes having NDR's in other potential regions.[4] The NDR's arise from various factors[2] such as the formation of inactive layers at the electrode surface, the formation or disappearance of surface catalysts, and the electrostatic repulsion between ionic electroactive species and polarized electrodes. Of these, the NDR's arising from surface catalysts are especially interesting because their studies can serve for exploration of new electrocatalytic reactions and their clarification.

The author reported previously[5-7] that adsorbed OH (and adsorbed iodine) on Pt electrodes promoted the dissociative adsorption of H_2O_2. The author also reported[8] that adsorbed OH on Au and Pt promoted the dissociative adsorption of $S_2O_8^{2-}$. Such a catalytic effect of adsorbed OH caused the appearances of NDR's and electrochemical oscillations in potential regions where the surface coverage of adsorbed OH (θ_{OH}) decreases steeply.[5-8]

In the present paper, the author reports that adsorbed bromine also acts as a catalyst for the dissociative adsorption of H_2O_2 and $S_2O_8^{2-}$, causing the appearance of new NDR's and oscillations.

Experimental

Single-crystal Pt(111), (100), and (110) electrodes with atomically flat surfaces were prepared by the method of Clavilier et al.[9] The details of the preparation method were described elsewhere.[5] Polycrystalline Au (99.99 % in purity) discs of about 6.0 mm in diameter were also used as the working electrode. The poly-Au discs were polished with 0.06-μm alumina slurry, and immersed in hot $HNO_3 + H_2O_2$ for 10 min to remove surface contamination.

Current density (j) vs. potential (U) curves were measured with a potentiogalvanostat (Nikko-Keisoku NPGS-301) and a potential programmer (Nikko-Keisoku NPS-2), using a Pt plate (10×10 mm^2) as the counter electrode, and a saturated calomel electrode (SCE) as the reference electrode. The data were recorded with a data-storing system (instruNET, GW Instruments) with a sampling frequency of 1 kHz. Electrolyte solutions were prepared using special grade chemicals and pure water, the latter of which was obtained by purification of deionised water with a Milli-Q water purification system. The electrolyte solutions were kept stagnant during measurements. The ohmic drops in the solution between the working and the reference electrodes were not corrected in the present work.

Results

Figures 1(a) and 1(b) show, for reference, reported j vs. U curves for H_2O_2 reduction on atomically flat single crystal Pt(111) electrode in relatively low and high H_2O_2 concentrations (0.2 M H_2O_2 + 0.3 M H_2SO_4 and 1.0 M H_2O_2 + 0.3 M H_2SO_4), respectively, under potential-controlled conditions. A cathodic current in a potential region from about +0.55 to –0.08 V is due to the H_2O_2 reduction, which starts at about +0.80 V. Hydrogen evolution starts at about –0.1 V. The H_2O_2-reduction current in 0.2 M H_2O_2 + 0.3 M H_2SO_4 shows two NDR's in regions from +0.02 to –0.08 V and from +0.25 to +0.15 V, as designated as NDR-H and NDR-OH in Fig. 1(a). The origins of the NDR's can be explained as follows. The H_2O_2 reduction is initiated by dissociative adsorption of H_2O_2

$$2Pt + H_2O_2 \rightarrow 2Pt\text{-}OH \qquad (1)$$

followed by electrochemical reduction of the resultant Pt-OH

$$Pt\text{-}OH + H^+ + e^- \rightarrow Pt + H_2O \qquad (2).$$

The potential-independent H_2O_2-reduction current in +0.55 to –0.08 V indicates that reaction-1 is the rate-determining step.[5,6,10] The NDR-H arises from the suppression of reaction-1 by the formation of underpotential deposited hydrogen (upd-H).[10,11] On the other hand, the NDR-OH arises from a decrease in the coverage (θ_{OH}) of adsorbed OH (Pt-OH), which acts as an autocatalyst for reaction-1, with a negative potential shift.[5-7] Namely, the rate constant, k_1, for reaction-1 is expressed as follows

$$k_1 = k_{10} + \kappa\theta_{OH} \qquad (3)$$

where k_{10} is a normal rate constant, and κ is a proportional constant. A negative shift in U leads to a decrease in θ_{OH}, which in turn leads to a decrease in k_1 (equation (3)) and hence a decrease in j. Thus, an NDR (NDR-OH) appears. In a high H_2O_2 concentration (1.0 M H_2O_2 + 0.3 M H_2SO_4), two oscillations, called oscillation A and E, appear in the regions of these NDR-H and NDR-OH (Fig. 1b). Slight shifts in potential between the NDR's and oscillations in Figs. 1a and 1b can be attributed to ohmic drops in the solution.

Figures 1c and 1d show j-U curves when 2 μM KBr was added to 0.2 M H_2O_2 + 0.3 M H_2SO_4 and 0.7 M H_2O_2 + 0.3 M H_2SO_4, respectively. A new NDR, named NDR-Br in Fig. 1c, appears. In accordance with the appearance of the NDR, a new oscillation, named oscillation F, appears in a solution of high H_2O_2 concentration (Fig. 1d).

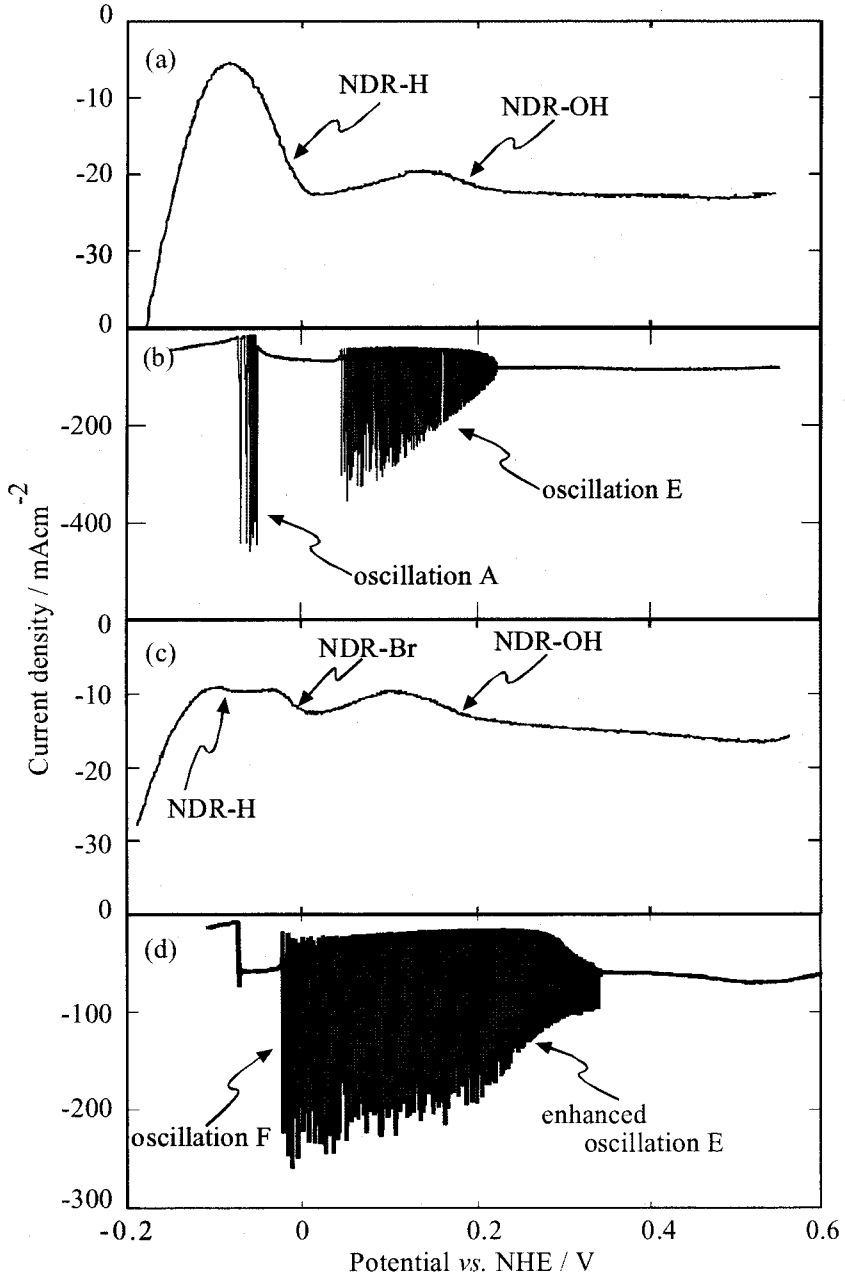

Fig. 1 Effect of Br^- addition on *j-U* curves for H_2O_2 reduction on Pt(111) under potential-controlled conditions. Electrolyte: (a) 0.2 M H_2O_2 + 0.3 M H_2SO_4, (b) 1.0 M H_2O_2 + 0.3 M H_2SO_4, (c) 0.2 M H_2O_2 + 0.3 M H_2SO_4 + 2 μM KBr, and (d) 0.7 M H_2O_2 + 0.3 M H_2SO_4 + 2 μM KBr. Scan rate: (a) and (c) 100 mV/s, and (b) and (d) 10 mV/s.

A similar result was obtained for Pt(100) electrodes, as shown in Fig. 2. The NDR-OH is not so prominent for Pt(100) (Fig. 2a),[5] and oscillation E appears only in some experiments (Fig. 2b). When Br^- was added to the solutions, the NDR-Br and oscillation F appear (Fig. 2c and d), similar to the case of Pt(111). It may be noted that another oscillation, named oscillation G in Fig. 2(d), is observed for Pt(100) in a region of +0.52 ~ +0.46 V, though the origin is unknown at present.

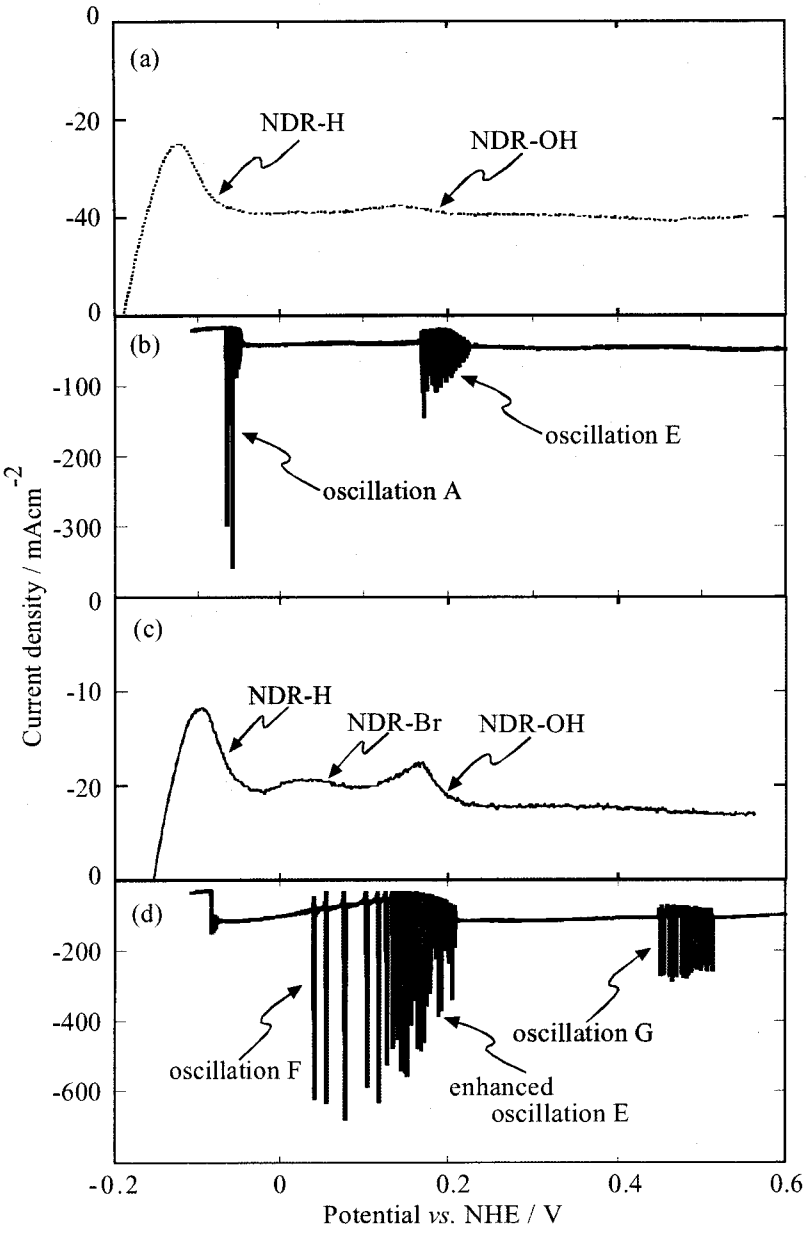

Fig. 2 The same as Fig. 1, except that Pt(100) is used and the H_2O_2 concentration in (b) is 0.7 M.

Figure 3 shows results of similar experiments for Pt(110) electrodes. Neither NDR-OH nor oscillation E appears for Pt(110), contrary to the cases of Pt(111) and Pt(100). Furthermore, neither NDR-Br nor oscillation F appears when Br^- was added.

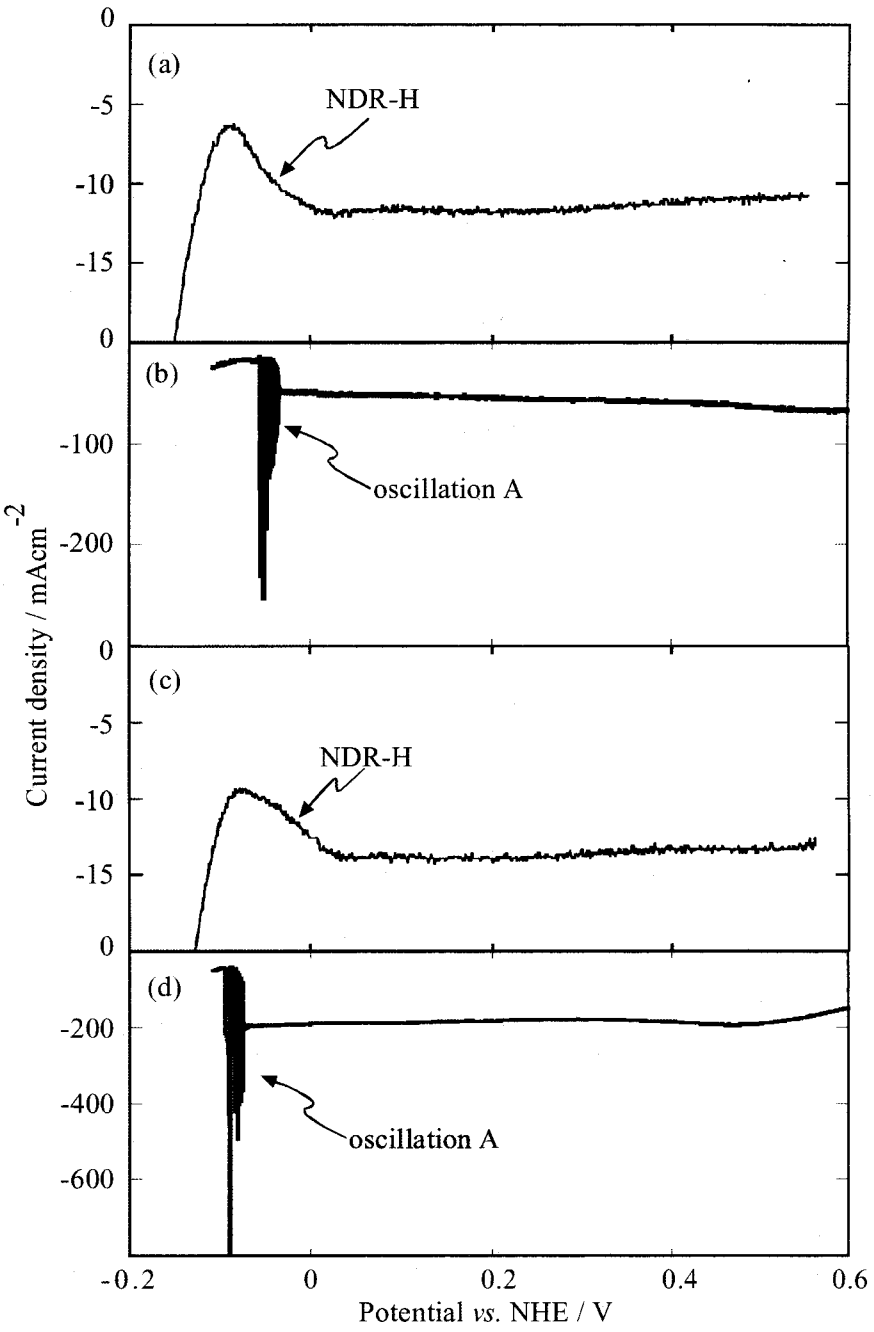

Fig. 3 The same as Fig. 2, except that Pt(110) is used.

Figure 4(a) shows a *j-U* curve for $S_2O_8^{2-}$ reduction on a polycrystalline Au-disc electrode under a potential controlled condition. Two NDR's, NDR-OH and NDR-X (the origin of NDR-X is unknown), are observed in 0.5 M $Na_2S_2O_8$ + 0.5 M $HClO_4$. The $S_2O_8^{2-}$ reduction is reported[12,13] to proceed via the following mechanism in the potential region of NDR-OH,

$$S_2O_8^{2-} \rightarrow 2SO_4\cdot^-_{ad} \quad (4)$$

$$2SO_4\cdot^-_{ad} \rightarrow SO_4^{2-}{}_{ad} \quad (5).$$

Thus, the NDR-OH arises[8] from a catalytic effect of adsorbed OH on the dissociative adsorption of $S_2O_8^{2}$ (reaction-4), similar to the case of the H_2O_2-reduction system. Under current-controlled conditions, a potential oscillation (named oscillation γ) appears in the potential region of NDR-OH[8] (Fig. 4c).

When Br^- ions were added to the solution, a new NDR, named NDR-Br, appears between NDR-OH and NDR-X (Fig. 4b), with the NDR-X shifted to the negative potential. In accordance with the appearance of the NDR-Br, a new oscillation, named oscillation ζ, is observed under current-controlled conditions (Figs. 4d and 4e). It is to be noted that oscillation ζ in the present work appears in a potential region similar to oscillation δ (the mechanism for oscillation δ is unknown) reported previously,[8] though the amplitude of the former is much smaller than that of the latter.

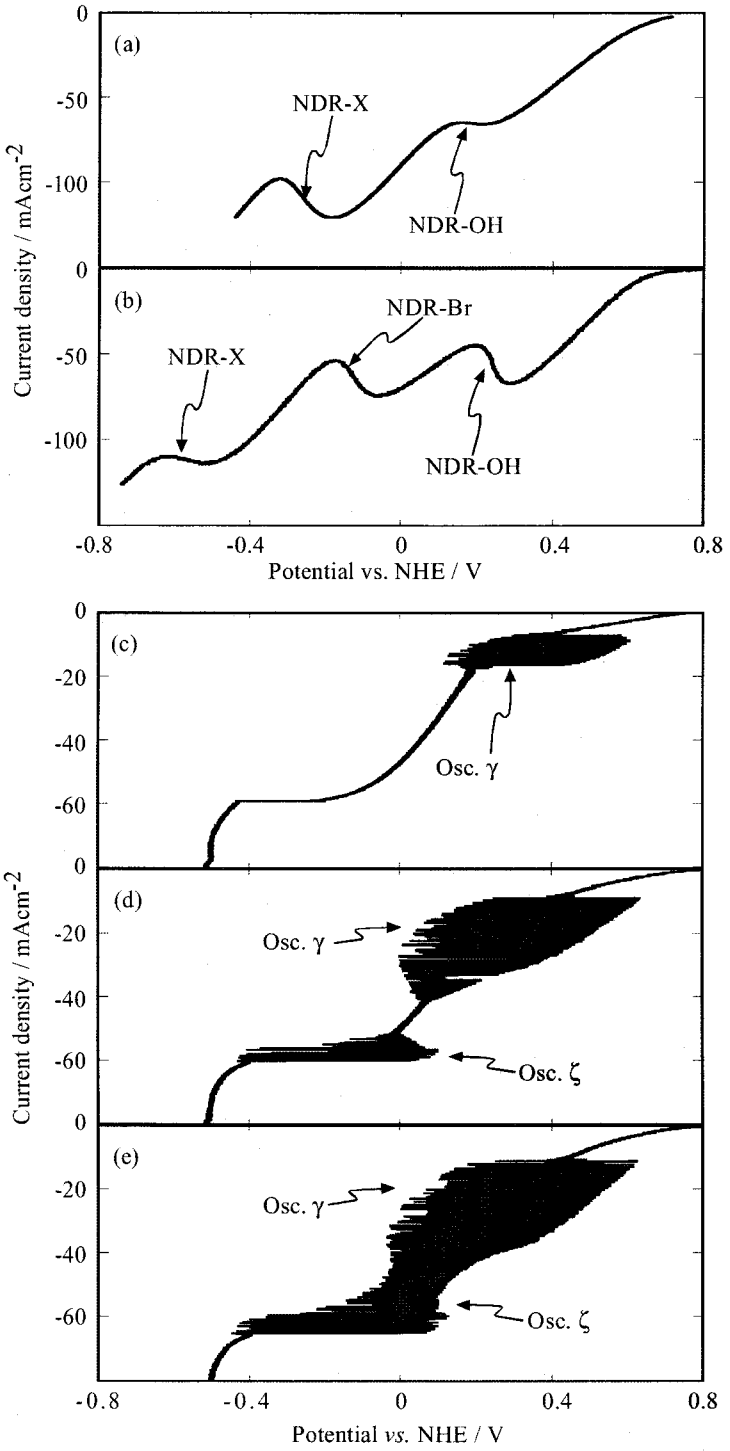

Fig. 4 Effect of Br^- addition on *j-U* curves for $S_2O_8^{2-}$ reduction on poly-Au under, (a) and (b), potential-controlled, and (c)-(e), current-controlled conditions. Electrolyte: (a) and (c) 0.5 M $Na_2S_2O_8$ + 0.5 M $HClO_4$, (b) and (e) 0.5 M $Na_2S_2O_8$ + 0.5 M $HClO_4$ + 15 μM KBr, and (d) 0.5 M $Na_2S_2O_8$ + 0.5 M $HClO_4$ + 12.5 μM KBr. Scan rate: (a) and (b) 100 mV/s, (c), (d), and (e) 1 mA/s.

Discussion

The experimental results clearly show that the addition of Br^- ions to the solution causes the appearances of NDR-Br (Figs. 1c, 2c and 4b) and the corresponding oscillations (oscillation F and ζ) (Figs. 1d, 2d, 4d and 4e). It is to be noted here that the reported potential regions in which the surface coverage (θ_{Br}) of adsorbed Br on Pt and Au changes largely are in good agreement with the potential regions of NDR-Br for Pt and Au electrodes (Figs. 1c, 2c, and 4b), respectively. For example, Ross et al. reported[14] that adsorbed Br on Pt(111) in 0.1 M $HClO_4$ was desorbed in a potential region from +0.10 to –0.12 V. Weaver et al. reported,[15] by surface enhanced Raman spectroscopy (SERS), that adsorbed Br on Pt was desorbed in a region more negative than –0.17 V. They also reported[16] that adsorbed Br on Au was desorbed in a region of –0.17 to –0.57 V. The author can thus conclude that the NDR-Br and oscillations F and ζ arise from adsorbed Br.

The appearance of NDR-Br can be explained quite in the same way as that of NDR-OH.[5,7,8] If adsorbed Br acts as a catalyst for the dissociative adsorption of H_2O_2 (reaction-1) and that of $S_2O_8^{2-}$ (reaction-4), the rate constants for these reactions can be expressed as

$$k_1 = k_{10} + \kappa' \theta_{Br} \quad (6)$$

$$k_4 = k_{40} + \kappa'' \theta_{Br} \quad (7)$$

where k_{10} and k_{40} are normal rate constants for reaction-1 and -4, and κ' and κ'' are proportional constants. Thus, a decrease in θ_{Br} by a negative shift in U leads to a decreases in k_1 or k_4 and hence decrease a in j, resulting in an NDR (NDR-Br). It is to be noted that the Br^- concentration is very low (2 μm) in the present work and thus θ_{Br} is considerably smaller than one even in positive potentials where θ_{Br} is saturated. This allows the appearances of NDR-OH and oscillation E or γ even in the presence of Br^- (Figs. 1, 2, and 4).

The dependence of NDR-Br and oscillations F and ζ on the crystallographic structure of the electrode surface can also be explained in the same way as that of NDR-OH and oscillation E.[5] The NDR-Br and oscillation F appear most prominently for Pt(111) (Figs. 1-3), similarly to NDR-OH and oscillation E reported.[5,7,8] This difference was attributed to the difference in the number of positively polarized Pt (or Au) atoms near an adsorbed OH among the (111), (100), and (110) faces.[5,7,8] The same should hold for adsorbed Br, as schematically shown in Fig. 5.

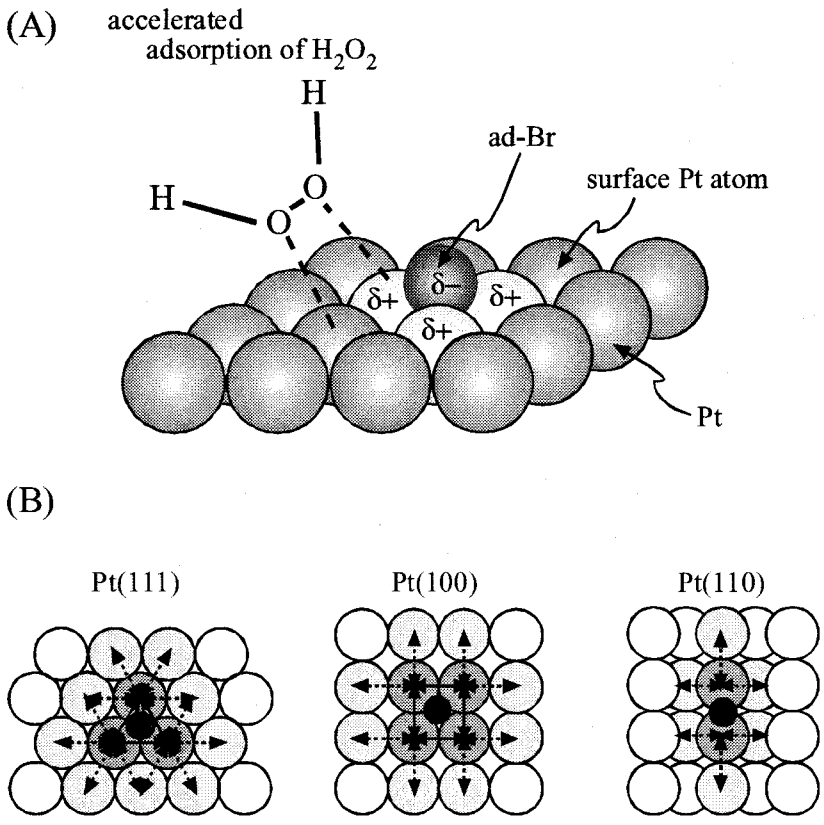

Fig. 5 (A) Schematic illustration of a catalytic effect of adsorbed Br on the dissociative adsorption of H_2O_2 on Pt. (B) The difference in the number of Pt pairs on which accelerated adsorption of H_2O_2 can occur, among Pt(111), (100), and (110).

Based on the arguments described thus far and reported results, Table 1 summarizes the oscillations appearing in the H_2O_2 and $S_2O_8^{2-}$ reduction on Pt and Au electrodes. For oscillations whose mechanisms are clarified, the NDR-inducing species, the slow processes, and the classes according to mechanical classification are indicated. Oscillation F in the H_2O_2-Pt system in the present work is classified into NDR (Class III) oscillators, whereas oscillation ζ is classified into HNDR (Class IV.2) oscillators, though they have a common NDR. The mechanism of oscillation F can be explained in the same way as oscillation E[5] by considering adsorbed Br instead of adsorbed OH. On the other hand, the mechanism of oscillation ζ can be explained in the same way as oscillation γ,[8] also by considering θ_{Br} instead of θ_{OH}.

In conclusion, the present work has revealed that adsorbed Br has a catalytic effect on the dissociative adsorption of H_2O_2 and $S_2O_8^{2-}$, causing new NDR's and oscillations (oscillations F and ζ). The presented results as well as the reported ones for the H_2O_2 and $S_2O_8^{2-}$ reduction on Pt or Au electrodes confirm the generality of a catalytic (or an autocatalytic) effect of adsorbed electronegative species such as adsorbed OH, I, and Br on the dissociative adsorption of peroxides like H_2O_2 and $S_2O_8^{2-}$.

Table 1. A variety of oscillations appearing in the H_2O_2 reduction on Pt and the $S_2O_8^{2-}$ reduction on Pt or Au, together with their characteristics and classification.

NDR-inducing species	Slow process	Name of oscillation[*1]		Classification
		H_2O_2 - system	$S_2O_8^{2-}$ - system	
Adsorbed-OH	H_2O_2 diffusion	Osc. E [5]	———	NDR (Class III)
	H_2O_2 diffusion	enhanced Osc. E [7,*2]	———	NDR (Class III)
	Desorption of adsorbed Cl^-, Br^-, or SO_4^{2-}	Osc. C [10,17]	Osc. γ [8]	HNDR (Class IV.2)
Adsorbed-Br	H_2O_2 diffusion	Osc. F[*3]	———	NDR (Class III)
	Desorption of adsorbed SO_4^{2-}	———	Osc. ζ[*3]	HNDR (Class IV.2)
Upd-H	H_2O_2 diffusion	Osc. A [18-20]	Osc. α [8]	NDR (Class III)
	H_2O_2 diffusion	Osc. B [4]	———	CNDR (Class V)
Adsorbed OH and Upd-H	Desorption of adsorbed Br^-	Osc. D [10,17]	———	HNDR (Class IV.4)
unknown	$S_2O_8^{2-}$ diffusion	———	Osc. β [8]	HNDR[*4](Class IV.3)
	Desorption of adsorbed SO_4^{2-}	———	Osc. δ [8]	HNDR[*4](Class IV.2)

*1 Numerals attached on the names of oscillations refer to the reference numbers. *2 Enhanced by a catalytic effect of adsorbed iodine. *3 The present work. *4 Determined by impedance spectroscopy (an unpublished result).

References

1. M. T. M. Koper, "Advances in Chemical Physics Vol. 92", ed by I. Prigogine and S. A. Rice, p.161, John Willey & Sons, New York (1996).
2. K. Krischer, "Modern Aspects of Electrochemistry Vol. 32", ed by R. E. White, J. O'M. Bockris, and R. E. Conway, p.1, Plenum, New York (1995).
3. M. T. M. Koper, J. H. Sluyters, *J. Electroanal. Chem.*, **371**, 149 (1994).
4. Y. Mukouyama, S. Nakanishi, H. Konishi, Y. Ikeshima, Y. Nakato, *J. Phys. Chem. B*, **105**,10905 (2001).
5. S. Nakanishi, Y. Mukouyama, K. Karasumi, A. Imanishi, N. Furuya, Y. Nakato, *J. Phys. Chem. B*, **104**, 4181 (2000).
6. Y. Mukouyama, S. Nakanishi, H. Konishi, K. Kouhei, Y. Nakato, *Phys. Chem. Chem. Phys.*, **3**, 3284 (2001).
7. S. Nakanishi, Y. Mukouyama, Y. Nakato, *J. Phys. Chem. B*, **105**, 5751 (2001).
8. S. Nakanishi, S. -I. Sakai, M. Hatou, Y. Mukouyama, Y. Nakato, *J. Phys. Chem. B*, in press.
9. J. Clavilier, R. Faure, G. Guinet, D. Durand, *J. Electrochem. Soc.*, **107**, 205 (1980).
10. Y. Mukouyama, S. Nakanishi, H. Konishi, and Y. Nakato, *J. Electroanal. Chem.*, **473**, 156 (1999).
11. Y. Mukouyama, S. Nakanishi, Y. Nakato, *Bull. Chem. Soc. Jpn.*, **72**, 2573 (1999).
12. L. Müller, *J. Electroanal. Chem.*, **13**, 275 (1967).
13. L. Treindl, K. Doblhofer, K. Krischer, Z. Samec, *Electrochim. Acta*, **44**, 3963 (1999).
14. H. A. Gasteiger, N. M. Markovic, P. N. Ross, *Langmuir*, **12**, 1414 (1996).
15. M. F. Mrozek, M. J. Weaver, *J. Am. Chem. Soc.*, **122**, 150 (2000).
16. P. Gao, M. J. Weaver, *J. Phys. Chem.*, **90**, 4057 (1986).
17. Y. Mukouyama, S. Nakanishi, T. Chiba, K. Murakoshi, Y. Nakato, *J. Phys. Chem. B*, **105**, 7246 (2001).
18. Y. Mukouyama, H. Hommura, S. Nakanishi, T. Nishimura, H. Konishi, Y. Nakato, *Bull. Chem. Soc. Jpn.*, **72**, 1247 (1999).
19. T. Matsuda, H. Hommura, Y. Mukouyama, S. Yae, Y. Nakato, *J. Electrochem. Soc.*, **144**, 1988 (1997).
20. S. Nakanishi, Y. Mukouyama, Y. Nakato, *J. Electrochem. Soc.*, **148**, E405 (2001).

Chapter 6

Control of the Period of an Electrochemical Oscillation by Atomic- or Nanometer-Scale Modifications and Structural Changes of Electrode Surfaces in a System of H_2O_2 Reduction at Pt Electrodes

Introduction

Electrochemical oscillations are of much interest from the point of view of dynamic self-organization of molecular systems. They have been reported in various reactions including metal dissolution, metal deposition, and electrocatalytic reactions, as summarized in recent reviews.[1-4] Mechanistic studies have also made rapid progress recently,[4-6] especially since the work by Koper and Sluyters.[7,8] Growing attention has nowadays been paid to observation and mechanism of spatiotemporal patterns.[9-13] The mechanism of transitions from stationary to oscillatory-current states has also been investigated.[14]

Another interesting aspect of electrochemical oscillations is the investigation of influences of structural perturbations and modifications of the electrode surface on atomic and nanometer scales. In living bodies, unique functions originate from dynamic well-organized structures of molecular sizes, indicating a possibility of great advance in studies in this direction. Although there are a number of reports on the modulation of the oscillation period by changes in the electrode potential[15] and the reactant concentrations[15-18] or by application of external potential[19,20] and light[20,21] pulses, little work has been done on the influences of atomic- or nanometer-scale modifications and structural changes of the electrode surface.

The author has studied electrochemical oscillations observed for hydrogen peroxide (H_2O_2) reduction on Pt electrodes in acidic solutions, and found[15,20,22-24] that five oscillations of different types, named oscillation A, B, C, D, and E, appear, depending on the electrode potential, the presence or absence of halide ions in the electrolyte, and the atomic flatness of the electrode surface. The mechanisms of the oscillations were all revealed with an aid of mathematical simulation. Oscillations A[15,20,22] and E[20,23,24] were classified into NDR (negative differential resistance) oscillators, whereas oscillations C and D[20,25,26] were classified into hidden NDR (HNDR) oscillators. Oscillation B was classified into a new-type category, which may be called a coupled NDR (CNDR) oscillator.[27]

In the present paper, the author reports on the influences of modifications and structural changes of the electrode surface on oscillation A. Some preliminary results were reported in previous papers.[20,28]

Experimental

Two kinds of Pt electrodes were used as the working electrode. One is polycrystalline Pt (99.97 % in purity) disc electrodes (about 0.3 mm in diameter). The electrodes were polished with emery paper and aluminum slurry. The other is thin Pt-layer electrodes, prepared by electron-beam evaporation of Pt onto single crystal p-Si(100) wafers (2 × 2 mm in area) at room temperature or 300°C. The average thickness of the Pt layer was ca. 100 nm. The p-Si(100) surfaces were etched with 25 % HF and washed successively under ultrasonic agitation with acetone for 40 min, ethanol for 15 min, and pure water for 15 min, before Pt deposition. Electrical measurements showed that the deposited Pt layer and p-Si formed ohmic contact.

Electrochemical measurements were done using a normal three-electrode system and a beaker-type Pyrex glass cell. The working electrode was placed in a static manner without solution stirring. The counter electrode was a Pt plate (10 × 10 mm in area), and a saturated calomel electrode (SCE) was used as the reference electrode. Just before measurements, cyclic potential scans were performed several times in 0.3 M H_2SO_4 (M = mol/dm^3) between –0.30 and 1.25 V vs. SCE to clean the electrode surface. Electrolyte solutions were prepared using special grade chemicals and water purified from deionized water with a Milli-Q water purification system.

Current density (j) vs. potential (U) curves and j vs. time (t) curves were both measured with a Hokuto-Denko HA-501 potentiogalvanostat and a Nikko-Keisoku NPS-2 potential programmer. They were either recorded with a National VP-6415A X-Y recorder or stored digitally at 1 kHz with a Mac ADIOS II/16 (GW Instruments). XPS spectra were measured with a Shimadzu ESCA 1000 spectrometer. The inspection of electrode surfaces was performed by a high-resolution scanning electron microscope (SEM, Hitachi S-5000).

Results

Figure 1 shows, for reference, a reported *j-U* curve for a Pt-disc electrode in 0.3 M H_2SO_4 + 0.7 M H_2O_2 under a potential-controlled condition.[15,20,22] The H_2O_2-reduction (cathodic) current starts at about 0.60 V vs. SCE, and is independent of the potential between about –0.25 and +0.40 V. The potential-independent current is explained[20,23,25] by assuming that the H_2O_2 reduction is initiated by the dissociative adsorption of H_2O_2

$$2\,Pt + H_2O_2 \xrightarrow{k_1} 2\,Pt\text{-}OH \qquad (1)$$

followed by electrochemical reduction of the resultant Pt-OH

$$Pt\text{-}OH + H^+ + e^- \xrightarrow{k_2} Pt + H_2O \qquad (2)$$

and that the former (reaction (1)) is the rate-determining step. An NDR appears in a potential region of about –0.30 to –0.25 V vs. SCE (just before hydrogen evolution) owing to suppression of the dissociative adsorption of H_2O_2 (reaction (1)) by formation of under-potential deposited hydrogen (upd-H) of a nearly full coverage.[20,23,25] In the potential region of this NDR, oscillation A appears. Hydrogen evolution starts at about –0.30 V, and oscillation B appears in the region of hydrogen evolution.[20,22,27]

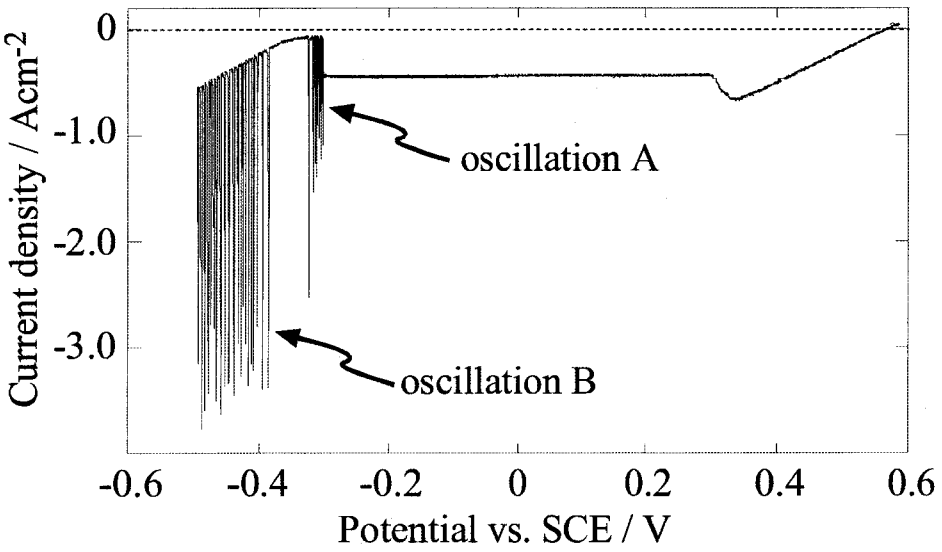

Fig. 1 Current density (*j*) vs. potential (*U*) curve for a Pt disc electrode in 0.7 M H_2O_2 + 0.3 M H_2SO_4. The scan rate is 10 mV/s.

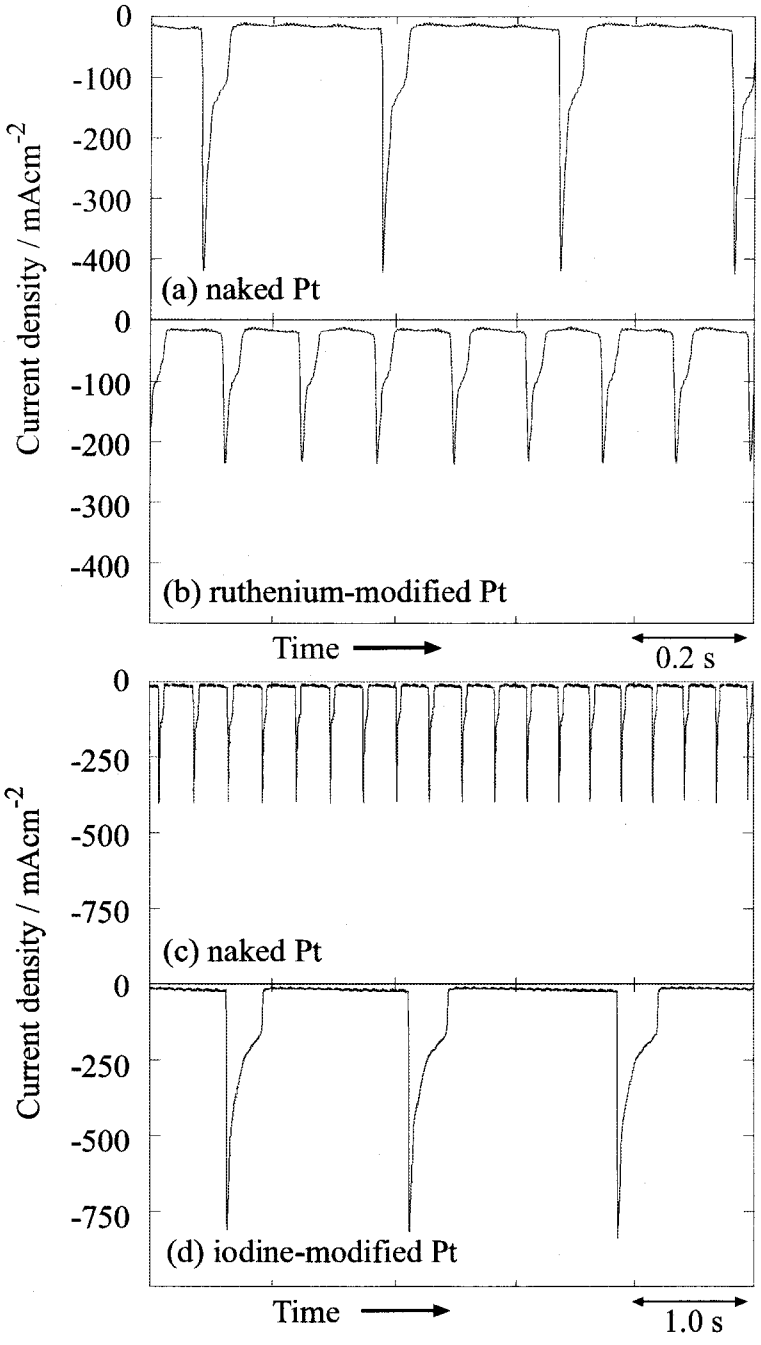

Fig. 2 Time courses of oscillation A at –0.31 V vs. SCE for (a) naked Pt, (b) Ru-modified Pt, (c) naked Pt, and (d) I-modified Pt. Note that the time scale is different between (a), (b) and (c), (d). Electrolyte: 0.7 M H_2O_2 + 0.3 M H_2SO_4.

Figures 2(a) and (b) show *j-t* curves for oscillation A at –0.31 V vs. SCE in 0.3 M H_2SO_4 + 0.7 M H_2O_2 for naked and Ru-modified Pt disc electrodes, respectively, and Figs. 2(c) and (d) those for naked and iodine-modified Pt electrodes, respectively. The Ru- and iodine-modified electrodes were obtained by immersing naked Pt discs in 1 μM $RuCl_3$ for 30 s and in 10 μM KI for 8 s, respectively. The surface coverage was estimated from a decrease in the current peaks of upd-H desorption (explained later in more detail) to be about 0.2 for Ru and about 0.3 for iodine. For Ru-modified Pt, the oscillation period became shorter than for naked Pt, with almost no change in the wave shape, whereas for iodine-modified Pt, the oscillation period became longer. Both the oscillations for the modified electrodes continued long, indicating that the Ru and iodine atoms were stable without desorption during oscillations.

The author reported previously[15,20,22] that the oscillation period for oscillation A strongly depended on the electrode potential, the amplitude increasing nearly in parallel to the period. For example, the oscillation period for a naked Pt electrode in 0.7 M H_2O_2 + 0.3 M H_2SO_4 changed from about 0.02 s at –0.29 V vs. SCE to 0.55 s at –0.32 V[15,20]. Nevertheless, similar results to Fig. 2 were obtained at any potential where oscillation A appeared. The Ru and iodine modifications caused no detectable shift in the potential region of oscillation A.

Figure 3 shows *j-t* curves in another type of experiments. Namely, a naked Pt-disc electrode was immersed in 0.3 M H_2SO_4 + 0.7 M H_2O_2 containing 1.6 μM $CuSO_4$, and the electrode potential was stepped from the rest potential (lying at about 0.60 V) to –0.31 V at which oscillation A appeared (see Fig. 1). The time in Figs. 3(b) ~ (d) was measured from the time of the potential step. Figure 3(a) is a *j-t* curve in the absence of Cu^{2+}, in which the oscillation continued steadily for more than 1 h. In the presence of Cu^{2+}, the oscillation period became shorter with time, and finally the oscillation stopped.

Figure 4 shows a result of a similar experiment to Fig. 3, in which 1.6 μM $AgNO_3$ was added to the solution. Contrary to the case of Cu^{2+} addition, the oscillation period became longer with time, and then the oscillation stopped. Figure 5 plots the oscillation periods of Figs. 3 and 4 as a function of time. In the presence of Cu^{2+}, the oscillation period decreased initially but slightly increased later in a range of 100 to 120 s and then the oscillation stopped, though this is not necessarily clear in Fig. 3. The addition of Ru^{3+} and $AuCl_4^-$ to the solution gave essentially the same results as the addition of Cu^{2+}, including the slight increase of the period in a time range of around 20 s just before the stop of the oscillation.

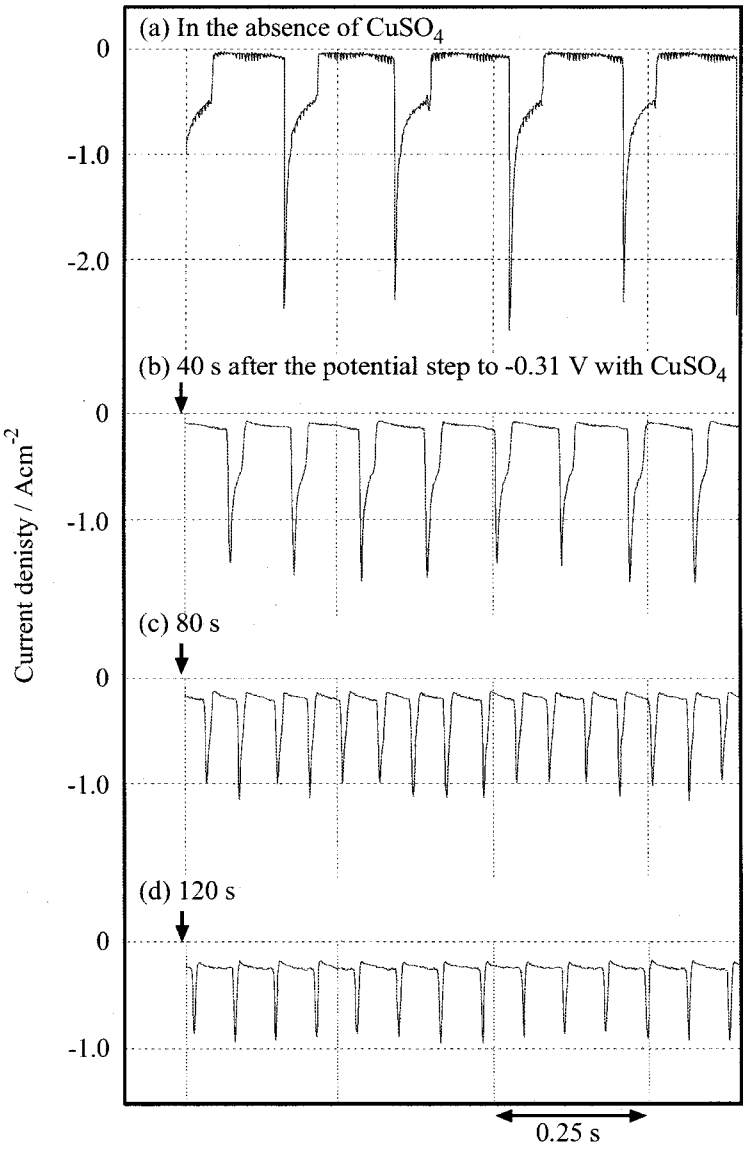

Fig. 3 (a) A time course of oscillation A for naked Pt at –0.31 V vs. SCE in 0.7 M H_2O_2 + 0.3 M H_2SO_4, and (b) ~ (d) those in the presence of 1.6×10^{-6} M $CuSO_4$. See text for details.

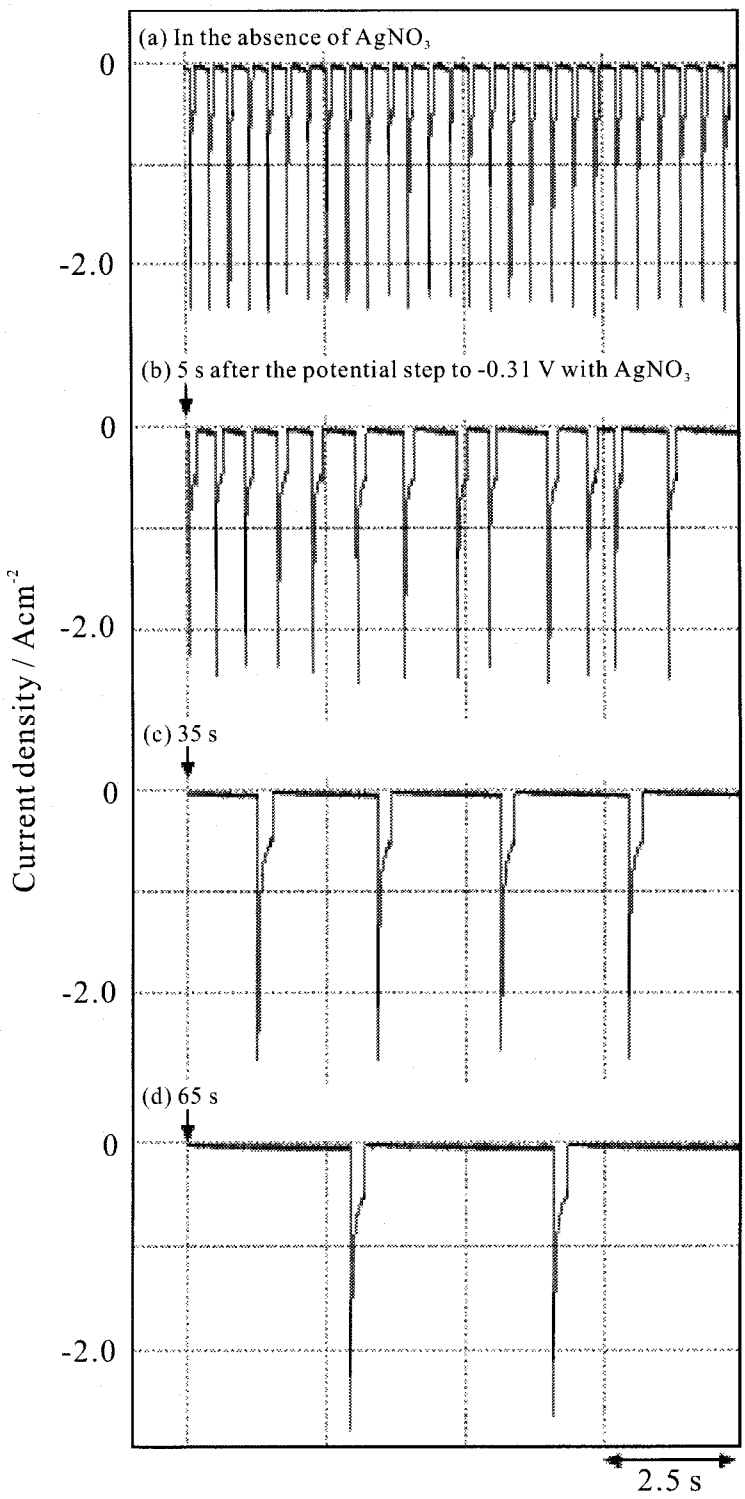

Fig. 4 (a) A time course of oscillation A for naked Pt at –0.31 V vs. SCE in 0.7 M H_2O_2 + 0.3 M H_2SO_4, and (b) ~ (d) those in the presence of 1.6×10^{-6} M $AgNO_3$.

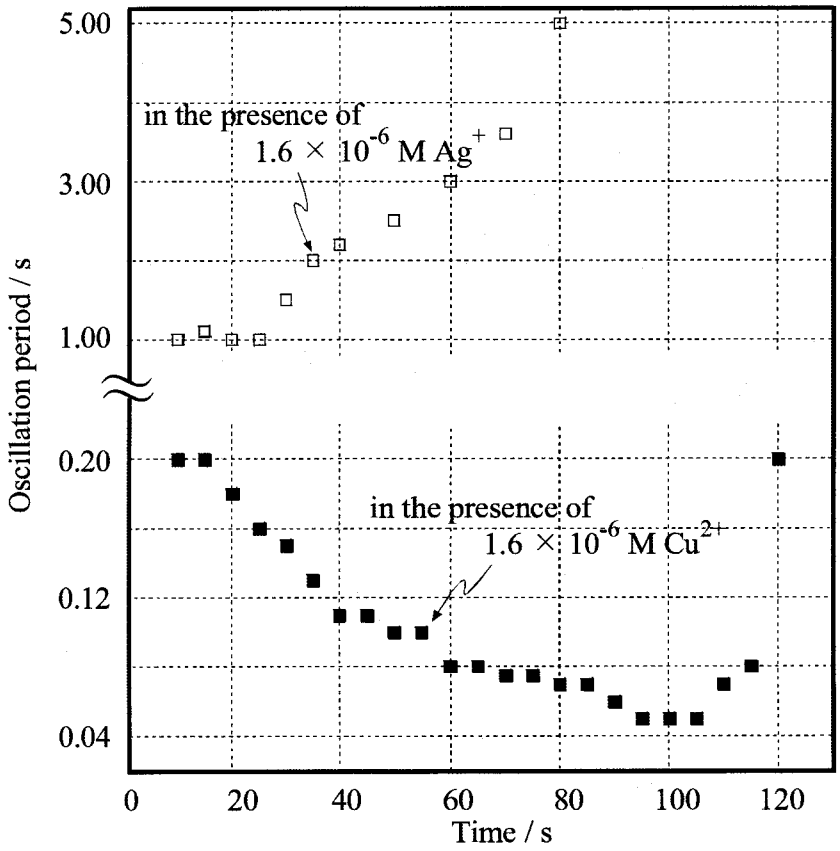

Fig. 5 The oscillation period as a function of time in the presence of Cu^{2+} and Ag^{+} ions in the solution.

It may be noted here that the oscillation period for naked Pt electrodes varied from electrode to electrode even at the same potential and in the same electrolyte composition (see for example Figs. 2(a), 2(c), 3(a) and 4(a)) probably because of slight differences in the initial condition and pretreatment of the electrode. However, the relative changes of the period by the addition of metal ions were well reproduced. Moreover, the decrease and increase of the oscillation period as well as the stopping of the oscillation were observed similarly at any electrode potential.

The above-mentioned changes of the oscillation period are expected to occur by electrochemical deposition of metals such as Cu, Ag, Ru and Au during oscillations, because the potentials in which oscillation A appears are much more negative than the standard redox potentials for depositions of these metals[28-30]. The author investigated how much metals were deposited just after the oscillation had stopped in experiments such as Figs. 3 and 4, by measuring the current peaks of the upd-H formation and disappearance. Figure 6 shows a cyclic voltammogram (dashed line) in 0.3 M H_2SO_4 for the Pt disc electrode just after the oscillation stopped in 0.7 M H_2O_2 + 0.3 M H_2SO_4 + 1.6 μM $HAuCl_4$, compared with that (solid line) for naked Pt. Two peaks in a region from –0.3 to 0.1 V are attributed to desorption (oxidation) of upd-H. The coverage of Au was estimated from the lowering of the current peaks to be about 0.3. XPS spectra of the electrode surface just after the oscillation stopped showed peaks assigned to Au $3d_{3/2}$ and $3d_{1/2}$, indicating that Au was really deposited during oscillation. Analysis of the peak intensities for Pt 4f and Au 3d, by taking account of the coverage of Au of 0.3 as mentioned above, showed that the average thickness of adsorbed Au was nearly one monolayer.

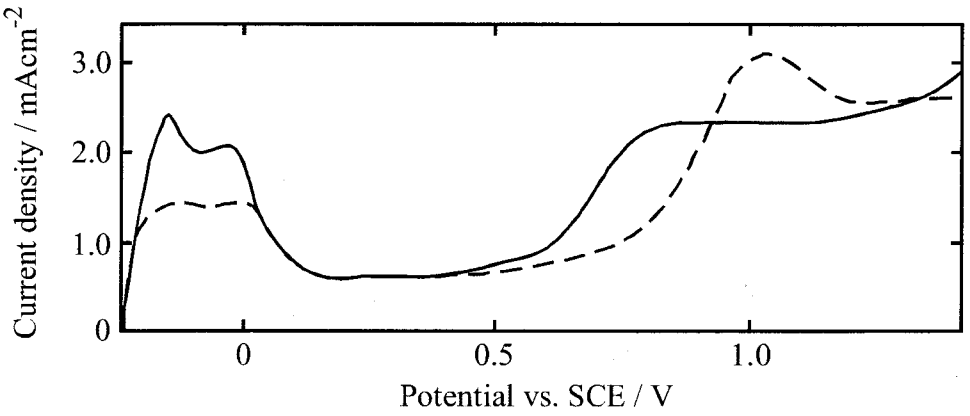

Fig. 6 *j-U* curves in 0.3 M H_2SO_4 for naked Pt (solid line) and Au-modified Pt just after the oscillation stopped in 0.7 M H_2O_2 + 0.3 M H_2SO_4 + 1.6×10^{-6} M $HAuCl_4$ (dashed line). The scan rate is 100 mV/s.

That only a sub-monolayer amount of metal was deposited when the oscillation had stopped was supported by another experiment. Figure 7 shows a *j-t* curve under the same experimental conditions as Fig. 4, on a long time scale. After the oscillation stopped in ca. 150 s, the stationary current still increased with time until it reached a constant value of ca. 0.2 Acm^{-2} in around 3000 s. This implies that the Ag deposition still proceeded after the oscillation had stopped, accompanied by the increase in the stationary H_2O_2-reduction current, or in other words, only a sub-monolayer amount of Ag was deposited in the form of atomic dispersion just after the oscillation had stopped, as discussed in detail in the Discussion section.

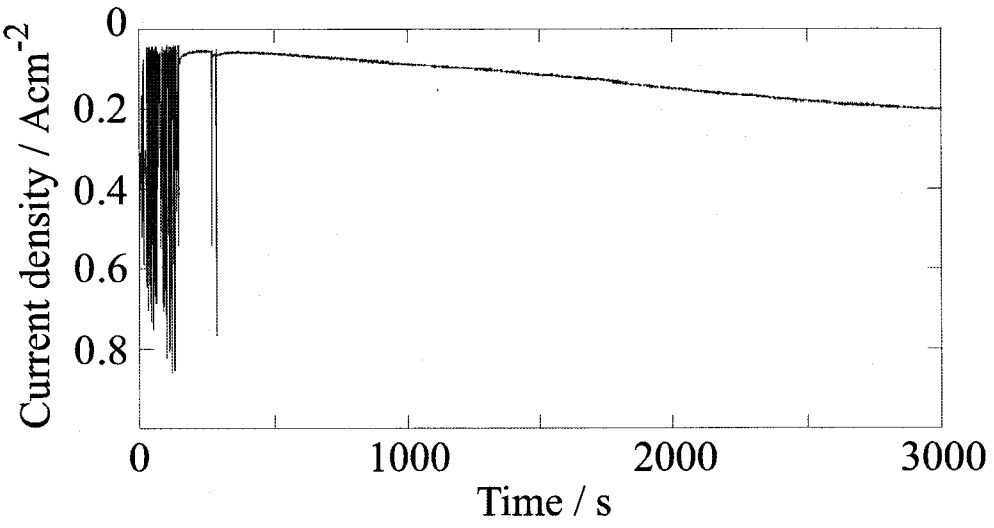

Fig. 7 Time course of oscillation A for naked Pt at –0.31 V vs. SCE in 0.7 M H_2O_2 + 0.3 M H_2SO_4 containing 1.6×10^{-6} M $AgNO_3$ on a long time scale.

Figures 8(a) and (b) show *j-t* curves at –0.31 V vs. SCE for thin Pt-layer electrodes, obtained by Pt deposition on p-Si at room temperature and 300°C, respectively. SEM images, shown in Fig. 9, indicate that Pt layers (white parts) are deposited in the form of islands, which are very small with small inter-island gaps for deposition at room temperature (Fig. 9(a)), whereas large with large inter-island gaps for deposition at 300°C (Fig. 9(b)). Comparison of Figs. 8 and 9 indicates that the oscillation period becomes long for large Pt islands with large inter-island gaps. The result was independent of the applied potential. No detectable shift in the potential region of oscillation A was observed between the large and small Pt islands.

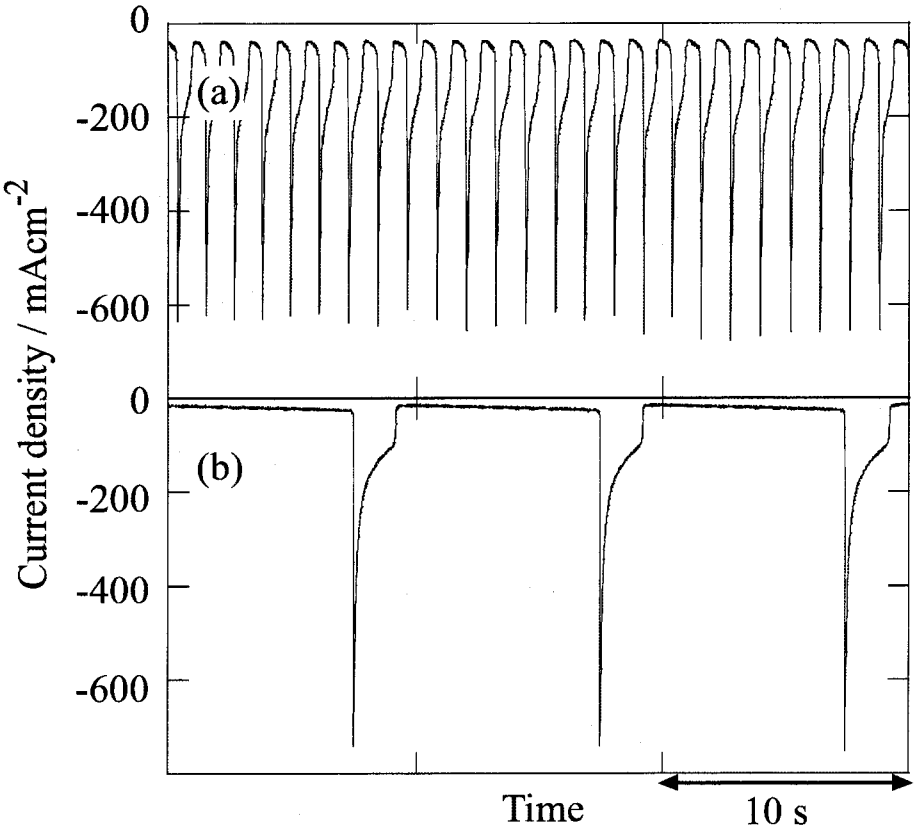

Fig. 8 Time courses of oscillation A at –0.31 V vs. SCE for electrodes of thin Pt layers, deposited on p-Si at (a) room temperature and (b) 300°C. Electrolyte: 0.7 M H_2O_2 + 0.3 M H_2SO_4. See also Fig. 9.

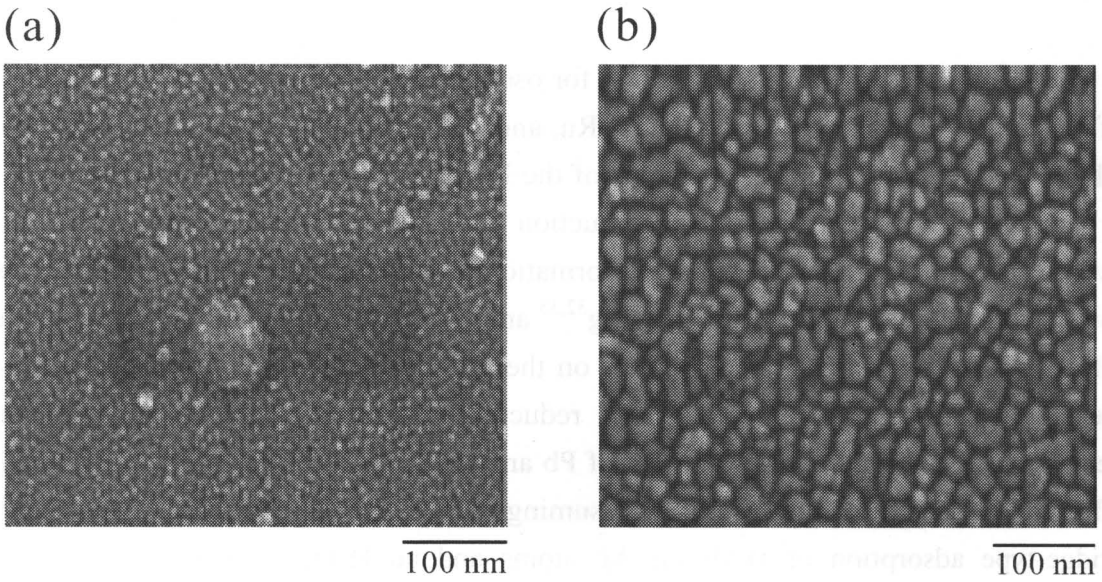

Fig. 9 SEM images of thin Pt layers deposited on p-Si at (a) room temperature and (b) 300°C.

Mathematical Simulation

Why does the oscillation period for oscillation A become longer for deposition of Ag, and shorter for deposition of Cu, Ru, and Au? The question can be answered by taking account of different mechanisms of the H_2O_2 reduction on these metal atoms. It is reported[31-35] that oxygen (O_2) reduction on Au electrodes proceeds by two two-electron reduction mechanisms via formation of H_2O_2,[31] whereas it proceeds by one four-electron reduction mechanism on Ag[32,33] and Pt[34,35] electrodes. Jüttner[36] studied the effect of deposition of Pb and Bi atoms on the O_2 and H_2O_2 reduction on Ag and Au electrodes, and reported that the H_2O_2 reduction on Ag was slowed down by the deposition of a sub-monolayer amount of Pb and Bi atoms, whereas on Au it was little affected. He explained the results by assuming that the H_2O_2 reduction proceeded via bridge-type adsorption of H_2O_2 on Ag atoms and no H_2O_2 reduction occurred on atomically dispersed Ag atoms, whereas on Au atoms, the reduction proceeded via head-on-type adsorption and hence it occurred even on atomically dispersed Au atoms.

The explanation by Jüttner is in harmony with the results of Figs. 4 and 7. The increase in the stationary H_2O_2-reduction current with time after the oscillation stopped (Fig. 7) indicates that the H_2O_2 reduction becomes more effective with the increase of the Ag coverage, i.e., the H_2O_2 reduction can occur on Ag islands or aggregates. On the other hand, in Fig. 4, the current density in the low-current state of oscillation A (a state of a nearly full coverage of upd-H and almost no H_2O_2 reduction on the Pt surface) shows no increase in the absolute value with time (i.e. with the Ag deposition). This implies that the Ag deposition in the initial stage occurs in the form of atomic dispersion and no H_2O_2 reduction occurs on atomically dispersed Ag atoms. For the deposition of Cu, Au or Ru, the author cannot know whether the deposition in the initial stage occurs in the form of atomic dispersion or islands, because the H_2O_2 reduction will occur in both the forms. Actually the current density in the low-current state of oscillation A in the electrolyte containing Cu^{2+} increases in the absolute value with time (Fig. 3), contrary to the case of Ag deposition. Similar results were obtained for the electrolytes containing $AuCl_4^-$ and Ru^{3+}.

The author can assume that no H_2O_2 reduction occurs on adsorbed iodine atoms. Thus, the author has three types of electrode surfaces, a surface (such as naked Pt) on which the H_2O_2 reduction occurs oscillatorily, a surface (such as a Au-covered part) on which it occurs steadily, and a surface (such as an atomic-Ag-covered part) on which no H_2O_2 reduction occurs. The observed modulation of the oscillation period can be reproduced by mathematical simulation on the basis of this idea, as explained below.

Let us first consider a Pt electrode, partially covered with Ag or I atoms on which no H_2O_2 reduction occurs. The following reactions can occur on the naked Pt surface,[20,23,25] in addition to the aforementioned reactions (1) and (2).

$$\mathrm{Pt} + \mathrm{H^+} + \mathrm{e^-} \underset{k_{-3}}{\overset{k_3}{\leftrightarrow}} \mathrm{Pt\text{-}H\ (upd\text{-}H)} \tag{3}$$

$$2\mathrm{Pt\text{-}OH} \xrightarrow{k_4} 2\mathrm{Pt} + \mathrm{O_2} + 2\mathrm{H^+} + 2\mathrm{e^-} \tag{4}$$

$$\mathrm{Pt} + \mathrm{H^+} + \mathrm{e^-} \underset{k_{-5}}{\overset{k_5}{\leftrightarrow}} \mathrm{Pt\text{-}H\ (on\text{-}top\text{-}H)} \tag{5}$$

$$\mathrm{Pt\text{-}H\ (on\text{-}top\text{-}H)} + \mathrm{Pt\text{-}H\ (on\text{-}top\text{-}H)} \xrightarrow{k_6} \mathrm{H_2} \tag{6}$$

The differential equations for a current balance, mass balances, and rate equations can be expressed as follows as reported previously,[20,23,25]

$$I = jA = (U - E)/R_\Omega = I_C + I_F = AC_{DL}(dE/dt) + I_F \tag{7}$$

$$I_F = AF\{-k_3 C_{H+}{}^S(1 - \theta_H - \theta_{OH} - \theta_M) + k_{-3}\theta_H - k_2 C_{H+}{}^s\theta_{OH} + k_4\theta_{OH}{}^2 - k_5 C_{H+}{}^s(1 - \Theta_H) + k_{-5}\Theta_H\} \tag{8}$$

$$dE/dt = (U - E)/AC_{DL}R_\Omega - I_F/AC_{DL} \tag{9}$$

$$(\delta_{HO}/2)\, dC_{HO}{}^s/dt = (D_{HO}/\delta_{HO})(C_{HO}{}^b - C_{HO}{}^s) - k_1 C_{HO}{}^s (1 - \theta_H - \theta_{OH} - \theta_M)^2 \tag{10}$$

$$N_0 d\theta_{OH}/dt = k_1 C_{HO}{}^s(1 - \theta_H - \theta_{OH} - \theta_M)^2 - k_2 C_{H+}{}^s\theta_{OH} - k_4\theta_{OH}{}^2 \tag{11}$$

$$N_0 d\theta_H/dt = k_3 C_{H+}{}^s(1 - \theta_H - \theta_{OH} - \theta_M) - k_{-3}\theta_H \tag{12}$$

$$N_0 d\Theta_H/dt = k_5 C_{H+}{}^s(1 - \Theta_H) - k_{-5}\Theta_H - 2k_6\Theta_H{}^2 \tag{13}$$

where I is the total current, A the electrode area, j the current density, U the external (or applied) electrode potential, E the true electrode potential, $(U - E)$ the ohmic drop between the electrode surface and the position of the reference electrode, R_Ω the solution resistance in the same place as above, $I_C = AC_{DL}(dE/dt)$ the charging current, C_{DL} the double-layer capacitance, and I_F the Faradaic current. $C_{HO}{}^s$ and $C_{H+}{}^s$ are the concentrations of H_2O_2 and H^+ ions at the electrode surface, respectively, $C_{HO}{}^b$ and $C_{H+}{}^b$ the concentrations of H_2O_2 and H^+ in the solution bulk, respectively, and θ_{OH}, θ_H, Θ_H, and θ_M are the surface coverages of Pt-OH, upd-H, on-top-H, and deposited Ag or I atoms, respectively. D_{HO} is the diffusion coefficients for H_2O_2, and δ_{HO} the thickness of the diffusion layers for H_2O_2. N_0 schematically represents the total amount of surface Pt

sites per unit area. In the present work, $C_{H+}{}^{s} = C_{H+}{}^{b}$ was assumed owing to a high mobility (high diffusion rate) of H^+ compared to H_2O_2.

The effect of deposition of Ag or I atoms, on which no H_2O_2 reduction occurs, is taken into account in the above equations by introducing such terms as $(1 - \theta_H - \theta_{OH} - \theta_M)$, which means that the H_2O_2 reduction occurs only on naked Pt. The rate constants, k_2, k_3, k_{-3}, k_4, k_5, and k_{-5}, are expressed by the Butler-Volmer equations,

$$k_i = k_{i0}\exp[-\alpha_i n_i F(E-E_{i0})/RT] \qquad \text{for i = 2, 3 and 5} \qquad (14)$$

$$k_i = k_{i0}\exp[(1-\alpha_i)n_i F(E-E_{i0})/RT] \qquad \text{for i = -3, 4 and –5} \qquad (15)$$

where k_{i0} is the rate constant at $E = E_{i0}$, E_{i0} the equilibrium redox potential for the i-th reaction, α_i the transfer coefficient, n_i the number of transferred electrons.

Figures 10(a) ~ (d) show the *j-t* curves calculated by expressing the coverage θ_M approximately as follows,

$$\theta_M = mt \quad (0 < \theta_M < 1) \qquad (16)$$

where m is a proportional constant. This approximation is reasonable because the Ag deposition proceeds very slowly compared with the oscillating reactions, or in other words, the coverage of Ag can be regarded to be nearly constant for a few cycles of the oscillation, as can be seen from Fig. 4. The oscillation period in Figs. 10(a) ~ (d) became longer with time, in good agreement with the observed result (Fig. 4). The calculation also showed that the oscillation finally stopped, again in agreement with the experiment.

For a Pt electrode, partially covered with Cu, Au, or Ru atoms (hereafter denoted as N) on which the H_2O_2 reduction occurs steadily, the following reactions on the N atoms are considered in addition to reactions (1) ~ (6).

$$N + H_2O_2 + 2H^+ + 2e^- \xrightarrow{k_{17}} N + 2H_2O \qquad (17)$$

$$N + H^+ + e^- \underset{k_{-18}}{\overset{k_{18}}{\leftrightarrow}} N\text{-}H \qquad (18)$$

$$N\text{-}H + N\text{-}H \xrightarrow{k_{19}} H_2 \qquad (19)$$

Reactions (18) and (19), together with reactions (5) and (6), were not necessarily essential in the present work but included to keep a consistency with our previous calculation[15,20].

The author divides the surface into two parts, the areas of the parts being expressed as $\theta_N A$ and $(1-\theta_N)A$, where θ_N is the coverage of the adsorbed metal atoms, N. The Faradaic current I_F can be expressed as follows,

$$I_F = (1-\theta_N)AF\{(-k_2 C_{H^+}{}^s \theta_{OH} - k_3 C_{H^+}{}^S(1-\theta_H-\theta_{OH}) + k_{-3}\theta_H$$
$$- k_5 C_{H^+}{}^s(1-\Theta_H) + k_{-5}\Theta_H + k_4\theta_{OH}{}^2)\} + \theta_N AF\{-2k_{17} C_{HO}{}^s C_{H^+}{}^{s2}$$
$$- k_{18} C_{H^+}{}^s(1-\Theta_{N\text{-}H}) + k_{-18}\Theta_{N\text{-}H}\} \qquad (8)'$$

where $\Theta_{N\text{-}H}$ is the coverage of N-H with respect to the whole Pt surface. The other equations are also modified as follows.

$$(\delta_{HO}/2)\, dC_{HO}{}^s/dt = (D_{HO}{}^s/\delta_{HO})(C_{HO}{}^b - C_{HO}{}^s)$$
$$- (1-\theta_N)k_1 C_{HO}{}^s (1-\theta_H-\theta_{OH}-\theta_N)^2 - \theta_N k_{18} C_{HO}{}^s C_{H^+}{}^2 \qquad (10)'$$

$$(1-\theta_N)N_0 d\theta_{OH}/dt = k_1 C_{HO}{}^s(1-\theta_H-\theta_{OH})^2 - k_3 C_{H^+}{}^s \theta_{OH} - k_4\theta_{OH}{}^2 \qquad (11)'$$

$$(1-\theta_N)N_0 d\theta_H/dt = k_3 C_{H^+}{}^s(1-\theta_H-\theta_{OH}) - k_{-3}\theta_H \qquad (12)'$$

$$(1-\theta_N)N_0 d\Theta_H/dt = k_5 C_{H^+}{}^s(1-\Theta_H) - k_{-5}\Theta_H - 2k_6\Theta_H{}^2 \qquad (13)'$$

Furthermore, another differential equation for the coverage of N-H is added.

$$\theta_N N_0 d\Theta_{N\text{-}H}/dt = k_{18} C_{H^+}{}^s(1-\Theta_{N\text{-}H}) - k_{-18}\Theta_{N\text{-}H} - 2k_{19}\Theta_{N\text{-}H}{}^2 \qquad (20)$$

The rate constants, k_{17}, k_{18}, and k_{-18} are expressed similarly to equations (14) and (15).

Figures 10(e) ~ (h) show calculated *j-t* curves, with θ_N expressed approximately as follows,

$$\theta_N = nt \quad (0 < \theta_N < 1) \qquad (21)$$

where n is a proportional constant. The calculation showed that the oscillation period became shorter with time and finally the oscillation stopped, in good agreement with the experiments (Fig. 3).

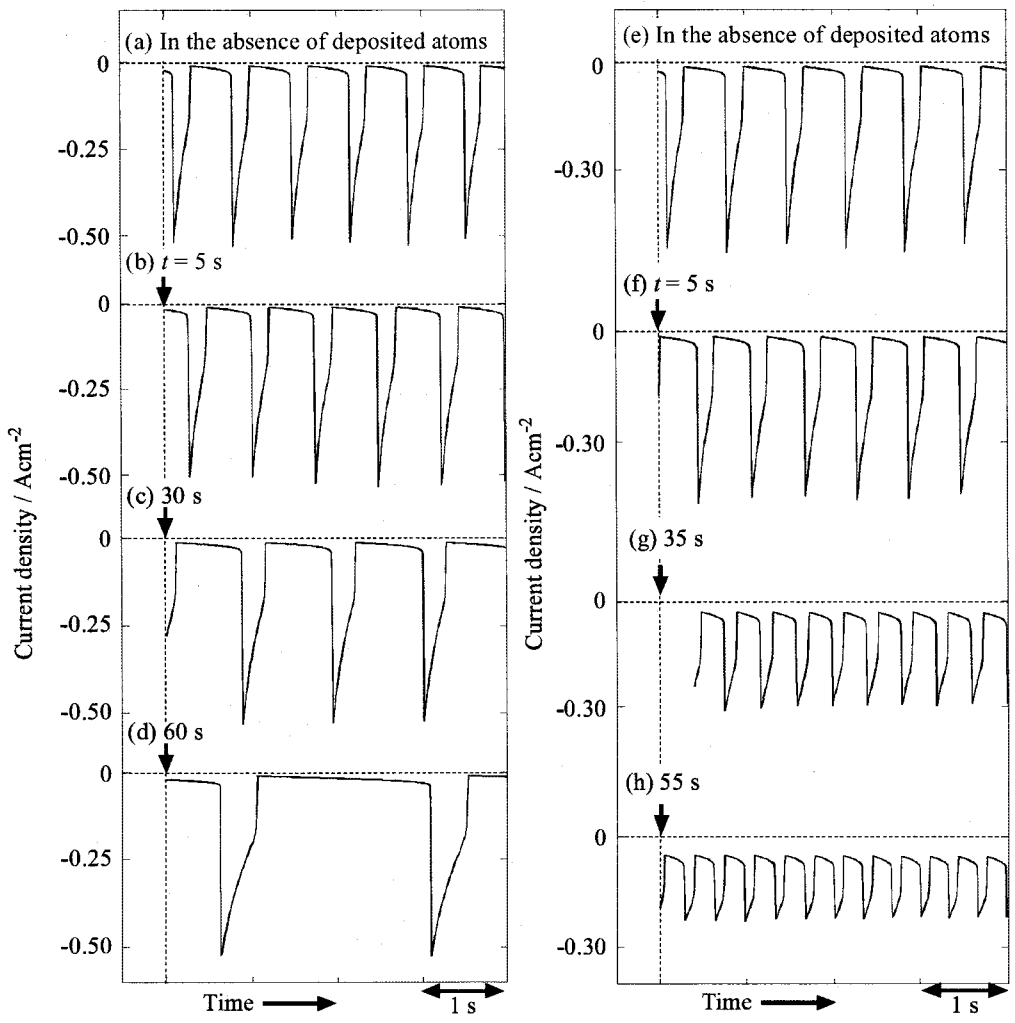

Fig. 10 Calculated time courses (a) ~ (d) for deposition of atoms (such as Ag and I) on which no H_2O_2 reduction occur, and (e) ~ (h) for deposition of atoms (such as Au, Cu, and Ru) on which the H_2O_2 reduction occurs continuously. The coverage of the deposited atoms, θ_M or θ_N, was expressed as $\theta_M = mt$ or $\theta_N = nt$, with $m = n = 0.01$ s^{-1}. U was kept constant at -0.27 V vs. SCE. The other parameter values are as follows: $C_{HO}^{b} = 0.7 \times 10^{-3}$ mol cm^{-3}, $\delta_{HO} = 0.01$ cm, $D_{HO} = 1.7 \times 10^{-5}$ cm^2 s^{-1}, $C_{H+}^{b} = 0.3 \times 10^{-3}$ mol cm^{-3}, $A = 0.01$ cm^2, $C_{DL} = 2.0 \times 10^{-5}$ F cm^{-2}, $N_0 = 2.2 \times 10^{-9}$ mol cm^{-2}, $R_\Omega = 60$ Ω, $T = 300$ K, $\alpha_i = 0.25$ (i = 2) and 0.50 (i $\neq$ 2), $n = 1$, $k_{10} = 4 \times 10^{-2}$ cm s^{-1}, $k_{20} = 1 \times 10^{-5}$ cm s^{-1}, $k_{30} = 1 \times 10^{-2}$ cm s^{-1}, $k_{-30} = 1 \times 10^{-5}$ mol cm^{-2} s^{-1}, $k_{40} = 1 \times 10^{-8}$ mol cm^{-2} s^{-1}, $k_{50} = 5 \times 10^{-3}$ cm s^{-1}, $k_{-50} = 5 \times 10^{-6}$ mol cm^{-2} s^{-1}, $k_6 = 5 \times 10^{-6}$ mol cm^{-2} s^{-1}, $k_{17} = 4 \times 10^{-5}$ cm^7 mol^{-3} s^{-1}, $k_{18} = 5 \times 10^{-3}$ cm s^{-1}, $k_{-18} = 5 \times 10^{-6}$ mol cm^{-2} s^{-1}, $k_{19} = 5 \times 10^{-6}$ mol cm^{-2} s^{-1}, $E_{20} = 1.10$ V vs. NHE, $E_{50} = E_{-50} = 0$-0.19 V, $E_{170} = 0.80$ V, and $E_{180} = E_{-180} = -0.19$ V.

Discussion

The experiments and mathematical simulation show that the modulation of the oscillation period is caused by the presence of adsorbed foreign atoms having different mechanisms (or different current densities) for the H_2O_2 reduction. The essential point can be understood by considering a surface model schematically shown in Figs. 11(a) ~ (c). When the averaged current density (j_{av}) at a position slightly (a few or a few tens nm) apart from the electrode surface is the same among Figs. 11(a), (b), and (c), the local current density at the naked Pt surface (j_{Pt}^{s}) is low for deposition of Cu, Au, or Ru atoms on which the H_2O_2 reduction occurs steadily (Fig. 11(a)), whereas the j_{Pt}^{s} is high for deposition of Ag or I atoms on which no H_2O_2 reduction occurs (Fig. 11(c)). The difference in j_{Pt}^{s} leads to the difference in the oscillation period.

This is explained as follows. According to our previous work,[15,20] the period of oscillation A is mainly determined by the time (t_{LC}) of the low-current state, and the t_{LC} is determined by the time in which the current density (j) in the low-current state increases (in the absolute value) and reaches a certain critical value, j_{cr} (see Fig. 11(d)). This is because the increase in j leads to a positive shift of E under a potentiostatic condition (U constant) by the relation of $U = E + AjR$ (j is negative for cathodic current), and when E becomes positive enough to remove upd-H, a rapid increase in j occurs owing to a rapid decrease in θ_H. For atomic or nm-scale dispersion of deposited metals, not the j_{Pt}^{s} but the j_{av} in Fig. 11 determines the ohmic drop (AjR) in the solution. This implies that the oscillation period for the modified Pt electrodes is mainly determined by the time in which the j_{av} reaches j_{cr}. It is easily understood that it takes only a short time for j_{av} to reach j_{cr} in case of Fig. 11(a) because the j_{Pt}^{s} only needs to reach a lower value than j_{cr}, whereas it takes a long time in case of Fig. 11(c) because the j_{Pt}^{s} needs to reach a higher value than j_{cr}.

The results for thin Pt-layer electrodes (Fig. 8) can be explained similarly. When large Pt islands are deposited with *large* inter-island gaps on p-Si, high j_{Pt}^{s} at the Pt island is needed for j_{av} to reach j_{cr}, because the H_2O_2 reduction does not occur on Si. This leads to a long oscillation period, in agreement with the experiment (Fig. 8).

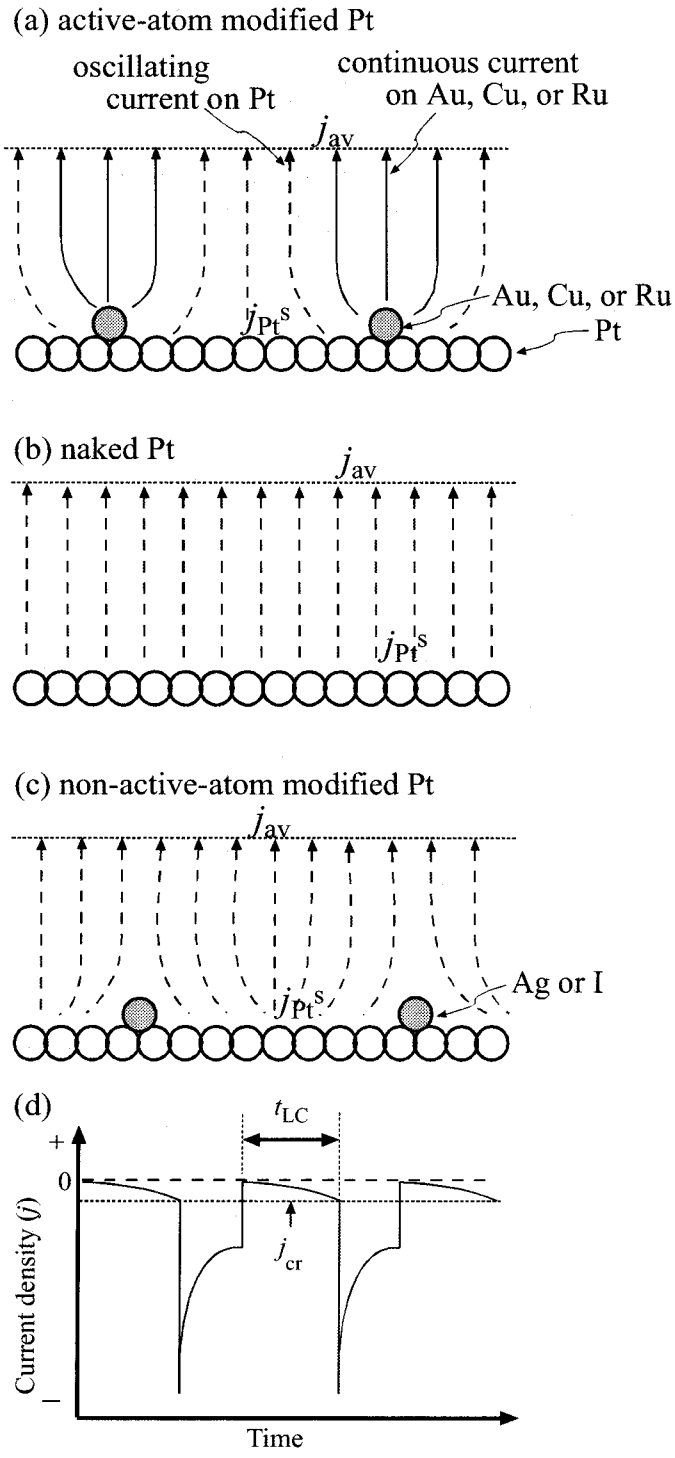

Fig. 11 (a) ~ (c) Schematic illustrations of current flows near the electrode surface for three different-type Pt electrodes. (d) Schematic illustration of a time course of oscillation A.

It is to be noted that the present results clearly indicate that the Ag deposition in the initial stage occurs in the form of atomic dispersion and no H_2O_2 reduction occurs on atomically dispersed Ag atoms, giving confirmative support to the mechanism of the H_2O_2 reduction on Ag, suggested by Jüttner.[36] For the modifications with Au, Cu, Ru, and I atoms, the author can get no definite conclusion on whether they are deposited in the form of atomic dispersion or islands, as mentioned before, because both the forms will have the same reactivity concerning the H_2O_2 reduction. However, as the deposited islands are expected to have nm-scale size, the author can conclude that the oscillation period is modulated by the atomic- or nm-scale modification of the Pt surface.

It may be noted also that the decrease and increase of the oscillation period by the electrode modification can be explained in another way, by considering shifts of the potential region of oscillation A. The deposition of I or atomically dispersed Ag atoms, for example, leads to a decrease in the H_2O_2-reduction current compared with that for a naked Pt electrode, and hence should in principle cause a shift of the oscillatory (potential) region toward the positive, though no definite shift was observed experimentally, as mentioned in the Results section. Because the oscillation period increases steeply with a negative potential shift, also as mentioned in the Results section, the slight positive shift of the oscillatory region by the Ag or I deposition can lead to a considerable increase of the oscillation period at a fixed (measured) potential. A similar explanation is possible for the results of the Cu, Au, and Ru-modified Pt electrodes and the Pt-deposited p-Si electrodes.

Finally the author has to note that the oscillation period in the solution containing Cu^{2+}, Ru^{3+}, or $AuCl_4^-$ decreases initially but increases slightly in a time range of around 20 s just before the oscillation stops (Fig. 5). The increase of the period just before the oscillation stops can be attributed to a decrease in the surface H_2O_2 concentration (C_{HO}^s) due to the increase in the coverage of Cu, Ru, or Au, on which the H_2O_2 reduction occurs steadily, and the diffusion limit of H_2O_2. Actually the author reported previously[15,20] that the period of oscillation A increased largely with the decreasing C_{HO}^s. The author can thus say that, for the deposition of Cu, Ru, or Au, the decrease in the oscillation period by the increase in j_{av} (cf. Fig. 11) contends with the increase in the period by the decrease in C_{HO}^s and the latter surpasses the former to some extent in a time range just before the oscillation stops.

In conclusion, the present work has revealed that the oscillation period of oscillation A for H_2O_2 reduction on Pt electrodes can be modulated by modifications and structural changes of the electrode surface on atomic or nanometer scales. The detailed analyses of the behavior, combined with mathematical simulation, have shown

that the mixing of surface areas having different mechanisms for the H_2O_2 reduction leads to the modulation of the oscillation period.

This work was partly supported by a Grant-in-Aid for Scientific Research on Priority Area of "Electrochemistry of Ordered Interfaces" (No. 09237105) from the Ministry of Education, Culture, Sports, Science and Technology, Japan

References

1. J. L. Hudson and T. T. Tsotsis, *Chem. Eng. Sci.*, **49**, 1493 (1994).
2. T. Z. Fahiday and Z. H. Gu, "Modern Aspects of Electrochemistry Vol. 27", ed by R. E. White, J. O'M. Bockris, and R. E. Conway, Plenum, New York (1995), p.383.
3. M. T. M. Koper, "Advances in Chemical Physics Vol. 92", ed by I. Prigogine and S. A. Rice, John Willey & Sons, New York (1996), p.161.
4. K. Krischer, "Modern Aspects of Electrochemistry Vol. 32", ed by R. E. White, J. O'M. Bockris, and R. E. Conway, Plenum, New York (1995), p.1.
5. M. T. M. Koper, J. H. Sluyters, *J. Electroanal. Chem.*, **371**, 149 (1994).
6. P. Strasser, M. Eiswirth, M. T. M. Koper, *J. Electroanal. Chem.*, **478**, 50 (1999).
7. M. T. M. Koper, J. H. Sluyters, *J. Electroanal. Chem.*, **303**, 73 (1991).
8. M. T. M. Koper, J. H. Sluyters, *J. Electroanal. Chem.*, **347**, 31 (1993).
9. G. Flätgen, K. Krischer, B. Pettinger, K. Doblhofer, H. Junkes, G. Ertl, *Science*, **269**, 668 (1995).
10. I. Z. Kiss, V. Gaspar, J. L. Hudson, *J. Phys. Chem. B*, **104**, 7554 (2000).
11. J. Christoph, R. D. Otterstedt, M. Eiswirth, N. I. Jaeger, J. L. Hudson, *J. Chem. Phys.* **110**, 8614 (1999)
12. P. Strasser, J. Christoph, W. F. Lin, M. Eiswirth, J. L. Hudson, *J. Phys. Chem. A*, **104**, 1854 (2000).
13. N. Mazouz, K. Krischer, G. Flätgen, G. Ertl, *J. Phys. Chem. B*, **101**, 2403 (1997).
14. Y. Mukouyama, T. Nishimura, S. Nakanishi, Y. Nakato, *J. Phys. Chem. B*, **104**, 11186 (2000).
15. Y. Mukouayama, H. Hommura, S. Nakanishi, T. Nishimura, H. Konishi, Y. Nakato, *Bull. Chem. Soc. Jpn.*, **72**, 1247 (1999).
16. J. J. Podesta, R. C. A. Piatti, A. J. Arvia, *J. Electrochem. Soc.*, **126**, 1363 (1979).
17. P. Russell, J. Newman, *J. Electrochem. Soc.*, **133**, 2093 (1986).
18. W. Lou, K. Ogura, *Electrochim. Acta*, **40**, 667 (1995).
19. T. Nishimura, Y. Mukouyama, S. Nakanishi, H. Konishi, Y. Nakato, *Kagaku-Kogaku Ronbun-shu (in Japanese)*, **25**, 510 (1999).
20. Y. Mukouyama, S. Nakanishi, Y. Nakato, *Bull. Chem. Soc. Jpn.*, **72**, 2573 (1999).
21. H. Tributsch, *Ber. der Bunsenges. Phys. Chem.*, **79**, 580 (1975).
22. T. Matsuda, H. Hommura, Y. Mukouyama, S. Yae, Y. Nakato, *J. Electrochem. Soc.*, **144**, 1988 (1997).
23. S. Nakanishi, Y. Mukouayma, K. Karasumi, A. Imanishi, N. Furuya, Y. Nakato, *J.*

Phys. Chem. B, **104**, 4181 (2000).
24. S. Nakanishi, Y. Mukouyama, Y. Nakato, *J. Phys. Chem. B*, **105**, 5751 (2001).
25. Y. Mukouyama, S. Nakanishi, H. Konishi, and Y. Nakato, *J. Electroanal. Chem.*, **473**, 156 (1999).
26. Y. Mukouyama, S. Nakanishi, T. Chiba, K. Murakoshi, Y. Nakato, *J. Phys. Chem. B*, **105**, 7246 (2001).
27. Y. Mukouyama, S. Nakanishi, H. Konishi, Y. Ikeshima, Y. Nakato, *J. Phys. Chem. B*, **105**, 10905 (2001).
28. S. Nakanishi, H. Hommura, Y. Mukouyama, Y. Matsuda, and Y. Nakato, *Chem. Lett.*, 977 (1998).
29. D. M. Kolb, M. Przasbyski, and H. Gerischer, *J. Electroanal. Chem.*, **54**, 25 (1974).
30. "Chemical Handbook (Kagaku Binran)," 4th ed, Basic Part II, The Chemical Society of Japan, Maruzen, Tokyo(1993). P.II-466.
31. R. Zurilla, R. Sen, E. Yeager, *J. Electroanal. Chem.*, **125**, 1103 (1978).
32. A. J. Appleby, "Modern Aspects of Electrochemistry Vol. 9", ed by J. O'M. Bockris, and R. E. Conway, Plenum, New York (1974).
33. E. Yeager, C. Krouse, K. V. Rao, *Electrochim. Acta*, **9**, 1075 (1964).
34. P. Fischer, J. Heitbaum, *J. Electroanal. Chem.*, **112**, 231 (1980).
35. J. Huang, R. Sen, E. Yeager, *J. Electrochem. Soc.*, **126**, 785 (1979).
36. K. Jűttner, *Electrochim. Acta*, **243**, 445 (1988).

General Conclusions

Studies on electrochemical oscillations have made rapid progress recently, but the detailed mechanisms have still remained unclear. The present work studied the mechanisms of electrochemical oscillations for the reduction reaction of H_2O_2 and $S_2O_8^{2-}$ on Pt or Au electrodes, with an emphasis placed on the elucidation of the influence of the atomic-level structure of the electrode surfaces on electrochemical oscillations, and revealed a new important autocatalytic mechanism and found a variety of new electrochemical oscillations. The main results can be summarized as follows.

The present work has revealed that adsorbed electronegative species such as adsorbed OH, Br, and I have an (auto)catalytic effect on the dissociative adsorption of some peroxides (such as H_2O_2 and $S_2O_8^{2-}$). The effect is really of a new type, depending strongly on the atomic-level structure of the electrode surface, and causes a variety of electrochemical oscillations, such as oscillations A, B, C, D, E, F, and G for the H_2O_2 reduction, and oscillations α, β, γ, δ, and ζ for the $S_2O_8^{2-}$ reduction.

Oscillation E in the "H_2O_2 reduction on Pt electrode" system (Chapter 1) and oscillation γ in the "$S_2O_8^{2-}$ reduction on Pt or Au electrode" system (Chapter 4) is caused by the (auto)catalytic effect of adsorbed OH. The (auto)catalytic effect can be explained by a mechanism that adsorbed OH induces positive polarization at surface metal atoms in the neighborhood by the electronegativity difference between metal atoms and OH group. The adsorption of H_2O_2 and $S_2O_8^{2-}$ are accelerated on such positively polarized metal atoms by electrostatic interaction. The fact that adsorbed OH and adsorbed bromine and iodine have similar (auto)catalytic effects strongly supports the above model.

The present work also discovered the presence of two stationary states of low and high current densities for the H_2O_2 reduction on Pt electrodes, which confirms further the above model because the high-current-density state can be induced only by the autocatalytic effect of adsorbed OH (Chapter 2). The observation of the two stationary states gives confirmative evidence for the presence of the autocatalytic effect of adsorbed OH.

The present work has in addition studied the influences of the various modifications of electrode surface and structural changes on the behavior of oscillation

A, and revealed that the oscillation period is determined by the ratio of the areas of active and the passive surfaces, introduced by surface modifications. The result is a first successful example for the control of electrochemical oscillatory behavior by modification of the electrode surface.

The oscillations appearing in the H_2O_2 and $S_2O_8^{2-}$ reduction on Pt and Au electrodes, including the above-mentioned ones, are summarized in Table. For the oscillations whose mechanisms are clarified, the NDR-inducing species, the slow process, and the class (or type) are indicated according to the improved classification based on the oscillation mechanisms. It is clear that the H_2O_2- and $S_2O_8^{2-}$-reduction systems studied in the present work are very interesting ones, showing not only a variety of electrochemical oscillations, oscillations A, B, C, D, E, F, and G and α, β, γ, δ, and ζ, but also a variety of oscillation mechanisms.

The present work has investigated the electrochemical oscillations systematically from the point of view of the structural control of the electrode surfaces on atomic-level or nanometer scale, and exploited new mechanism and a new research field for the electrochemical oscillations. The present work has also shown that the study of electrochemical oscillations is important not only for the understanding of nonlinear chemical dynamics of molecular systems but also for the elucidation of the mechanisms of electrochemical reactions themselves.

Table. A variety of oscillations appearing the H_2O_2 reduction on Pt and the $S_2O_8^{2-}$ reduction on Pt or Au, together with their characteristics and classification.

NDR-inducing species	Slow process	Name of oscillation		Classification
		H_2O_2 - system	$S_2O_8^{2-}$ - system	
Adsorbed-OH	H_2O_2 diffusion	Osc. E	———	NDR (Class III)
	H_2O_2 diffusion	enhanced Osc. E	———	NDR (Class III)
	Desorption of adsorbed Cl^-, Br^-, or SO_4^{2-}	Osc. C	Osc. γ	HNDR (Class IV.2)
Adsorbed-Br	H_2O_2 diffusion	Osc. F	———	NDR (Class III)
	Desorption of adsorbed SO_4^{2-}	———	Osc. ζ	HNDR (Class IV.2)
Upd-H	H_2O_2 diffusion	Osc. A	Osc. α	NDR (Class III)
	H_2O_2 diffusion	Osc. B	———	CNDR (Class V)
Adsorbed OH and Upd-H	Desorption of adsorbed Br^-	Osc. D	———	HNDR (Class IV.4)
unknown	$S_2O_8^{2-}$ diffusion	———	Osc. β	HNDR(Class IV.3)
	Desorption of adsorbed SO_4^{2-}	———	Osc. δ	HNDR(Class IV.2)

List of Publications

1. *Modulation of the Oscillation Period for an Electrochemical Oscillation in an "H_2O_2-Acid-Pt Electrode" System by Deposition of a Small Amounts of Metal Atoms*
   S. Nakanishi, H. Hommura, Y. Mukouyama, T. Matsuda, Y. Nakato
   Chem. Lett., 977, (1998).

2. *Appearance of an Oscillation through Autocatalytic Mechanism by Control of the Atomic-Level Structure of Electrode Surfaces in Electrochemical H_2O_2 Reduction at Pt Electrodes*
   S. Nakanishi, Y. Mukouyama, K. Karasumi, A. Imanishi, N. Furuya, Y. Nakato
   J. Phys. Chem. B, **104**, 4181 (2000).

3. *Catalytic Effect of Adsorbed Iodine on Hydrogen Peroxide Reduction at Single Crystal Pt Electrodes, Causing Enhanced Current Oscillations*
   S. Nakanishi, Y. Mukouyama, Y. Nakato
   J. Phys. Chem. B, **105**, 5751 (2001).

4. *Observation of Two Stationary States of Low and High H_2O_2-Reduction Currents at a Pt Electrode, Arising from the Occurrence of a Positive Feedback Mechanism Including Solution-Stirring by Gas Evolution*
   Y. Mukouyama, S. Nakanishi, H. Konishi, K. Karasumi, Y. Nakato
   Phys. Chem. Chem. Phys., **3**, 3284 (2001).

5. *Control of the Period of an Electrochemical Oscillation by Atomic-Scale Modifications and nm-Scale Structural Changes of Electrode Surfaces in a System of H_2O_2 Reduction at Pt Electrodes*
   S. Nakanishi, Y. Mukouyama, Y. Nakato
   J. Electrochem. Soc., **148**, E405 (2001).

6. *Oscillatory Peroxodisulfate Reduction on Pt and Au Electrodes under High Ionic Strength Conditions, Caused by Catalytic Effect of Adsorbed OH*
   S. Nakanishi, S. –I. Sakai, M. Hatou, Y. Mukouyama, Y. Nakato
   J. Phys. Chem. B, **106**, 2287 (2002).

7. *Promoted Dissociative Adsorption of Hydrogen Peroxide and Persulfate Ions by a Catalytic Effect of Adsorbed Bromine, Causing Electrochemical Oscillations*
   S. Nakanishi, S. –I. Sakai, M. Hatou, K. Fukami, Y. Nakato
   J. Electrochem. Soc., submitted for publication.

The papers not included in the present thesis:

8. *Appearance of a New Oscillation (Named Oscillation C) in H_2O_2-Reduction Reaction on a Pt Electrode in Acidic Solutions by Addition of a Small Amount of Chloride Ions*
   Y. Mukouyama, H. Konishi, S. Nakanishi, Y. Nakato
   Chem. Lett., 1009 (1998).

9. *Mechanism and Simulation of Electrochemical Current Oscillations Observed in the H_2O_2-Reduction Reaction on Platinum Electrodes in Acidic Solutions*
   Y. Mukouyama, H. Hommura, S. Nakanishi, T. Nishimura, H. Konishi, Y. Nakato
   Bull. Chem. Soc. Jpn., **72**, 1247 (1999).

10. *Modulation of Electrochemical Oscillations in an H_2O_2-H_2SO_4-Pt System by External Potential Pulses*
    T. Nishimura, Y. Mukouyama, S. Nakanishi, H. Konishi, Y. Nakato
    Kagaku Kogaku Ronbunshu, **25**, 510 (1999).

11. *Positive Feedback Mechanism, Autocatalysis Mechanism, and Dependence on Atomic-Level Surface Structures in Electrochemical Oscillations for H_2O_2 Reduction on Pt Electrodes*
    Y. Mukouyama, S. Nakanishi, Y. Nakato
    Bull. Chem. Soc. Jpn., **72**, 2573 (1999).

12. *Electrochemical Oscillations of a New Type in an H_2O_2 + H_2SO_4 / Pt-Electrode System, Appearing by Addition of Small Amounts of Halide Ions*
    Y. Mukouyama, S. Nakanishi, H. Konishi, Y. Nakato
    J. Electroanal. Chem., **473**, 156 (1999).

13. *Roles of Local Deviations and Fluctuations of the Helmholtz-Layer Potential in*

Transition from Stationary to Oscillatory Currents in an "H_2O_2-Acid-Pt" Electrochemical System
Y. Mukouyama, T. Nishimura, S. Nakanishi, Y. Nakato
J. Phys. Chem. B, **104**, 11186 (2000).

14. *New-Type Electrochemical Oscillation Caused by Electrode-Surface Inhomogeneity and Electrical Coupling as Well as Solution Stirring through Electrochemical Gas Evolution Reaction*
Y. Mukouyama, S. Nakanishi, H. Konishi, Y. Ikeshima, Y. Nakato
J. Phys. Chem. B, **105**, 10905 (2001).

15. *Mechanisms of Electrochemical Oscillations of Two Types, Observed for H_2O_2 Reduction on Pt Electrodes in the Presence of Small Amounts of Halide Ions*
Y. Mukouyama, S. Nakanishi, T. Chiba, K. Murakoshi, Y. Nakato
J. Phys. Chem. B, **105**, 7246 (2001).

16. *New Autocatalytic Mechanism for Metal Electrodeposition Leading to Oscillations and Fern-Leaf-Shaped Deposits*
S. Nakanishi, K. Fukami, S. –I. Sakai, Y. Nakato
Chem. Lett., in press (2002).

17. *Oscillation-Induced Layer-by-Layer Electrodeposition Producing Alternate Metal and Metal-Alloy Multilayers on a Nanometer Scale*
S. –I. Sakai, S. Nakanishi, K. Fukami, Y. Nakato
Chem. Lett., in press (2002).

Acknowledgments

The author would like to express his sincerest gratitude to Professor Yoshihiro Nakato for his continuous guidance and encouragement through this work. The author is also extremely indebted to Associate Professor Kei Murakoshi and Research Associate Akihito Imanishi for their valuable suggestions.

The author would like to express his deep thanks to Professor Nagakazu Furuya (Yamanashi University) for his kind instruction on the preparation of single crystal metal electrodes, and to Professor Kingo Itaya (Tohoku University) for his kind guidance on STM measurements. The author wishes to thank Assistant Professor Shinji Yae (Himeji Institute of Technology) and Dr. Yoshiharu Mukouyama (Tokyo Denki University) for their valuable discussions through this work.

Furthermore, the author wishes to thank Assistant Noriko Wada and all the members of Prof. Nakato's laboratory.

Finally, the author is grateful to his wife for her continuous support.

April 2002

Shuji Nakanishi